Project porcupine : the MF mutual-impedance probe experiment. Part II : Flight F3 and F4 (March 1979)

L.R.O. Storey, J. Thiel, J.M. Illiano

CENTRE NATIONAL D'ETUDES DES TELECOMMUNICATIONS

CENTRE NATIONAL DE LA RECHERCHE SCIENTIFIQUE

CENTRE DE RECHERCHES EN PHYSIQUE DE L'ENVIRONNEMENT TERRESTRE ET PLANETAIRE

CRPE

NOTE TECHNIQUE
C.R.P.E. 94

PROJET PROCUPINE

THE MF MUTUAL - IMPEDANCE PROBE EXPERIMENT PART 2 :- FLIGHTS F3 and F4 (MARCH 1979)

by

L.R.O. STOREY . J. THIEL and J.M. ILLIANO

C.R.P.E. / R.P.E.
45045 ORLEANS CEDEX.

CENTRE NATIONAL D'ETUDES
DES TELECOMMUNICATIONS

CENTRE NATIONAL DE
LA RECHERCHE SCIENTIFIQUE

CENTRE DE RECHERCHES EN PHYSIQUE DE

L'ENVIRONNEMENT TERRESTRE ET PLANETAIRE

NOTE TECHNIQUE CRPE/94

PROJECT PORCUPINE

THE MF MUTUAL-IMPEDANCE PROBE EXPERIMENT

PART 2 : - FLIGHTS F3 and F4 (MARCH 1979)

By

L.R.O. STOREY, J. THIEL, and J.M. ILLIANO

C.R.P.E./R.P.E.

45045 ORLEANS CEDEX

Le 1er Novembre 1981

CONTENTS

PART 2 :- FLIGHTS F3 and F4 (MARCH 1979)

6. PREFACE

This is the second part of a report on the results from the medium-frequency (MF) mutual-impedance probe experiment that was supplied by the Centre for Research in Environmental Physics (CRPE, Orléans, France) as a contribution to the West-German Porcupine program of research on auroral physics during the International Magnetospheric Study.

The subject of Part 1 was the results from the first successful flight, named F2, which took place from ESRANGE (Kiruna, Sweden) on 20 March 1977. On that occasion, the MF probe experiment did not succeed in its objective of detecting field-aligned drift motion of the thermal electrons in the auroral ionosphere. The non-reciprocal shift of the lower oblique resonance (L.O.R.) frequency that this motion should have produced was masked by a similar but much larger shift that was obviously spurious, since it varied, more or less sinusoidally, as a function of the spin-phase angle. Various conceivable physical causes for this spurious shift were studied, but were rejected. The question of whether the true cause was some other physical phenomenon, as yet unidentified, or whether it was technological in nature, had to be left open. The results from the flight F2 nevertheless suggested a number of ways in which the experiment could be improved, and these were discussed in Section 5, which concluded Part 1 of the report.

In Part 2, after the present preface, Section 7 describes how these and other modifications were made to the MF probe, in preparation for the flights F3 and F4. The changes that were made to some of the other instruments on board are mentioned also.

The flight F3 took place on the evening of 19 March 1979, during a quiet interval within a period of repeated auroral activity. A weak negative magnetic bay of about 100 γ ($K_p = 2_-$) was in progress at the time of launch : see § 7.2. of the report by *Häusler et al.* [1982]. The aurora failed to evolve as anticipated, and the payload did not pass through any discrete arc. These relatively calm conditions, which disappointed the other experimenters, were ideal for determining whether

the various modifications had improved the MF probe. In Section 8, where the results of the F3 experiment are presented, emphasis is therefore laid on analysis of the technical performance of the probe.

The flight F4, on the evening of 31 March 1979, took place during a strong magnetic substorm ($K_p = 5_+$). At the time of launch, a discrete visual arc was present with a sharp northern edge, and the trajectory of the payload crossed this edge ; see § 7.3. of the report by *Häusler et al.* [1982] . Stronger electric fields were encountered on this flight than on F3, and much of our study of the experimental results in Section 9 has been devoted to clarifying certain effects that appear to have been caused by these fields, and which resemble the spurious effects already observed on F2 inasmuch as they depended on spin phase and masked the interesting effects that we were looking for.

The conclusions, presented in Section 10, are drawn from the results of all three successful flights. They substantiate the progress made in the development of the MF mutual-impedance probe as a means for measuring the field-aligned drift velocity of the thermal electrons, and indicate how, by further development, it might be made into a reliable instrument for this purpose.

7. INSTRUMENTAL MODIFICATIONS

7.1. MF SENSOR

In Section 5, a discussion of the results from the flight F2 led to several suggestions for improvements in the design of the MF sensor, which may be summarized as follows :

- that the double-monopole layout of the sensor units be adopted definitively, to the exclusion of the various quadripole layouts ;

- that the spin axis of the payload be aligned with the Earth's magnetic field, instead of being set at an angle of 30° to the field ;

- that one of the telescopic booms that support the two sensor units be made longer than the other, in order that the sensor axis (i.e. the line joining the centres of the two electrodes) may still be inclined at about 30° to the field.

Together, these modifications led to the design of double-monopole sensor illustrated in Figure 20 (see Part 1).

The particular dimensions shown in the figure were chosen so as to minimize the mechanical changes that would be required. Thus the spacing of the two booms along the payload axis, and also the length of one of them, were the same as on F2. The sole mechanical change was the lengthening of the other boom by 0.5 m.

On F2 there were four boom-mounted sensor units, and the decision was taken to have the same number on each of the F3 and F4 payloads, though this was not strictly necessary. The main reason for this choice was to insure against the risk of failure either of a boom or of a sensor unit, such as occurred on F2 and plagued the interpretation of the data. With four booms spaced uniformly along the payload axis, it is possible to compose a sensor of the type shown in Figure 20 in three possible ways, one for each pair of adjacent sensor units. The requirement that adjacent units be on booms of different lengths led finally to the design illustrated in Figure 21.

In comparison with the arrangement on F2, on the flights F3 and F4 the four booms were turned through 45° around the payload axis so as to increase the distances between the sensor units and the payload base, in the hope of reducing interference from the telemetry system.

Because of the higher degree of symmetry that this new system possesses, it should be unaffected by most of the possible causes of the spurious L.O.R. frequency-shifts that were observed on F2, and have been discussed in § 4.3. Specifically, it should be immune to the effects of the perturbation of the supra-thermal electron population by the payload body (§ 4.3.2.), to electromagnetic effects (§ 4.3.3.), and to certain technological defects (§4.3.4.). Only the perturbation of the thermal plasma may still produce spurious frequency-shifts.

Moreover, one merit of a sensor system of this type is that if ever the mode of origin of an observed L.O.R. frequency-shift is uncertain, it may be identifiable by comparison of the data from two adjacent pairs of units. The comparison concerns the dependence of the frequency-shift upon the spin-phase angle,and before discussing it, we must first define these two quantities unambiguously.

As regards the frequency-shift, the only point at issue is its sign. This was defined in § 4.2., and we now recall the definition : the shift Δf is counted as positive if the L.O.R frequency is higher when the direction of transmission is towards the base of the payload, than when it is towards the tip.

For the spin-phase angle, however, we must now adopt a definition different from the one used in Part 1. The old and the new definitions are compared in Figure 22. In the old definition, the origin of the spin-phase angle ϕ was taken as the projection of the magnetic-field vector $\mathbf{B}_o$ into the plane perpendicular to the payload spin axis (Fig. 22 a). The angle so defined will henceforth be called ϕ_b. It is not useful for the study of the data from the flights F3 and F4, during each of which the spin axis was almost parallel to $\mathbf{B}_o$, because in these circumstances a small change in the direction of this axis in space could lead to a large change in ϕ_b. Accordingly we now prefer to take the origin of the spin-phase angle to be the projection of the cross-field plasma drift velocity $\mathbf{V}_\perp$ into the plane perpendicular to the spin axis (Fig. 22 b), which is

the theoretical direction of the plasma wake of the payload. With this new definition, the spin-phase angle will be called ϕ_v.

By comparing the variations of Δf versus ϕ_v, measured on two adjacent pairs of sensor units, it may be possible to identify any of the following four causes of L.O.R. frequency-shifts :

(a) Field-aligned drift motion,
(b) Cross-field drift motion,
(c) Isotropic density perturbation,
(d) Anisotropic density perturbation.

How (a) and (b) give rise to frequency-shifts was explained in § 2.1. From our point of view, such shifts are genuine, while those caused by (c) or (d) are spurious. The shapes of the corresponding functions $\Delta f(\phi_v)$ are indicated in Fig. 23, and will now be commented on briefly.

a) Field aligned drift motion

Frequency-shifts due to field-aligned drift motion of the thermal electrons should be independent of spin phase, and should have the same sign on adjacent pairs of units.

b) Cross-field drift motion

In contrast, the frequency-shifts due to cross-field drift motion of the thermal plasma should vary sinusoidally as a function of spin phase, with an average value of zero, and should have opposite signs on adjacent pairs of units.

c) Isotropic density perturbation

The perturbation of the thermal plasma by the payload body was discussed in § 4.3.1. When the drift velocity of the plasma is zero, or when it is parallel to the axis of the payload, the perturbation is isotropic in the sense that it is independent of azimuth at a given radial distance from the axis. It can affect a sensor system of the type shown in Fig. 21, because the plasma is more severely perturbed near the sensor unit on the end of the short boom than it is near the unit on the end of the long boom. Accordingly the resultant frequency-shift should be independent of spin phase, but opposite in sign on adjacent pairs of units.

(d) Anisotropic density perturbation

When the drift velocity of the plasma relative to the payload body has a non-zero cross-field component , the plasma perturbation is anisotropic : the reduction of plasma density is greatest in the wake. In this case, therefore, the frequency-shift should vary with spin phase, though without changing sign, which distinguishes it from shifts due to (b). As with (c), the sign is opposite on adjacent pairs of units. At low cross-field drift velocities the variation might be more or less sinusoidal, though with non-zero mean value, but at large velocities, giving rise to a well-defined wake, it would be markedly non-sinusoidal as is shown in the figure.

Of course, paragraphs (c) and (d) presuppose a mechanism whereby changes in the density of the thermal plasma, greater near one of the sensor units of a pair than near the other, can give rise to non-reciprocal L.O.R. frequency-shifts. The possible nature of this mechanism will be considered in § 9.3.2.

The features illustrated in Fig. 23 allow any of the four causes of frequency-shifts to be identified, whenever it occurs on its own. This is not always possible, however. For instance, the effect (d) is inevitably accompanied by (b), which means that they are difficult to distinguish from one another. On the other hand, when the genuine effects (a) and (b) occur together in the absence of the spurious effects (c) and (d), it should be possible to distinguish between them, even in the data from a single pair of sensor units, by analyzing the functional dependence of the frequency-shift Δf on the spin-phase angle ϕ_v.

Fig. 24 shows the same data as Fig. 23, but graphed as polar plots of Δf versus ϕ_v. The thin circle is the origin of Δf : points inside and outside it correspond to negative and to positive values of Δf respectively. This type of graph will be used subsequently for presenting the experimental data from the new sensor system shown in Fig. 21.

In addition to these modifications of the mechanical layout of the sensor, some improvements were made to the miniature electronics that formed part of each of the four sensor units. In particular, the electrostatic screening of the circuits was improved so as to eliminate the breakthrough from the emission to the reception that spoilt the self-impedance

measurements on F2. Figure 25 presents the electronic circuit diagram of the sensor units used on F3 and F4.

7.2. ELECTRONICS

On the whole, the main electronics associated with the MF probe underwent very little change between the flight F2 in 1977 and the flights F3 and F4 in 1979.

One noteworthy change was a reduction of the gain of the receiver. On F2, the strongest resonances had saturated its high-level output. Moreover, the internal noise level had been about 15 dB above the bottom of the dynamic range of the low-level output. For these reasons, the gain was reduced by about 5 dB, so that the noise level on F3 and F4 was about 10 dB above the bottom of the total dynamic range. Thus, in comparison with F2, the useful part of this dynamic range was enlarged by 5 dB, and the risk of saturation diminished.

Most of the other significant changes were direct consequences of those made to the layout of the sensor, described in § 7.1. above. Thus the decision to use the four sensor units as a set of three double-monopole sensors led to a modification of the measurement cycle. The new cycle is shown in Figure 26. In the first half of it, devoted to the active measurements, the three double-monopole layouts were used sequentially ; the layout involving the central pair of sensor units was used twice, and the others once each.

During the second half-cycle, passive measurements were made using each of the four sensor units in turn as a monopole antenna, and also using various combinations of two units as dipole antennas. These new arrangements, particularly the use of single monopole antennas, were meant to help in identifying the sources of technological interference.

These minor changes in the cycle of MF measurements were brought about by modifying the logical circuits of the experiment programmer (Figure 7).

Equally minor changes had to be made in the arrangements for

the external calibrations (see § 3.4.). The calibration box containing discrete capacitances that was used on F2 (Figure 10) was replaced on F3 and F4 by a set of four coaxial cables yielding a distributed capacitance of the same order of magnitude (Figure 27). During the time when the sensor units were stowed in the payload, one end of each cable was connected to the electrode of one such unit. The opposite ends of the four cables were joined together. The combined capacitance of all four amounted to about 1100 pF.

Changes of greater importance were made to the HF probe system : in particular, the passive HF measurements were made in a new way, by on-board analogue calculation of the cross-spectrum of the signals received on the two dipole antennas of the HF sensor [*Pottelette and Illiano*, 1982] . This fact must be mentioned here because it had a certain incidence on the passive measurements at MF. The cross-spectrum was measured continuously throughout the second half-cycle, and therefore, during half of this period, these passive HF measurements overlapped those being made at MF (Figure 26). At such times a conflict arose between the MF and HF experiments, inasmuch as they were generating data at a total rate exceeding their joint allowance of telemetry, which was the same as it had been on F2. Fortunately the telemetry requirements of the new passive HF experiment were more modest than on F2, so it was feasible to satisfy them at the expense of the passive MF experiment. From time to time, at the interface between the CRPE instrument and the PCM telemetry system (Figure 7), a word of HF data was inserted into the stream of words of MF data, one of the latter then being lost. Since the passive MF data were used only for survey purposes, and were not analyzed quantitatively, this loss of a few of them was of no consequence.

7.3. OTHER INSTRUMENTS

Besides the two RF mutual-impedance probes, several of the other instruments aboard the Porcupine payload were modified between the flights F2 and F3.

The only modification that had a significant impact on the CRPE experiment concerned the Russian ejectable plasma source. On flight F2 a cesium plasma source was used, but it failed to function. On flights F3 and F4 it was replaced by a xenon plasma source, which functioned correctly

[*Haerendel and Sagdeev*, 1981 ; *Häusler et al.*, 1982] . When the source was in action, the xenon plasma beam perturbed the ionospheric plasma, and also caused waves to be generated. Effects of the beam were observed by both the MF and HF probes, in both their active and their passive modes, but these are not discussed in the present report. Neither do we discuss the effects of the barium ion jet, nor those of the emissions of freon from the attitude-control system. A brief account of some of these effects has been published elsewhere [*Thiel*, 1981].

8.1.2. Sensor system

The main phase of the flight was distinguished by correct deployment of all four booms of the MF sensor, together with correct operation of all four sensor units. These circumstances, together with the relatively calm state of the ionosphere, lent themselves to an appraisal of the performance of the MF mutual-impedance probe in its prime role as a device for measuring field-aligned electron drifts. The scientific data from the flight F3 will be viewed below in this perspective.

8.1.3. Passive mode

The passive measurements made during the flight F3 can be divided into two main groups : those made before any of the booms were deployed, and those made after all four booms were deployed. Some data also were obtained during the short period when booms 1-3 were deployed, while boom 4 was not yet deployed, but these will not be discussed.

Before boom deployment, the four electrodes of the sensor unit were joined together electrically, and were connected jointly to ground via the capacitance of the external calibration system (Fig. 27). For the layouts * R * * , R * * * , R * R * and * R * R, the noise level was about 22 dB above the bottom of the dynamic range of the low-level channel of the receiver, while for the layouts * * * R ,* * R *,* * RR and RR * * The corresponding figure was about 16 dB. The power spectra were more or less flat in all cases.

When all four booms were deployed, the observed noise spectra were as shown in Figure 29. At the highest frequencies, the noise level was much the same in all layouts, namely about 14 dB above the bottom of the low-level channel ; this figure is less than those observed before deployment, and is only about 4 dB larger than those measured in the laboratory, before the instrument was installed in the payload (see § 7.2.). However, the noise exceeded this level at lower frequencies, below about 1 MHz for the monopole layouts and below about 0.5 MHz for the dipole layouts (see Fig. 26). At these frequencies, the noise was stronger in the monopole than in the dipole layouts, as was expected.

8. PORCUPINE F3

8.1. TECHNICAL ASPECTS

The Aries rocket carrying the F3 payload was launched at 22 h 75 m 0 s UT on the evening of 19 March 1979. The geographic azimuth at launch was 352°, and the payload attained an altitude of 464.1 km at apogee.

8.1.1. Calibrations

The data collected before the launch and during the initial phase of the flight consisted entirely of calibrations. On this occasion all the calibrations, both internal and external, were performed correctly, apart from a few minor troubles.

In the internal calibrations, for instance, the measurements of the frequencies for the first ten steps of the frequency-sweep (see § 3.3.) were unsatisfactory throughout the flight, but this was of no consequence since all the frequencies concerned were below 100 kHz.

Some representative quick-look plots of the external calibration signals are given in Figure 28, for each of the four layouts of the sensor. The signal levels were about 10 dB below the top of the dynamic range of the high-level channel of the receiver. A certain amount of noise, broad-band but including several spectral lines, accompanied these signals. It was worse in some layouts than in others. In some layouts, moreover, the noise level depended distinctly on which of the two sensor units in service was emitting and which was receiving. This is understandable, because the two units were separated by nearly 1 m, so any localized source of technological noise within the payload was likely to affect them differently.

How the external calibration data were processed, in order to overcome the effects of the noise, will be explained in § 8.1.4., after the presentation in § 8.1.3. of the noise observed, in the absence of signals, in the passive mode of operation of the probe.

That it is not the case at lower frequencies is a consequence of the procedure that was followed in calculating the transfer impedance of the probe in the plasma, starting from the relevant telemetry data. For each measurement, the latter consisted of two numbers representing the amplitudes of the RF potentials measured by the detectors at the two outputs of the receiver (Fig. 5). First, making use of the internal calibration data, these two numbers were combined into a single one (V, say) which was proportional, by an unknown factor, to the RF potential at the input of the receiver. Then this number was inserted into the following expression for the modulus of the transfer impedance :

$$(8) \qquad | Z_t(f) | = \frac{V(f)}{V_c(f)} | Z_c(f) |$$

where $V_c(f)$ is the corresponding number obtained, with the same layout of the sensor and at the same frequency f, in the course of the external calibrations, and $Z_c(f)$ is the known transfer impedance of the external calibration network. More precisely, for a given sensor layout, the set of numbers representing the function $V_c(f)$ was obtained by averaging all the relevant external calibration curves and then smoothing the average curve, so as to minimize the effects of noise. Now our need for detailed analysis of the experimental transfer functions was limited to the frequency range 0.5 - 1.0 MHz, in which the L.O.R. was almost always located (see below). Moreover, it happened that in this range, and indeed at all frequencies above about 0.5 MHz, the calibration curves were approximately straight lines, as can be seen from Figure 28. Therefore, in order to simplify the numerical computations, we adopted for the function $V_c(f)$, over the entire frequency range 0.1 - 1.5 MHz, the straight line that fitted the average calibration curve best in the range 0.5 - 1.0 MHz. Hence the functions $| Z_t(f) |$, derived from the experimental data V(f) by the procedure outlined above, were slightly in error at frequencies below 0.5 MHz. This fact had no serious consequences, but it explains why, when the same procedure is applied to an individual calibration curve, as was done in preparing Figure 30, the resulting curve is not constant below about 0.5 MHz.

When applied to the active mode measurements made with the sensor units immersed in the plasma, the above procedure, which referred all transfer impedances to the standard constituted by the capacitance

The excess noise observed in flight, compared with that measured in the laboratory, is almost certainly caused by technological interference from other items of equipment on board. In particular, we consider that the rise in the noise levels at the lower frequencies is probably due to interference from the telemetry transmitter. A comparison of the levels observed in all the different layouts is consistent with this view. For instance, the data from the dipole layouts clearly suggest that the noise was coming from the base of the payload. In the monopole layouts, however, the substantially higher levels were much the same in all four cases, but this can be understood by supposing that the extra noise was due to fluctuations in the potential of the payload. Throughout the flight all these noise levels remained fairly steady, except for events linked with the ejections of xenon plasma, of barium ions, and of freon.

As regards its spectral composition, the noise was wide-band apart from a few weak but well-defined lines, for example at 240 kHz, 395 kHz and 915 kHz. Their amplitudes were near the bottom of the lower half of the dynamic range of the receiver, so they did not interfere significantly with the active measurements.

8.1.4. Active mode

For the purpose of discussion, the data got in the active mode will be divided into the same two groups as in § 8.1.3.

Before boom deployment, the active-mode data consisted of external calibrations, as already noted in § 8.1.1. Some qualitative plots of them appeared in Figure 28. One other example is graphed quantitatively in Figure 30. The abscissa is the frequency, while the ordinate is the measured transfer impedance of the calibration circuit (Fig. 27), divided by the theoretical transfer impedance, in a vacuum, of the double-monopole sensor illustrated in Figure 20 ; we recall that the MF probe experiment used, successively, three independent sensors of this type (Fig. 21).

Since both of these transfer impedances are capacitive, their ratio should be constant, independent of frequency. In Figure 30, we see that at all frequencies above about 0.5 MHz this is indeed the case, apart from random fluctuations and some spikes due to narrow-band interference.

disagreements with the theory, mainly concerning the amplitude and similar to those already noticed in the data from the flight F2 (see § 4.1.4.), were also observed on F3.

Figure 33 shows the L.O.R. frequency-shifts, normalized with respect to the local electron cyclotron frequency (i.e. the gyrofrequency), graphed as functions of the time after launch. The four parts of the figure refer to the four double-monopole layouts that were used for the active measurements (Figure 26). The labels A - D correspond to the order of appearance of these various layouts in the measurement cycle, as follows :

Label	Sensor units	Layout
A	1 and 2	ER * */RE * *
B	2 and 3	*ER */ * RE *
C	3 and 4	** ER/ * * RE
D	2 and 3	* ER*/ * RE *

Thus the data shown in parts A and C of the figure represent truly independent measurements, made at different instants of time with different layouts ; they are independent of one another, and also of the data shown in parts B and D. But the latter are only partially independent of one another, having been made with the same layout, though again at different instants.

One most interesting result is immediately apparent from the figure : in spite of the scatter of the measurements, all four sets of data agree in showing a positive frequency-shift, particularly in the middle of the flight. This feature was noted in § 7.1. as being the characteristic signature of field-aligned drift (see Figure 22). If all the data are lumped together and are averaged over the entire flight, the mean frequency-shift is $\Delta f = 7$ kHz ; its value normalized with respect to the electron cyclotron frequency f_c is $\Delta F = \Delta f / f_c \simeq 0.0054$. For the given design of the probe, under the conditions of the flight F3 ($\beta \simeq 32.5°$, $f_p \simeq 5$ MHz, $T_e \simeq 1500$ K), the relation between the field-aligned drift velocity $V_{//}$ of the thermal electrons and the resulting frequency-shift

of the calibration network, yielded the function $|Z_t(f)|$ without our having to know either the emitted RF current or the gain of the receiver, or how these quantities varied with the frequency.

On the F3 flight, all four booms carrying the MF sensor units were deployed without accidents. Thereafter, in all of the four double-monopole layouts, the probe functioned correctly and resonances of good quality were observed ; two examples are given in Figure 31.

At the peaks of the resonances, the signal levels were situated lower down in the dynamic range of the receiver than they had been on F2 : on F3, they were near the bottom of the upper half of this range, i.e. the half covered by the high-level output (see § 3.2.). One reason for this was the reduction in the gain of the receiver, mentioned in § 7.2. Additionally, however, the actual transfer impedances at resonance were less on F3, because, during most of the flight, the ambient electron density was higher : typically, the plasma frequency was around 5 MHz, compared with 2.5 MHz on F2. Only near the end of the flight, when less dense plasma was encountered, did the peak signal levels rise systematically towards the middle of the dynamic range of the high-level output, though transient density reductions and signal enhancements accompanied the earlier ejections of freon and of barium ; see Figs. 85 - 88 on pages 181 - 183 of the thesis by *Thiel* [1981].

The situation of the peak signal levels, saturating the low-level (LL) output but not rising far above the bottom of the dynamic range of the high-level (HL) output, was unfortunate in that it gave rise to additional noise. When digitized in the telemetry interface, such signals were coded into relatively small binary numbers. A signal that, in the LL channel, yielded the number 255 corresponding to the full-scale output, yielded a number of about 10 at the output from the HL channel. Consequently signals at slightly higher levels, which saturated the LL channel but lay near the bottom of the dynamic range of the HL channel, were subject to quantization errors of up to $\pm$ 5 %. Thus the quantization noise was more severe than it would have been for signals in the middle or at the top of the HL dynamic range.

is approximately

$$\Delta F \simeq 0.4 \quad V_{//} / V_{th} \tag{9}$$

where V_{th} is the electron thermal velocity ; here, of course, $V_{//}$ is expressed in coordinates that are fixed with respect to the payload. With $V_{th} \simeq 200$ km/s, corresponding to the assumed value of T_e, the parallel drift velocity is found to be about 3 km/s downwards, which, for a typical plasma frequency of 5 MHz, corresponds to an upward current density of about 1.3×10^{-4} A/m^2.

This figure is so large that it must be regarded with scepticism, particularly since the aurora was not very active during the F3 flight (see Section 6). However, it is not impossibly large, and in view of the interest that there would be in a direct measurement of field-aligned drift velocity, the data appear to be worth analyzing in greater detail.

To begin with, we shall look for evidence as to how the L.O.R. frequency-shift, and hence the apparent parallel drift velocity, varied during the flight. For this purpose, although the measurements are scattered and to lump them all together would reduce statistical errors, it seems better to keep the data from the layouts A - D separate in the first instance. Then they can be compared in order to see how well they agree with one another, and to detect any systematic errors.

Accordingly the four sets of data have been analyzed separately. The analysis consisted of smoothing each of them by means of a polynomial :

$$\Delta f(t) = a_o + a_1 t + a_2 t^2 + \ldots\ldots \tag{10}$$

The coefficients a_o, a_1, etc... were adjusted so as to minimize the variance of the data with respect to the smooth curve. Polynomials of different orders were tried, from 1 up to 8. The complete set of the results of this analysis are shown in Fig. 34, separately for the four sensor layouts, while in Fig. 35a the four results obtained with the polynomial of order 8 have been superposed.

In order to determine the frequencies of the resonance peaks, and also their amplitudes, as accurately as possible in spite of the noise, the measured transfer functions were analyzed in a sophisticated way. After normalization with respect to the theoretical transfer function for the probe in a vacuum, as explained above in connection with Figure 30, each experimental curve was smoothed by fitting a high-order polynomial to it in the neighbourhood of the peak. Since, for the given design of the probe (Fig. 20), the L.O.R. frequency was nominally around 750 kHz, the curve-fitting was performed routinely over the range 0.3 - 1.2 MHz ; this corresponded to about 150 consecutive measurements, that is, to about 75 for each of the two directions of propagation (see § 3.2.). Exceptionally, for instance when the probe was perturbed by the freon emissions, other frequency ranges were used. Figure 32 illustrates the process of curve-fitting. It concerns a case where the raw data were of decent quality : later, an example will be given of a case with a much poorer signal-to-noise ratio (Fig. 47). The coefficients of the best-fitting polynomial were found by an iterative process, using a weighted-least-squares error criterion which assigned low weights to any measurements that lay far from the smooth polynomial curve. For any one frequency-sweep, two such curves were fitted to the data, one for each of the two directions of propagation. Then the maximum of each curve was located, and the corresponding values of the frequency and of the normalized transfer impedance were noted. These items of information were the main input to the scientific study of the experimental data.

8.2. SCIENTIFIC RESULTS

8.2.1. Frequency-shifts

As before, this study will be concerned mainly with the non-reciprocal frequency-shifts of the L.O.R., i.e. the difference in the resonance frequencies for the two directions of propagation. Other aspects of the resonance, such as the average frequency for the two directions and also the average amplitude, have been discussed on pages 182 - 184 of the degree thesis of *Thiel* [1981] ; moreover, the relationship between the amplitude and the electron density is the subject of a forthcoming paper [*Thiel et al.*, 1983] . Suffice it here to say that certain

These velocities and current densities are too large to be credible, in view of the relatively calm ionospheric conditions that prevailed during the F3 flight. Moreover, had they been real, the resultant perturbation of the Earth's magnetic field would have been detectable by the triaxial magnetometer in the payload, but no such perturbations were observed [B. Theile, Private communication, 1980] . Therefore they must be branded as spurious, in spite of the apparent agreement between three independent sets of measurements.

In § 8.3. we shall continue the discussion of these spurious field-aligned drift velocities, but first we shall try to answer the question, previously left in suspense, as to why one of the four sets of measurements disagrees with the other three.

8.2.2. Spin-dependence

In Figures 33 - 35, which present graphs of the L.O.R. frequency-shift Δf versus time of flight for the four layouts of the probe, there is disagreement between the results from the layout D and those from the layouts A - C. It is most noticeable towards the end of the flight, where Δf is large and positive for the layout D, but is relatively small, and in one case negative, for the other three layouts. This disagreement is all the more surprising when we recall that the layout D is nominally the same as B.

In seeking ways in which these two layouts could differ in practice, we have been able to identify only two possibilities : the sensor in the layout D was perturbed either by some other instrument on board, or by some effect related to the spin of the payload. That another instrument might perturb the sensor in the layout D, but not in the layout A - C, is possible because all the scientific and technological instruments on board were synchronized from the same central programmer. No such perturbation appeared during the pre-flight testing, however. None the less, it might have occurred during the flight in the presence of the ionospheric plasma, but this possibility is not now verifiable. Accordingly we have concentrated on the second possibility, namely that of a perturbation related to the spin-phase angle ϕ_v (see Fig. 22).

A comparison of the data from the layouts A, B and C reveals general agreement, though with some exceptions, at most orders of the polynomial (Fig. 34). According to the highest-order curves (Fig. 35a), the frequency-shift Δf is small at the start of the data set, rises to a maximum at about one third of the way through the set, returns to small values at about two thirds, and then remains small until the end of the set. The agreement between the data from the layouts A - C suggests that these temporal variations are genuine.

Unfortunately this agreement is spoilt by the results from the layout D. In the first half of the data set, the variation of Δf is similar to that found from the other three sets, but in the second half Δf rises progressively. This discrepancy calls for detailed discussion, which we shall, however, postpone until § 8.2.2.

Meanwhile, we shall analyze the data in terms of an apparent parallel drift velocity, and we begin by averaging the results presented in Fig. 35 a. Clearly the outcome depends on whether or not the discrepant results from the layout D are included. In Fig. 35 b, the broken curve shows the average of the results from the layouts A, B and C only, while the solid line shows the average of the results from all the layouts, D included. The analysis will be based on the solid curve, which embodies all of the available data.

The lower part of Fig. 36 shows the temporal variations of the apparent parallel (i.e. field-aligned) drift velocity $V_{//}$. This velocity is expressed in a frame of reference fixed with respect to the Earth, and has been calculated taking the parallel component of the payload orbital velocity into account. No curve is traced for flight times before 160 s, at which the payload becomes stabilized with its axis parallel to $\mathbf{B}_o$ (see Appendix 1). At this time $V_{//}$ is relatively small ($\simeq$ 1.1 km/s) and negative. Throughout the rest of the flight it becomes progressively more negative, though there is a momentary reversal of this trend after apogee. At the end of the measurements it is large (4 - 5 km/s) and negative : it would be small, however, if the data from the layout D were not included (see Fig. 35). The upper part of Fig. 36 shows the corresponding variations of the upward field-aligned current density.

for further evidence of a dependence of the frequency-shifts on spin phase.

Consequently we extended this search to the first half of the flight, when the ϕ_v were varying rapidly. First, the available data were divided into two main sets, one comprising all the data from layouts A and C, and the other all the data from layouts B and D. Then the data in each of these sets were subdivided into four groups, corresponding to the time intervals 170 - 240 s, 240 - 310 s, 310 - 380 s and 380 - 660 s after launch ; it was at about 380 s that the spin-rate changed (see Fig. 37). Finally, in each group, the normalized frequency-shifts ΔF were graphed against the corresponding values of ϕ_v, and an offset sinusoid of the form

$$(12) \qquad \Delta F = \Delta F_o + \Delta F_1 \cos (\phi_v - \phi_1)$$

was fitted to the data, by adjusting the parameters ΔF_o, ΔF_1, and ϕ_1 so as to minimize the least-square error. Fig. 39 shows the outcome of this analysis ; the dots are the individual measurements, while the broken lines are the best-fitting offset sinusoids.

During the time interval 170 - 240 s, the data contain significant sinusoidal components. These are approximately in antiphase for the two main data sets, which is consistent with their having been caused by cross-field plasma drift (see Fig. 24). On the other hand, the amplitudes of these sinusoids are much larger than the values that a simple theory of the influence of cross-field drift would lead us to expect. The observed amplitudes are $\Delta F_1 \simeq 8.64 \times 10^{-3}$ for layouts A + C, and $\Delta F_1 \simeq 2.21 \times 10^{-3}$ for layouts B + D. A crude theory of the influence of cross-field drift [*Michel et al.*, 1975] yields

$$(13) \qquad \Delta F_1 \simeq 0.2 \; V_\perp \; / \; V_{th}$$

which leads to $| \mathbf{V}_\perp |$ = 8.8 km/s and 3.7 km/s respectively. Of course, these values are much too large (see Fig. 38). Moreover, the phases ϕ of the sinusoids are too far away from their respective theoretical values of 180° and 0° : they are closer to 270° and 90°. The observed amplitudes and phases do, however, agree with the suggestion that whatever may have

In Fig. 37, the values of ϕ_v at the instants when the active MF measurements were made have been plotted against time during the flight F3, for the four layouts of the sensor. The companion Figure 38 shows the magnitude of the cross-field plasma drift velocity $\mathbf{V}_\perp$. Both the direction and the magnitude of this velocity were calculated from the expression

$$\mathbf{V}_\perp = \frac{\mathbf{E} \times \mathbf{B}_o}{B_o^2} - \mathbf{U}_\perp \qquad (11)$$

where $\mathbf{U}_\perp$ is the cross-field component of the payload orbital velocity, obtained from the trajectory data, while $\mathbf{E}$ is the ambient electric field, the data on which were supplied by R. Grabowski [Private communication, 1980] ; we smoothed them before using them to calculate $\mathbf{V}_\perp$. They are consistent with optical observations of the drift of the barium ion cloud, and the accuracy of the inferred direction of $\mathbf{V}_\perp$ has been confirmed by comparison with that of the plasma wake, as observed by the electrostatic probe (Experiment 2 in Table 1) ; the two directions agree within 15° [O.H Bauer, Private communication, 1981] .

It is evident from Figure 37 that the temporal variation of ϕ_v for a given layout was markedly different during the first and second halves of the flight. The reason for this was a change in the spin rate near apogee, resulting from an attitude-control manoeuvre. On the upleg, ϕ_v varied rapidly and covered the full range of values 0 - 360° several times. But on the downleg, the spin period was approximately an integer sub-multiple of the duration of the measurement cycle, and as a result of this near-synchronism ϕ_v varied relatively slowly, over a total range of about 90°. For the four layouts, the ranges of variation were roughly as follows : (A) 135° - 55° ; (B) 270° - 180° ; (C) 45° - 325° ; (D) 180° - 90°. The immediate comment that these figures provoke is there is no reason to expect that the range covered by the layout D should be the site of a spin-dependent perturbation, which seems more likely to be found in the wake, around $\phi_v = 0°$. Moreover part of this range is also covered, without any apparent perturbation, by the layout A, though earlier and hence at lower values of $|\mathbf{V}_\perp|$; see Figure 38. Nevertheless, the coincidence between the interval of time when the data from the layout D disagree with those from the layouts A - C, and the interval when the ϕ_v are varying relatively slowly, is an encouragement to search

sign convention that $\Delta|Z_t|$ is positive if $|Z_t|$ is higher when the direction of propagation is towards the base of the payload. Theoretically, under the sole influence of field-aligned drift, the sign of $\Delta|Z_t|$ should be opposite to that of Δf ; this may be seen from Fig. 1c, in which the transfer function with the higher resonance frequency has the lower peak amplitude. In the course of the analysis of the measured transfer functions to determine Δf, by the method outlined at the end of § 8.1.4., the corresponding values of $\Delta|Z_t|$ were obtained as a by-product. They have been normalized with respect to $|Z_r|$, the average of the resonant values of $|Z_t|$ for the two directions of propagation, and the ratios $\Delta\ |Z_t|\ /\ |Z_r|$ have been graphed against time of flight in Figure 40 ; as in Figure 33, the four graphs correspond to the four sensor layouts A - D.

The most obvious features common to all four graphs are the facts that the data points are scattered fairly randomly on either side of zero during most of the flight, but that towards the end of the flight the scatter is much reduced, and systematic trends appear that are different for the four layouts ; these findings are similar to those for Δf.

Fig. 41 shows what happens when the data for $\Delta|Z_t|$ are grouped, analyzed, and displayed in the same way as was done for Δf in Fig. 39. In fact, rather similar results emerge. During the first time interval, 170 - 240 s, the data contain significant sinusoidal components, which are roughly in antiphase for the layouts A + C and B + D. During the second and third intervals, the data are less spin-dependent in most cases, while during the fourth interval they are too scattered to reveal any significant trends.

At the very end of the flight, $\Delta|Z_t|$ is slightly negative for the layout A and strongly so for B, while it is slightly positive for C and strongly so for D. As in the case of Δf (see Fig. 33), the contrast between the results for the two nominally identical layouts B and D is particularly striking. Fig. 42 presents, for each of these two layouts, a set of five transfer functions measured during the period 650 - 660 s, which demonstrate the intensification of the non-reciprocity at this time.

It is of interest that, during most of the flight, the spin-independent component of $\Delta|Z_t|$ is negative, which is the sign opposite to that of ΔF_o and is consistent with the effect of field-aligned drift.

caused these spin-dependent frequency-shifts during the interval 170 - 240 s after launch, also caused the anomalous behaviour observed in the layout D towards the end of the flight.

During the intervals 240 - 310 s and 310 - 380 s, the amplitudes ΔF_1 of the sinusoidal component are relatively small, and it may be significant that $|\mathbf{V_1}|$ is less at these times than during the interval 170 - 240 s (see Fig. 38).

During the interval 380 - 660 s, due to the stroboscopic effect previously mentioned, the sampling in ϕ_v is insufficient to allow a significant fit of an offset sinusoid to the data. The anomalous behavior observed in the layout D around the end of the flight occurs with $\phi_v \simeq 90°$, which suggests that the cause, whatever it may be, is the same as that of the less striking effects observed during the interval 170 - 240 s.

On the whole, the situation is reminiscent of that encountered on the flight F2, involving spin-dependent frequency-shifts of unknown origin. Fortunately, on the flight F3 such frequency-shifts were much smaller, but their origin is no less obscure.

As a possible step towards identifying the origin of these spurious frequency-shifts, we shall now examine the accompanying shifts in the amplitude of the lower oblique resonance.

8.2.3. Amplitude-shifts

The non-reciprocal L.O.R. frequency-shifts Δf that are illustrated in Figure 33, and which have been discussed in § 8.2.1. and § 8.2.2., were accompanied by non-reciprocal shifts $\Delta|Z_t|$ in the amplitude of the resonance, i.e. in the maximum value of the modulus of the transfer function $Z_t(f)$. Such amplitude-shifts had been predicted theoretically by *Storey and Thiel*, [1978], but those observed on the flight F3 generally did not behave in accordance with the theory ; for example, compare Fig. 9 of *Storey and Thiel*, [1978] with Fig 31 b of the present report. As in the definition of Δf (see § 4.2.2.), we have adopted the

However, although the measurements in the layouts A - C agreed quite well with one another, the implied values of $V_{//}$ are not acceptable because they are too large. Thus the question arises of what was really being measured in this experiment, i.e. to what common influence the probe was responding in these three independent layouts. A related question is why discrepant results were obtained in the fourth layout D, which was nominally the same as B. For the moment, in the sole light of the data from the F3 experiment, these questions remain unanswered.

In this connection, it should be noted that although the ionospheric conditions were fairly calm during the F3 experiment, they were not entirely so. For instance, the retarding-potential analyzer in the main payload measured a rather high and constant precipitated supra-thermal electron flux of about 10^{10} m^{-2} s^{-1} sr^{-1} eV^{-1} within the lower hemisphere throughout the flight (Fig. 44). However, while it is conceivable that supra-thermal electrons could have a direct influence on the probe, there is not, as yet, any theoretical or experimental evidence to suggest that they could give rise to L.O.R. frequency-shifts of the observed magnitudes.

Summarizing, in its present state the MF mutual-impedance probe is not yet a sufficiently precise instrument to be useful geophysically for the measurement of field-aligned electron drift velocity. Its performance is spoilt by errors of two types : random and systematic. In order for it to become useful in the future, both these types of error must be reduced by at least a factor of ten.

8.3.2. Reduction of random errors

The prospects for reducing the random errors are quite encouraging. Such errors are due to the inadequate signal-to-noise (S/N) ratio, which is very noticeable in Figures 30 and 31 for instance. The S/N ratio can be increased by increasing the signal level and/or reducing the noise level.

The simplest way of increasing the signal level is to increase the emitted RF current. This possibility is limited by the onset of nonlinearity in the transfer function of the probe. However, the experimental

Fig. 43, which combines data from Figures 39 and 41, is a regression diagram of $\Delta|Z_t| / |Z_r|$ versus ΔF_o. The six points correspond to the layouts A + C and B + D, and to the first three time intervals which have been labelled from (1) to (3) in sequence. The regression line is shown dashed, while the solid line is theoretically, the slope of the regression line should be - 0.91, but the experimental value is - 2. : the amplitude-shifts, though of the right sign, are greater than would be expected from the observed frequency-shifts. Since the latter have already been stigmatized as unreasonably large, the same verdict must be pronounced on the amplitude-shifts.

8.3. DISCUSSION

In this Section 8, the data from the flight F3 have been examined mainly in order to assess the performance of the MF mutual-impedance probe as an instrument for measuring the field-aligned electron drift velocity $V_{//}$, and now it is appropriate to summarize and discuss the findings.

8.3.1. Summary of probe performance

When the values of $V_{//}$ deduced from the smoothed data in the lowermost row of Figure 34 are compared, in Fig. 35 a, for the three independent sensor layouts A - C, they are found to agree with one another to within $\pm$ 1 km/s throughout the flight. In this very restricted sense, the probe achieved the anticipated measurement accuracy of 2 km/s that was announced before the rocket experiments started [*Simon,* 1975].

Of course, the dispersion of the individual measurements around the smooth curve exceeds this value. If the data from these three layouts are combined, the standard deviation of the individual measurements with respect to the average smooth curve (i.e. the broken line in Fig. 35 b) amounts to 0.8 % in terms of the quantity $\Delta f/f$; in terms of $V_{//}$, it is about 4 km/s.

of the potential of the payload body with respect to the plasma. By using sensor layouts in which the receiving antenna is a dipole, this type of noise could be reduced.

It should also be possible to reduce the internal noise of the receiver to some extent. In the circuit of the sensor unit, a resistor of about 120 kΩ was placed between the spherical electrode and the gate of the field-effect transistor in the first stage of the preamplifier (see Fig. 25). Its purpose was to prevent the preamplifier from oscillating when the electrode was immersed in the plasma, but it did so at the price of increased noise. Perhaps a careful study of the electrical behaviour of the sensor unit in the plasma would reveal that this resistance could be reduced without risk of instability, or even eliminated if the preamplifier were redesigned. Moreover, a redesign study would be likely to reveal other ways of reducing the noise, since there is no reason to believe that the receiver used in the F3 experiment attained, in this respect, the limits of present-day technology.

8.3.3. Evidence of systematic errors

When the random errors in the frequency-shift data are reduced by smoothing (Fig. 34), the smoothed curves for the layouts A, B, and C agree quite well with one another during most of the flight (Fig. 35 a), from about 150 s to about 550 s after the launch. However, they exhibit systematic differences outside this interval, i.e. at the beginning and in the second half of the flight.

The anomalies at the beginning of the flight are of technological origin. Until about 160 s after the launch, the payload axis was not properly aligned with the Earth's magnetic field, so the angle β varied as the payload spun. Indeed, it was only through an oversight on our part that the data from these times were included in the analysis.

At subsequent times, the data perturbed by the ejections of freon, of xenon, and of barium were, of course, excluded (see Appendices 1 and 2). Nevertheless, between the smoothed curve for the layout D and

results of *Gonfalone* [1974] and of *Michel et al.* [1975] suggest that the current could be raised significantly above the value used in the Porcupine programme, without non-linearity becoming a serious problem.

Another way in which the signal level could effectively be increased is by reducing the extent of the frequency-sweep, so as just to cover a relatively narrow range of frequencies centred on the L.O.R. peak in the transfer function, for instance the range between the 3 dB points on either side of this peak. Such a change would be equivalent to an increase in signal level, because the important quantity is not the peak amplitude of the signal, but rather the average signal power per unit bandwidth in this range, from which come almost all the data that are useful for estimating the L.O.R. frequency.

In the circumstances of the F3 experiment, an increase in the signal level would, in itself, have reduced the noise level, since an appreciable part of the noise was due to quantization (see § 8.1.4.). In point of fact, the signal level did rise towards the end of the flight, when the payload moved into a region of less dense plasma. The resulting reduction in the scatter of the measurements at this time is evident in Figures 33 and 40. In any future experiment, quantization noise could be made negligible by technological artifices such as the provision of automatic gain control in the receiver.

Some of the noise picked up by the sensors is due to interference from the telemetry system (see § 8.1.3.). This should be corrigible, for instance by using the highest possible carrier frequency, and by siting the telemetry antennas as far away from the sensors as is possible.

In the sensor layouts used on the flight F3, the receiving antenna was always a monopole. From the passive-mode data presented in Fig. 29, it appears that the monopoles were noisier than the dipoles. This could perhaps be due to the interference mentioned above being closely correlated on the four sensor units, but this is unlikely because of their different distances from the telemetry antenna. More plausibly, the explanation is that much of this noise corresponds to fluctuations

those for the other three layouts, there is a large systematic difference which begins at about 400 s (Fig. 35 a). Then, from about 550 s onwards, the curves for the layouts A,B, and C disagree with each other, though to a lesser extent. It may be significant that, at these later times, the perpendicular component of the plasma drift velocity was higher (Fig. 38) and the ambient electron density lower (Fig. 42) than they were during the middle part of the flight.

These anomalies correspond, partly at least, to spurious frequency-shifts of unknown origin which depend on the spin-phase angle ϕ_v. They represent systematic errors which must be reduced considerably if the MF probe is ever to become a practical instrument for measuring field-aligned drift velocity. The discussion of how this might be done will be postponed, however, until consideration has been given to the similar but rather larger differences that were observed on the flight F4.

9.1.2. Sensor system

At the instant when the MF booms were deployed, 86 s after the launch, the sensor nearest to the tip of the payload (n° 1 in Fig. 21) suddenly ceased to function, both in emission and in reception. Hence no scientific data were got in the layout A, but fortunately the sensor system functioned correctly in the other three layouts (see § 8.2.1. for their definitions).

9.1.3. Passive mode

The passive observations of noise on the flight F4 were quite like those made on F3, apart from some clear differences due to the lack of observations below 240 kHz and to the failure of sensor unit n° 1. Technological noise caused by other devices in the payload, and physical noise accompanying the ejections of xenon plasma, of barium ions, and of freon, were observed as before.

9.1.4. Active mode

Similar remarks apply to the technological aspects of the active-mode observations on F4. The peaks of the resonances were mostly in the upper half of the dynamic range of the receiver, and were slightly higher than on F3, so there was less quantization noise. The signal levels were higher because the ambient plasma was less dense. On the other hand, narrow-band technological noise of the type described at the end of § 8.1.3. was more serious, causing significant interference. An example is given in Fig. 47, which also shows to what extent the deleterious effects of the interference can be countered by smoothing the transfer functions in the way explained in § 8.1.4.

9. PORCUPINE F4

9.1. TECHNICAL ASPECTS

The launch of the Aries with the F4 payload took place at 22 h 29 m 0 s UT on 31 March 1979. The launch azimuth was 346°, and the apogee altitude 451 km.

9.1.1. Calibrations

As on the previous flight, both the internal and external calibration systems behaved quite satisfactorily.

In the internal calibrations, good measurements were made of the frequencies for all the steps of the sweep. However, it was found that for the first 30 or so steps, the measured frequencies stayed more or less the same, at about 240 kHz, instead of increasing progressively as they should have done. Again, this was harmless because all the frequencies concerned were well below that of the L.O.R. A more serious trouble was that at about 500 s after the launch, the measured frequencies started to drift. This instability first appeared at the lowermost frequency-steps, then spread rapidly upwards. It was caused by a drop in the output from the converter that supplied the power for the CRPE experiment, and its effect was that, from this time onwards, the frequency scales of the measured transfer functions became progressively less accurate.

The external calibration data were better in some respects, and worse in others, than on the previous flight, as may be seen by comparing Fig. 46 with Fig. 30. Within the limits of error, the measured calibration curves were perfectly straight over the full frequency range covered by the instrument, which facilitated their analysis by the procedure outlined in § 8.1.4. ; the graphs of Fig. 46 are the products of such an analysis. On the other hand, interference of technological origin was stronger : it affected not only the external calibrations but also the physical measurements, both in the passive and in the active mode.

On the other hand, it seems likely that the differences observed, during the second half of this flight, between the data acquired in the three different sensor layouts, are due to a perturbation that is somehow related to the spin-phase angle ϕ_v. This interpretation is supported by the fact that the ambient electric field, and hence the cross-field plasma drift velocity, are greater during the second half of the flight. Thus, for F4 even more than for F3, there is an interest in studying the spin-dependence of the L.O.R. frequency-shifts.

9.2.2. Spin-dependence

Fig. 49, which is like Fig. 37, displays the values of the spin-phase angle ϕ_v at the instants when the L.O.R. measurements were made. From about 160 s onwards, a stroboscopic effect is apparent, just as there was during the second half of the flight F3. The spin period of the payload was almost exactly equal to the interval between a measurement in the layout B and one in the layout D. The consequences were, firstly, that the values of ϕ_v at which the measurements were made in these two layouts varied only slightly from one spin period to the next, and secondly, at any given time they differed by about 90° from the values at which measurements were being made in the layout C. Between about 360 and 370 s, the attitude control system was operated and the spin period changed. From then on, there was still a stroboscopic effect , but it was such that measurements were made in the layouts B, C, and D at spin-phase angles differing by 90°. These facts account for several features of the data of Fig. 8, namely the quasi-sinusoidal oscillations of Δf noted during the second half of the flight, and the phase relationships between these oscillations for the different sensor layouts.

Using the data shown in Fig. 48, the dependence of Δf on ϕ_v during the flight F4 has been studied in the same way as for F3 (see § 8.2.2.). First, these data were divided into two sets, one comprising the data from the layout C and the other the data from the layouts B and D combined. Then the data in each set were subdivided into four groups, corresponding to four different time intervals. Finally, a curve of the form (12) was fitted, by least squares, to the graph of Δf versus ϕ_v for each group.

9.2. SCIENTIFIC RESULTS

9.2.1. Frequency-shifts

Figure 48 shows the L.O.R. frequency-shifts measured on the flight F4, normalized with respect to f_c and graphed versus time after launch. It is similar to Fig. 33 for F3, except that it contains no data from the layout A.

Comparing the two figures, it appears that, for a given layout, the scatter of the measurements was slightly less on F4 than on F3. This is a consequence of the higher signal-to-noise ratio on F4.

When, in Fig. 48, the data from the three different layouts are compared, they are seen to agree fairly well with one another during the first half of the flight, when they all exhibit quite small frequency-shifts. This is the case up to about 330 s after launch, from which time onwards, however, relatively large shifts are observed. These vary in an oscillatory fashion as time goes on, and the variations are plainly not the same on the different layouts.

This behaviour must be viewed in the context of the magnetically disturbed geophysical situation that existed during the F4 flight, as described by *Häusler et al.* [1982] in their § 7.3. Shortly after launch the rocket entered an active auroral region, where it remained during the first half of the flight. At about 330 s it emerged from this region, and the ambient electric field measured by the double-probe experiment immediately became more intense [R. Grabowski, Private communication, 1980] . This state of affairs persisted during the second half of the flight, though the electric field decreased again from about 440 s onwards.

In the light of the results from F3, it appears unprofitable to analyze even the data from the first half of the flight F4 in terms of field-aligned drift velocity of the thermal electrons. Indeed, during this period and most of the second half as well, the spin-independent part of Δf had the opposite sign on the layout C in comparison with the layouts B and D (see Fig. 47 and § 9.2.2. below), which disagrees with the theoretically-predicted effects of field-aligned drift (see Figs. 23 and 24).

It is reasonable to conclude that the observed spin-dependent frequency-shifts are caused by cross-field plasma drift, but the mechanism is not the simple direct one explained in § 2.1. Confirmation is forthcoming from the fact, visible in § 2.1., that the phase of the sinusoidal component of $\Delta F(\phi_v)$ does not have the values 0° or 180° that the simple theory predicts. This is the same conclusion as was reached in § 8.2.2., on the basis of the less striking data from F3.

9.2.3. Amplitude-shifts

For the sake of completeness, data from the flight F4 concerning the non-reciprocal amplitude-shift $\Delta|Z_t|$ are presented in Fig. 53, in the same way as they were for F3 in Fig. 41.

In the case of F4, the spin-independent part of $\Delta|Z_t|$ is opposite in sign for the layout C and for the layouts B + D. Moreover, comparison with Fig. 53 shows that, for any one of these layouts, its sign is the same as that of the spin-independent part of Δf. These findings conflict with those for F3.

The spin-dependent part of $\Delta|Z_t|$ increases in amplitude from the second to the fourth time interval, while $V_\perp$ is decreasing, which is curious.

9.3. DISCUSSION

9.3.1. Summary of probe performance

On the flight F4, as on the two previous flights, the data from the MF probe proved to be inexplicable in terms of the direct effects of thermal electron drift that the instrument was designed to measure. This was unfortunate, since the geophysical conditions were ideal for the measurement : there was strong geomagnetic activity, and the payload sampled regions of the ionosphere both inside and outside an auroral arc.

The four time intervals were selected after inspection of the graph of the cross-field plasma drift velocity $V_\perp$ versus time after launch, which is given in Fig. 50. They are as follows : (1) 170 - 320 s ; (2) 340 - 440 s ; (3) 460 - 550 s ; (4) 550 - 655 s. The period (1) corresponds to the first half of the flight, when $V_\perp$ was relatively small. Period (2), in contrast, is the one during which $V_\perp$ was greatest ($\simeq$ 2.8 km/s). It declined during periods (3) and (4), though remaining larger, on the average, than during period (1).

Fig. 51 shows the results of this analysis of the frequency-shift data from F4, displayed in the same way as those for F3 were in Fig. 39, with which it should be compared. During the period (1), the data from F4 resemble those from the second, third, and fourth periods analysed for F3, inasmuch as the spin-dependent component of the frequency-shift is quite small. But during the periods (2), (3) and (4), as in the first period analyzed for F3, the functions $\Delta F(\phi_v)$ have sinusoidal components which are approximately in antiphase for the two main data sets. These components are much larger on F4 than they were on F3, which may be attributable to the larger values of $V_\perp$.

This view is corroborated by Fig. 52, in which the amplitude ΔF_1 of the sinusoidal component of $\Delta F(\phi_v)$ is plotted against the average value of $V_\perp / V_{th}$ for each of the four periods, V_{th} being the electron thermal velocity. Three facts should be noted on this figure :

- there is excellent agreement between the value of ΔF_1 for the layout C (dots) and those for the layouts B + D, which confirms the significance of our estimates of this quantity ;

- except during the first period (when $V_\perp$ is quite variable), ΔF_1 appears to vary linearly with the ratio $V_\perp / V_{th}$.

- however, the coefficient of proportionality is about ten times larger than that predicted theoretically for the direct effect of the cross-field plasma drift velocity, as given in Eq. (13).

The problem is to identify the causative mechanism, which cannot be the straightforward action of cross-field drift as described in § 2.1., since the observed shifts are about ten times greater than would be expected on this basis, and do not have extrema when the sensor booms are parallel or anti-parallel to $V_\perp$. Among the other possibilities, the most obvious are those that have been discussed already in § 4.3., in connection with the data from F2 ; they are listed on p. 33 of Part 1.

The correlation now observed between ΔF_1 and $V_\perp$ may be taken as evidence in favour of the first one on the list, namely an effect of the perturbation that the payload body creates in the thermal plasma around it. However, the same objection can be raised as was made in § 4.3.1., namely that the spin-dependent part of ΔF does not have a maximum or minimum in the wake, i.e. at $\phi_V = 0°$. On F4, the extremum of ΔF that came closest to the wake generally occurred between 0° and 90°, while on F2 it was near to 90°. It is very hard to see how an effect of the thermal plasma perturbation could be strongest elsewhere than in the wake.

There does exist one such possibility, however, namely that the sensor might be susceptible to the influence of the ambient electric field. This field is, of course, perpendicular to $\mathbf{V}_\perp$ in the plane perpendicular to $\mathbf{B}_o$, and corresponds to a gradient of plasma potential. The electric field may influence the behaviour of the sensor because, in its presence, any conductor acquires, with respect to the ambient plasma, a potential that depends on its position relative to the payload body, if it is connected to the body electrically. This is not the case for the spherical electrodes of the sensor units, which are biased at constant current, so that each one of them takes up, with respect to the plasma in its immediate neighbourhood, the same potential as all the others (see § 3.1.). But it is the case for the small metal boxes that house the miniature electronics associated with these electrodes, from which they are separated by only 7 cm. In any one of the layouts of the sensor, the two units in use are at different distances from the payload body, so their electronics boxes are at different potentials with respect to the plasma. It is just conceivable that, in this way, the electric field could influence the sensor, and give rise to spurious non-reciprocity.

During the first half of the flight, spent mostly inside the arc, the data were quite similar to those from F3. The frequency-shifts were small, and did not exhibit much spin-dependence.

During the second half of the flight, however, the frequency-shifts were larger and more strongly spin-dependent than those observed on F3. This behaviour appears to be related to the fact that the payload was then outside the arc, in a region where it encountered strong electric fields, and hence high plasma drift velocities across the magnetic field.

For present purposes, the observed frequency-shifts must be considered as being mostly spurious. They constitute systematic errors of measurement, which mask the interesting frequency-shifts caused directly by drift motion of the thermal electrons. In the circumstances, the best use for these data is in identifying the causes of the systematic errors, and in finding ways to reduce them.

9.3.2. Causes of systematic errors

In § 8.2.2. and § 9.2.2., the normalized frequency-shift data from F3 and F4 respectively were resolved, according to Eq. (12), into their spin-independent and spin-dependent parts, and these will now be discussed separately. However, it is economical to suppose that they have a common cause.

The spin-independent part ΔF_o is hard to interpret, because some aspects of its behaviour on F3 and on F4 are contradictory, and its variations do not correlate with those of any of the other physical phenomena observed.

On the other hand, a close correlation has been found between the spin-dependent part ΔF_1, and the component $V_\perp$ of the plasma drift velocity in the plane perpendicular to the Earth's magnetic field, measured with respect to the payload. This is illustrated best by Fig. 52. It suggests most strongly that cross-field plasma drift is the cause of the spin-dependent frequency-shifts.

reduced these perturbations, or tended to make them the same around all the electrodes in use at any one time.

Let us begin by considering the plasma perturbation caused by the electronics boxes. Clearly it could be reduced by biasing the boxes at constant current, as has already been done for the spherical electrodes. Of course, in order to minimize RF interference, it would probably be wise to ground the boxes capacitatively to the payload body.

The perturbation produced by the body in the plasma around the sensor units could be minimized by holding them away from the body on the longest possible booms. Moreover, any residual perturbation could be arranged to be approximately the same for all the units, by adopting a sensor layout in which they were all at the same distance from the body.

Finally, since spurious spin-dependent L.O.R. frequency-shifts well correlated with cross-field plasma drift were much in evidence in the Porcupine experiments, particularly on the flight F4, it seems advisable to give the sensor layout a symmetry that excludes the possibility of such frequency-shifts arising from cross-field drift alone. This requirement is met by the quadripole layout illustrated in Fig. 54, where the four electrodes are placed at the corners of a rectangle, one side of which is oriented parallel to the Earth's magnetic field.

In this layout, the propagation paths of interest are the diagonals of the rectangle. For a given plasma, the L.O.R. frequency is defined by the angle that they make with the magnetic field, which is 30° in the figure. Of course, there are two other propagation paths, along the sides parallel to the field, but the associated resonance occurs at a much lower frequency, specifically at the lower hybrid frequency, so it should not interfere with the observation of the L.O.R.

The symmetry of this layout is such that a cross-field plasma drift, whatever its direction, cannot give rise to a non-reciprocal frequency-shift. It can change the L.O.R. frequency, but the change should be of the second order in the ratio $V_\perp / V_{th}$, and should be the same for the two directions of propagation, (a) and (b) in Fig. 54. The symmetry does not rule out the possibility that the magnitude of the non-reciprocal

In § 4.3.1., it was explained that the perturbation of the plasma density by the payload body is accompanied by a perturbation of plasma potential, and hence by an electric field. If the plasma is stationary with respect to the body, then the field is independent of azimuth and is directed towards the body. If the plasma has a cross-field velocity with respect to the body, then the azimuthal symmetry is broken, the field being strongest in the wake. When this localized field is added to the large-scale field present in the plasma, and the radial component of the total field is taken, its absolute value is found to be greatest in the azimuthal range $0° \leqslant \phi_v \leqslant 90°$. It is this component of the field that gives rise to the difference between the ambient plasma potentials for the two sensor units used in each layout. Thus the fact that the spurious frequency-shifts are greatest in the range $0° \leqslant \phi_v \leqslant 90°$ is consistent with an explanation in terms of an influence of the ambient electric field.

However, we have not been able to suggest a specific mechanism by which the field may exert its influence, apart from noting that it affects the potentials of the electronics boxes relative to the plasma. These differences in potential could cause different plasma perturbations near the electrodes, in addition to the perturbations due directly to the proximity of the payload body. It seems reasonable to think that the cause of the systematic errors due to spurious non-reciprocity must be sought in differences in the state of the plasma around each of the two sensors in use, and much of the evidence is consistent with this view, but how these differences give rise to the observed non-reciprocity remains obscure.

9.3.3. Reduction of systematic errors

The findings of § 9.3.2. may be summarized by stating that although the causative mechanism of the systematic errors has not been identified, the causative agent is almost certainly the perturbation of the thermal plasma around the electrodes of the sensor, produced by the payload body and perhaps also by the electronics boxes.

If these findings are correct, it follows that the systematic errors could be reduced by modifying the sensor system in ways that either

of the body in the direction of the orbital motion, so that it is the first to encounter the oncoming plasma. It should be oriented with its plane perpendicular to the plane of the orbit, and with its axis vertical. Then at high latitudes, where the Earth's magnetic field is almost vertical, the probe axis would be approximately parallel to the field. This arrangement would be suitable for measuring the field-aligned drift velocity of the thermal electrons at high latitudes, where the interest in doing so is greatest.

frequency-shift due to field-aligned drift might be modified in the presence of cross-field drift, but again this effect is expected to be of the order of $(V_\perp / V_{th})^2$.

The use of a quadripole sensor layout, rather than the double-monopole layouts used on the flights F3 and F4 (Fig. 21), has an advantage mentioned in § 8.3.2. and illustrated by Fig. 29, namely that a dipole receiving antenna generally picks up less technological noise than a monopole does. Moreover, if all other things are equal, the use of four electrodes instead of two almost doubles the amplitude of the received signal ; this statement supposes that, at the L.O.R. frequency for oblique propagation along the diagonals, the signal received in this way is much stronger than that received along the sides parallel to $\mathbf{B}_o$, a point that needs to be checked by numerical calculation. If this is correct, then the adoption of the quadripole layout shown in Fig. 54 should lead to an improvement in the signal-to-noise ratio, and hence to a reduction of the random errors in the measurement of the L.O.R. frequency-shifts.

A disadvantage of this or any other quadripole layout, in comparison with the set of double-monopole layouts shown in Fig. 21, is that it can be put out of action completely by a failure of any one of the four sensor units, or of the four booms on which these units are mounted. This problem was encountered on the flight F2 (see Part 1). If it is to be avoided in the future, the booms and sensor units must be made more reliable.

Fig. 55 shows how a probe with the recommended layout could be mounted on the payload of a rocket such as the Aries. All four booms are of the same length, which is convenient. Also the fact that the four sensor units are all at the same distance from the payload body should minimize the effects of plasma perturbations (see § 9.2.2.).

The ideal platform for this probe would be a polar-orbiting satellite with 3-axis stabilization, one axis being the local vertical and another being in the plane of the orbit. To avoid plasma perturbations caused by the satellite body, the probe should be placed ahead

the magnitude of the cross-field drift velocity, but its phase did not correspond to the direction of this velocity. These findings suggest that the spurious frequency-shifts are due partly to the perturbation of the thermal plasma by the payload body, and perhaps also to a perturbation of the sensor by the electric field in the plasma.

In order for the MF probe to attain its objective of measuring the field-aligned drift velocity, and so to become a useful instrument for space research, its accuracy must be improved. This is mainly a matter of reducing the spurious frequency-shifts. The design changes made before the flight F3, in the light of the results from F2, have already reduced them tenfold. A reduction by a further factor of ten is necessary, and there is no reason to think that it cannot be achieved. The results from the flights F3 and F4 have suggested what improvements in the technology of the probe should be made for this purpose, and it is much to be hoped that an opportunity to try them out, on a rocket or preferably on a satellite, will occur in the not-too-distant future.

10. CONCLUSIONS

In its ultimate objective of determining the field-aligned drift velocity of the thermal electrons in the auroral ionosphere, by measuring the shift in frequency of the lower oblique resonance, the MF mutual-impedance probe experiment of Project Porcupine was not successful. Nevertheless, very substantial progress towards this objective was made in the course of the Porcupine program.

The MF probe experiment on the flight F2 was the first of its kind, so it included comparative tests of several different electrical layouts of the sensor system. Unfortunately, because of some accidents that occurred to the system during boom deployment, the data were difficult to interpret. The main finding was the existence of spurious L.O.R. frequency-shifts, resembling the anticipated effects of field-aligned drift, but much too large : interpreted as such, they implied drift velocities of 30 - 40 km/s. Though the cause of these spurious frequency-shifts could not be identified, their behaviour, in particular their strong dependence on the spin-phase angle of the payload, suggested that they might be reduced by modifying the sensor system in certain ways.

These suggestions were implemented on the flight F3, which offered an excellent opportunity to evaluate their effects, since it took place under fairly quiet magnetic conditions. On this occasion, the frequency-shifts showed relatively little dependence on spin phase. Also, fair agreement was found between the shifts measured with several independent sensor layouts. The measured values, which were roughly ten times smaller than on the previous flight, corresponded to drift velocities of about 3 km/s on the average. However, such velocities are still too large to be accepted as genuine.

On the final flight F4, the sensor system was the same as on F3, but the magnetic conditions were disturbed. As a result, the payload encountered strong ionospheric electric fields, involving plasma drift velocities of several kilometres per second across the magnetic field. This time the frequency-shifts were about twice as large as those observed on F3, and were markedly spin-dependent. The amplitude of the spin-dependent component of the frequency-shift was strongly correlated with

ACKNOWLEDGEMENTS

Project Porcupine was part of the national sounding rocket program of the Federal Republic of Germany during the International Magnetospheric Study (1976 - 1979). It was carried out by the Deutsche Forschungs- und Versuchsanstalt für Luft- und Raumfahrt, and funded by the Bundesministerium für Forschung und Technologie. The project management and overall engineering support were provided by the Max-Planck-Institut für Extraterrestrische Physik, at Garching. The participation by the Centre de Recherches en Physique de l'Environnement (CRPE), which is a joint institute of the Centre National de la Recherche Scientifique (CNRS) and the Centre National d'Etudes des Télécommunications (CNET), was sponsored by the Centre National d'Etudes Spatiales (CNES).

We are most grateful to the Principal Investigator, Dr. G. Haerendel, for the invitation to participate, and to the Project Manager, Dr. B. Häusler, for adapting the Aries payload so as to include the CRPE experiment. We particularly appreciated their acceptance of the modifications that we proposed between the flights F2 and F3. To them and to all the other scientists, engineers , and technicians who cooperated with us during the payload integration in Munich and during the launch campaigns at Kiruna, we express our warmest thanks.

The instrument for the MF probe experiment was built mainly by staff of the CRPE at Orleans, with vital assistance from the CNET at Issy-les-Moulineaux and from the CNES at Toulouse. The CNES also built an automatic test and calibration system, and processed most of the data that the experiment produced. We are very much beholden to all the persons concerned.

Finally we thank the other Porcupine experimenters with whom we have had many stimulating discussions, and who provided us with correlative data which we used in writing this report.

CLOUTIER, P.A., H.R. ANDERSON, R.J. PARK, R.R. VONDRAK, R.J. SPIGER, and B.R. SANDEL, Detection of geomagnetically aligned currents associated with an auroral arc, J. Geophys. Res., 75, 2595 - 2600, 1970.

D'ANGELO, N., Type III spectra of the radio aurora, J. Geophys. Res. 78, 3987 - 3990, 1973.

EVANS, D.S., Evidence for low altitude acceleration of auroral particles, in Physics of the Hot Plasma in the Magnetosphere, edited by B. Hultquist and L. Stenflo, pp. 319 - 340, Plenum Press, New York, 1975.

FISHER, R.K., and R.W. GOULD, Resonance cone in the field pattern of a radio frequency probe in a warm anisotropic plasma, Phys. Fluids, 14, 857 - 867, 1971.

GONFALONE, A., Oblique resonances in the ionosphere, Radio Sci. 9, 1159 - 1163, 1974.

GRARD, R.J.L. (Editor), Photon and Particle Interactions with Surfaces in Space, Reidel , Dordrecht, Holland, 1973.

HAERENDEL, G. (Editor), Project Porcupine, Summary of Scientific Objectives and Instrumentation, Max-Planck-Institut für Extraterrestrische Physik, Garching, Internal report, 1976.

HAERENDEL, G., E. RIEGER, A. VALENZUELA, H. FOPPL, H.C. STENBAEK-NIELSEN, and E.M. WESCOTT, First observation of electrostatic acceleration of barium ions into the magnetosphere, in European Programmes on Sounding-Rocket and Balloon Research in the Auroral Zone, European Space Agency, Report ESA- SP-115, August 1976.

HAERENDEL, G., and R.Z. SAGDEEV, Artificial plasma jet in the ionosphere, Adv. Space Res. 1, 29-46, 1981.

HAUSLER, B., G. HAERENDEL, O. BAUER, H. FÖPPL, E. RIEGER, R. TREUMANN and A. VALENZUELA, Projekt Porcupine, Max-Planck-Institut für Extraterrestrische Physik, Garching, Internal report, 1982.

REFERENCES

ANDERSON, H.R. and R.R. VONDRAK, Observations of Birkeland currents at auroral latitudes, J. Geophys. Res. 13, 243 - 262, 1975.

ARNOLDY, R.L., Auroral particle precipitation and Birkeland currents, Rev. Geophys. Space Phys., 12, 217 - 231, 1974.

BANKS, PM., C.R. CHAPPELL, and A.F. NAGY, A new model for the interaction of auroral electrons with the atmosphere : spectral degradation, backscatter, optical emission, and ionization, J. Geophys. Res. 79, 1459 - 1470, 1974.

BERING, E.A., M.C. KELLEY, and F.S. MOZER, Observations of an intense field-aligned thermal ion flow and associated intense narrow band electric field oscillations, J. Geophys. Res. 80, 4612 - 4620, 1975.

BOSWELL, R.W., and J. THIEL, Electron drift velocity deduced from lower oblique (whistler) resonance cone measurements, Phys. Fluids, 24, 2120 - 2122, 1981.

BUDDEN, K.G., and J.W. JULL, Reciprocity and non-reciprocity with magneto-ionic rays, Canad. J. Phys. 42, 113 - 130, 1964.

CARLSON, C.W., R.E. ERGUN and M.K. HUDSON, Observations of beam generated upper hybrid waves parametrically decaying to whistlers (Abstract only), Eos, 58, 1214, 1977.

BUSH, R., C.W. CARLSON, V.S. DOKOUKIN, R. GRABOWSKI, G. HAERENDEL, B. HAUSLER, D. JONES, M.C. KELLEY, V. J. KAPITANOV, V.G. KOROBEINIKOV, V.M. KOSTIN, E.V. MISHIN, A.J. MOROZOV, F.S. MOZER, V.N. ORAEVSKI, W. OTT, A. PEDERSEN, R. POTTELETTE, Ju. Ja. RUZHIN, R.Z. SAGDEEV, W. STUDEMANN, L.R.O. STOREY, A. URBAN, I.A. ZHULIN, K. WILHELM, H. WOLF, Artificial plasma jet in the ionosphere, IZMIRAN, Moscow, Preprint 21 (287), 1980.

CLOUTIER, P.A., and H.R. ANDERSON, Observations of Birkeland currents, Space Sci. Rev. 17, 563 - 587, 1975.

MICHEL, E., C. BEGHIN, A. GONFALONE, and I.F. IVANOV, Mesures de densité et température électroniques sur fusée dans l'ionosphère polaire par l'étude du cône de résonance, Ann. Géophys. 31,463 - 471, 1975.

MOZER, F.S., On the lowest attitude S3-3 observations of electrostatic shocks and parallel electric fields, Geophys. Res. Lett. 7, 1097 - 1098, 1980.

MOZER, F.S., C.W. CARLSON, M.K. HUDSON, R.B. TORBERT, B. PARADY, J. YATTEAU, and M.C. KELLEY, Observations of paired electrostatic shocks in the polar magnetosphere, Phys. Rev. Lett., 38, 292 - 295, 1977.

MOZER, F.S., C.A. CATTELL, M.K. HUDSON, R.L. LYSAK, M. TEMERIN, and R.B. TORBERT, Satellite measurements and theories of low altitude auroral particle acceleration, Space Sci. Rev. 27, 155 - 213, 1980.

POTTELETTE, R., Effet d'un mouvement du plasma parallèlement au champ magnétique sur la résonance oblique basse observée à l'aide d'une sonde quadripolaire, Ann. Géophys. 29, 201 - 226, 1973.

POTTELETTE, R., Méthodes actives et passives de diagnostic de plasmas hors d'équilibre au moyen d'une sonde quadripolaire : application aux plasmas spatiaux, Université de Paris VI, Thèse de Doctorat d'Etat, 1977.

POTTELETTE, R., and J.M. ILLIANO, Observation of weak HF electrostatic turbulence in the auroral ionosphere, J. Geophys. Res. 87, 5151 - 5158, 1982.

QUEMADA, D., Ondes dans les Plasmas, Hermann, Paris, 1968.

REME, H., and J.M. BOSQUED, Evidence near the auroral ionosphere of a parallel electric field deduced from energy and angular distributions of low-energy particles, J. Geophys. Res. 76, 7683-7693, 1971.

RUSSELL, C.T., High altitude observations of Birkeland currents, Ann. Geophys., 33, 435 - 442, 1977.

HULTQVIST, B., H. BORG, W. RIEDLER, and P. CHRISTOPHERSEN, Observations of a magnetic field-aligned anisotropy for 1 and 6 keV positive ions in the upper ionosphere, Planet. Space Sci., 19, 279 - 295, 1971.

ILLIANO, J.M., and R. POTTELETTE, Measurement of the collective motion of the electrons deduced from the shift of the lower oblique resonance frequency, Phys. Lett. 70 A, 315 - 316, 1979.

JONELEIT, D., Campaign handbook, Kiruna 12 a (IMS - Aries, Project Porcupine), Deutsche Forschungs- und Versuchsanstalt für Luft- und Raumfahrt, Oberpfaffenhofen, Technical Report, January 1976.

KINDEL, J.M., and C.F. KENNEL, Topside current instabilities, J. Geophys. Res., 76, 3055 - 3078, 1971.

KLUMPAR, D.M., J.R. BURROWS, and M.D. WILSON, Simultaneous observations of field-aligned currents and particle fluxes in the post-midnight sector, Geophys. Res. Letters, 3, 395 - 398, 1976.

KOONS, H.C., D.C. PRIDMORE-BROWN, and D.A. Mc PHERSON, Oblique resonances excited in the near field of a satellite borne electric dipole antenna, Radio Sci. 9, 541 - 545, 1974.

KUEHL, H.H., Electric field and potential near the plasma resonance cone, Phys. Fluids, 17, 1275 - 1283, 1974.

LUCKS, K., and M. KRAMER, Measurements of resonance cones influenced by ion dynamics and electron drift motion, Plasma Phys. 22, 879 - 892, 1980.

MALLINCDRODT, A.J., and C.W. CARLSON, Observations of auroral electron fluxes associated with high frequency plasma waves (Abstract only), Eos, 58, 1214, 1977.

MARTELLI, G., P.N. COLLIS, M. GILES and P.J. CHRISTIANSEN, Optical detection of electrostatic ion cyclotron waves in the auroral plasma, Planet. Space Sci. 25, 643 - 650, 1977.

STOREY,L.R.O.,and R. POTTELETTE, Possibilités d'utiliser la sonde quadripolaire pour la mesure de courants électriques dans la magnétosphère, Compt. Rend. (Sér. B), 273, 101 - 104, 1971.

STOREY,L.R.O.,and J. THIEL, Thermal and field-aligned-drift effects near the lower oblique resonance, Phys. Fluids, 21, 2325 - 2335, 1978.

STOREY,L.R.O.,J. THIEL, and R.W. BOSWELL, Location of the interference structure near the lower oblique (whistler) resonance cone, Phys. Fluids, 23, 654 - 655, 1980.

THEILE, B., and K. WILHELM, Field-aligned currents above an auroral arc, Planet. Space Sci. 28, 351 - 355, 1980.

THIEL, J., Etude sur le rayonnement d'un antenne dans un magnétoplasma maxwellien. Application au sondage in situ de l'ionosphère aurorale, Université d'Orléans, Thèse de Doctorat d'Etat ès Sciences Physiques, Juin 1981.

THIEL, J.,L.R.O.STOREY, and J.P. LEBRETON, Electron plasma density deduced from lower oblique resonance measurements, Phys. Fluids, to be published, 1983.

WESCOTT, E.M., H.C. STENBACK-NIELSEN, T.J. HALLINAN, and T.N. DAVIS, The Skylab barium plasma injection experiments. 2. Evidence for a double layer, J. Geophys. Res., 81, 4495 - 4502, 1976.

WILHELM, K., On the relation between magnetic field-aligned electrostatic electron acceleration and the resulting auroral energy flux, J. Geophys. 49, 69 - 73, 1981.

WILHELM, K., K.H. SAEGER, C. BECKER, R. SCHMIDT, and W. ENGELHARDT, Suprathermische elektronenexperimente TL 7 und KL 7, Max-Planck-Institut für Aeronomie, Katlenburg-Lindau, Report n° BMFT-FB W 79-46, June 1980.

ZMUDA, A.J., and J.C. ARMSTRONG, The diurnal flow patterns of field-aligned currents, J. Geophys. Res. 79, 4611 - 4619, 1974.

SAUVAUD, J.A. Analyse des précipitations aurorales observées à bord des satellites Auréole, Université de Toulouse, Thèse de Docteur ès-Sciences Physiques, 1977.

SCHMITT, G., IMS — Aries Project Porcupine Final Report, Kayser-Threde GMBH, Munich, October 1979.

SIMON, P. (Editor), French contribution to the IMS, Report of the French National Committee for the IMS, Meudon, 1975.

SINGH, N., Resonance cone and interference pattern in the field of a point charge in a flowing, warm magnetoplasma, Phys. Fluids, 20, 1692 - 1696, 1977.

SINGH, N., Resonance cones in non-Maxwellian plasmas, Radio Sci. 15, 881 - 889, 1980.

SINGH, N., and R.W. GOULD, Waves in a hot uniaxial plasma excited by a current source, Phys. Fluids, 16, 75 - 81, 1973.

SINGH, N., and R.W. GOULD, Radiation from a short electric dipole in a hot uniaxial magnetoplasma, Radio Sci., 6, 1151 - 1163, 1971.

SOJKA, J.J., W.J. RAITT, and A.D. JOHNSTONE, Suprathermal electron fluxes during various phases of auroral substorms, in European Programmes on Sounding-Rocket and Balloon Research in the Auroral Zone, European Space Agency, Report n° ESA-SP- 115, August 1976.

SPENNER, K., K. RAWER, and W. OTT, Thermal plasma and field aligned ion drift at the beginning of an auroral disturbance, in Space Research XIX, edited by M.J. Rycroft, pp. 331-334, Pergamon, Oxford, 1979.

STIX, T.H., The Theory of Plasma Waves, McGraw-Hill, New York, 1962.

STOREY, L.R.O., M.P. AUBRY, and P. MEYER, A quadripole probe for the study of ionospheric plasma resonances, in Plasma Waves in Space and in the Laboratory, edited by J.O. Thomas and B.J. Landmark, Volume 1, pp. 303 - 332, Edinburgh University Press, 1969.

29. Sketches of typical noise spectra observed at MF, in the passive mode, on the flight F3. The ordinate is roughly proportional to the detected output from the receiver.

30. Typical external calibration (flight F3) ; see text for explanation (§ 8.1.4.).

31. Examples of pairs of transfer functions measured on the flight F3, with the MF probe in the layouts ER * * (thick line) and RE * * (thin line) :
(a) pair showing no significant non-reciprocity (time after launch 587.74 s, altitude 254.90 km) ;
(b) pair similar to (a), but showing marked non-reciprocity (time after launch 89.76 s, altitude 128.47 km).

32. Illustrating how the experimental data on the probe transfer functions are smoothed by polynomial curve-fitting :
(a) raw data ; (b) smooth curves. In (b), the short vertical lines originating in the smooth curves indicate the positions of the raw data points.

33. Variation of the L.O.R. frequency-shift with time after the launch of F3, for the four sensor layouts. The scales on the right of the figure give the corresponding drift velocities of the thermal electrons, deduced from the approximate formulae (9) for $V_{//}$ and (13) for $V_{\perp}$.

34. Results of smoothing the data of Fig. 33, using polynomials of different orders, from 1 to 8.

35. Comparison, for the sensor layouts A - D, of the results of smoothing the data of Fig. 33 with a polynomial of order 8 :
(a) Individual results for the four layouts ;
(b) Average results for the layouts A, B, and C (broken line) and for all four layouts (solid line).

36. Apparent field-aligned drift velocity (below) and current density (above) for the flight F3. Both these quantities are here expressed in coordinates fixed with respect to the Earth, and are counted as positive when directed upwards.

FIGURE CAPTIONS

21. MF sensor system used on the flights F3 and F4.

22. Illustrating the definition of the two spin-phase angles : (a) ϕ_b ; (b) ϕ_v.

23. Illustrating how the L.O.R. frequency-shift Δf varies as a function of the spin-phase angle ϕ_v, for two different sensor layouts (uppermost panels) and for four different causative agents :

(a) Field-aligned drift motion ; the drift velocity vector is directed vertically downwards, parallel to $\mathbf{B}_o$.
(b) Cross-field drift motion ; the drift velocity vector is directed horizontally, from right to left.
(c) Isotropic density perturbation ; the drift velocity, if any, is parallel to $\mathbf{B}_o$.
(d) Anisotropic density perturbation ; the drift velocity is directed from right to left.

24. Same data as in Fig. 23, but graphed in polar coordinates.

25. Circuit diagram of one unit of the MF sensor, as used on the flights F3 and F4. The symbol F.P. denotes a filter pin.

26. Measurement cycle for the flights F3 and F4 : compare with Fig. 6 (b) for F2. The uppermost row refers to the HF probe ;
Z_s signifies self-impedance measurements,
Z_t transfer (i.e. mutual) impedance measurements.

27. External calibration circuit used on the flights F3 and F4 : compare with Fig. 7 for F2.

28. Quick-look data on the MF external calibration signals, from the high-level output of the receiver, between 65 s and 75 s after the launch of F3. The four vertical columns correspond to the four different electrical layouts of the sensor.

46. Typical external calibration (flight F4), to be compared with Fig. 30.

47. Example of a pair of transfer functions measured on the flight F4, in the presence of severe technological interference, (a) before and (b) after smoothing by the method illustrated in Fig. 32.

48. Variation of the L.O.R. frequency-shift with time after the launch of F4 ; for further details, see the caption of Fig. 33.

49. Values of the spin-phase angle ϕ_v at the instants when the L.O.R. frequency-shifts were measured, in each of the three operative sensor layouts (flight F4).

50. Magnitude of the cross-field plasma drift velocity, in coordinates fixed with respect to the payload (flight F4).

51. Similar to Fig. 39, but for the flight F4.

52. Regression diagram of the amplitude of the sinusoidal component of the normalized L.O.R. frequency-shift, versus the normalized cross-field plasma drift velocity.

53. Similar to Fig. 41, but for the flight F4.

54. MF sensor system recommended for future experiments. The broken lines represent the propagation paths from the emitting electrodes (E) to the receiving electrodes (R). The two parts of the figure show how the four electrodes are connected for propagation predominantly (a) parallel or (b) anti-parallel to the Earth's magnetic field.

55. Illustrating how the sensor system of Fig. 53 could be mounted on a rocket payload.

37. Values of the spin-phase angle ϕ_v at the instants when the L.O.R. frequency-shifts were measured in each of the four sensor layouts (flight F3).

38. Magnitude of the cross-field plasma drift velocity, in coordinates fixed with respect to the payload (flight F3).

39. Polar plots of the normalized L.O.R. frequency-shift $\Delta F = \Delta f / f_c$ versus the spin-phase angle ϕ_v, for the flight F3. The centre of each circle corresponds to $\Delta F = - 0.05$. For the definition of ϕ_v, see Fig. 22.

40. Variation of the L.O.R. amplitude-shift with time after the launch of F3, for the four sensor layouts.

41. Polar plots of the normalized L.O.R. amplitude-shift $\Delta |Z_t| \; / \; |Z_r|$ versus the spin-phase angle ϕ_v, for the flight F3. The centre of each circle corresponds to the value - 0.2.

42. Observations of the lower oblique resonance, at the end of the flight F3, in the two nominally identical layouts B and D. The time at the start of each frequency-sweep is given, in seconds after launch, above each pair of curves ; the thick curves refer to the layout * ER *, and the thin ones to * RE *.

43. Regression diagram of the spin-independent component of the normalized L.O.R. amplitude-shift versus the same component of the normalized frequency-shift. The solid line is their theoretical relationship, while the experimental regression line is dashed.

44. Downward flux of supra-thermal electrons, measured by a retarding-potential analyzer during the flight F3 [K. Spenner and W. Ott, Private communication, 1981] .

45. Plasma electron density (cm^{-3}) and temperature (eV) measured during the flight F3 by the electrostatic probe on the Berkeley free-flyer [C.W. Carlson, Private communication, 1981] .

TABLE 3

TIME (min, sec)	ALTITUDE (km)	RANGE (km)	EVENT
+ 0.01.23	112.2	3.8	Deployment of E-F booms
+ 0.01.25	117.2	4.0	Deployment of non-sym. booms
+ 0.01.36	144.0	5.1	Spinup (1.6 RPS)
+ 0.01.40	153.4	5.5	Spin mode ACS on
+ 0.01.47	169.6	6.1	Ejection of E-F probes
+ 0.01.57	191.9	7.1	Ejection of barium and xenon canisters
+ 0.02.00	198.4	7.3	Deployment of lower boom
+ 0.02.03	204.9	7.6	Spin mode ACS off
+ 0.02.13	225.7	8.6	Spin mode ACS on and vector 2 manoeuver
+ 0.02.33	264.6	10.4	Spin nozzle on (2.5 RPS)
+ 0.02.40	277.4	11.1	Spin mode ACS off
+ 0.06.00	460.3	29.3	Spin mode ACS on
+ 0.06.06	460.5	29.9	Apogee
+ 0.06.10	460.4	30.9	Spin mode ACS off
+ 0.06.30			Barium shaped charge

TABLE 4

119 - 137

147 - 152

162 - 167

192 - 197

222 - 227

292 - 297

422 - 427

572 - 577

TABLE CAPTIONS

Note. The data in these last two tables, which refer to flights F3 and F4, have been reproduced from the final report on Projekt Porcupine [*Häusler et al.*, 1982].

3. List of primary payload events. The times given in minutes and seconds after launch were fixed by the automatic programmer in the payload, while the trajectory data are nominal.

4. Pre-programmed xenon plasma injection times, in seconds after launch.

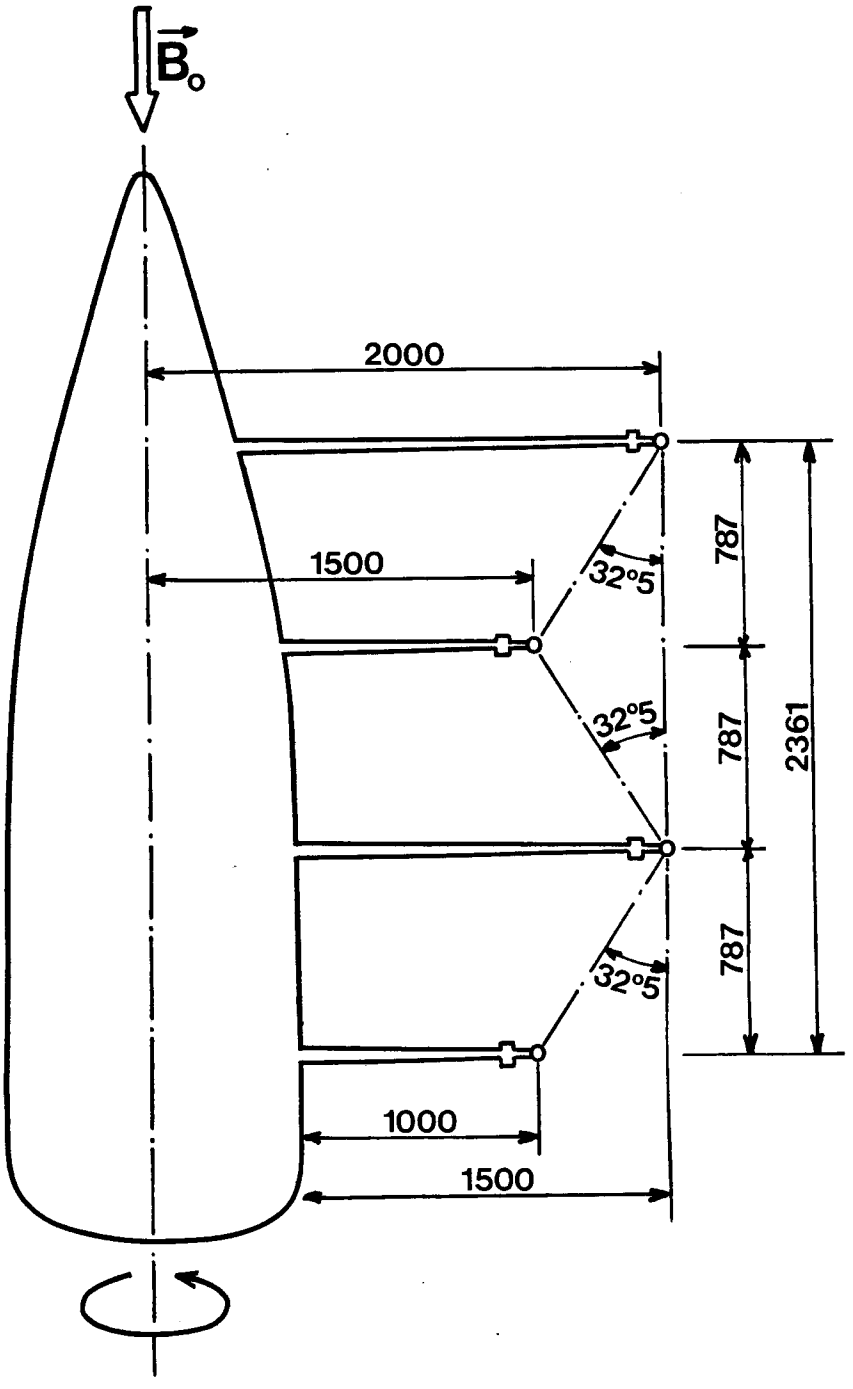

FIGURE 21

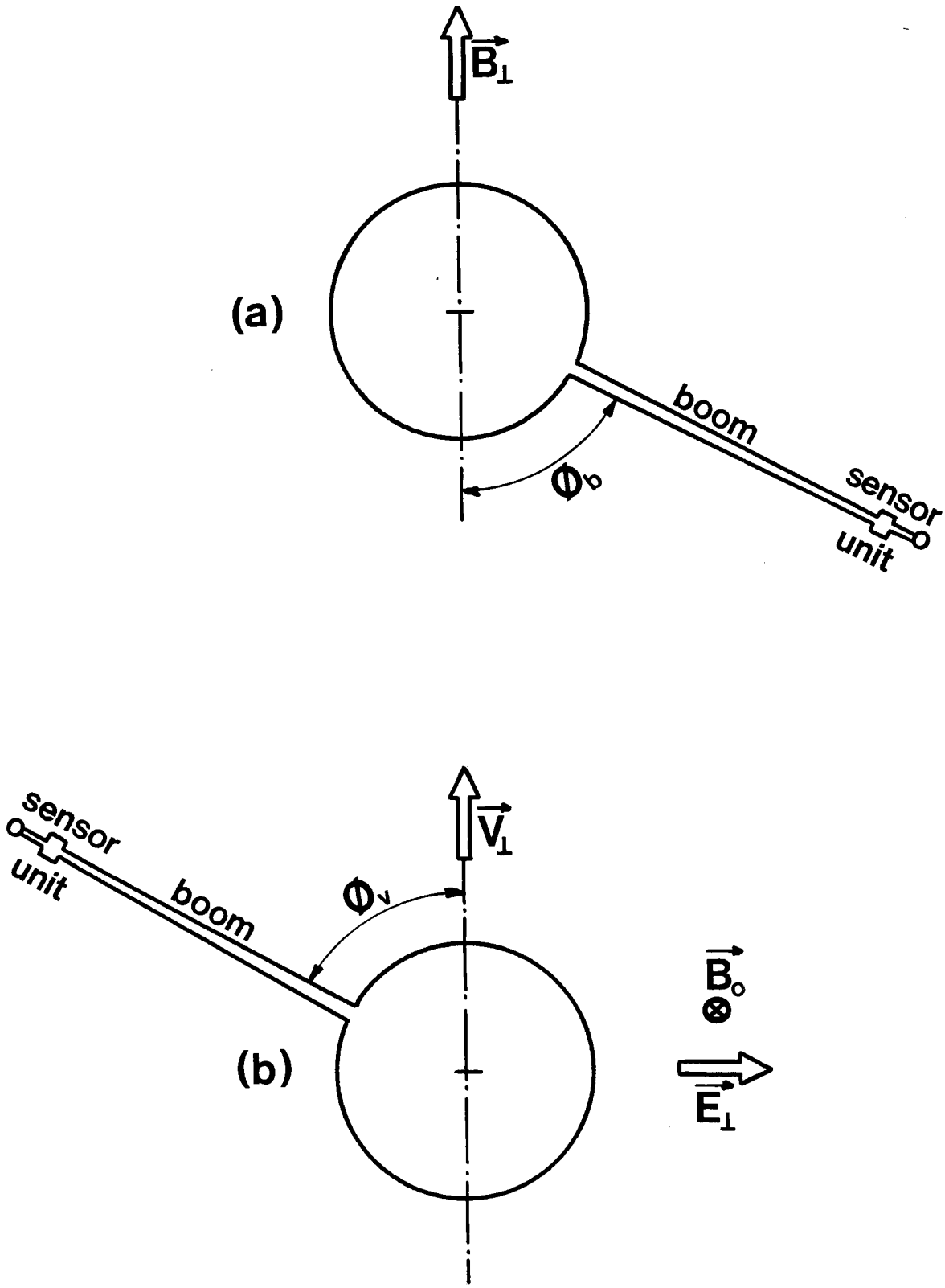
$\vec{B}_\perp$
(a)
boom
sensor
unit
Φ_b
sensor
unit
boom
Φ_v
$\vec{V}_\perp$
(b)
$\vec{B}_o$
$\vec{E}_\perp$

FIGURE 22

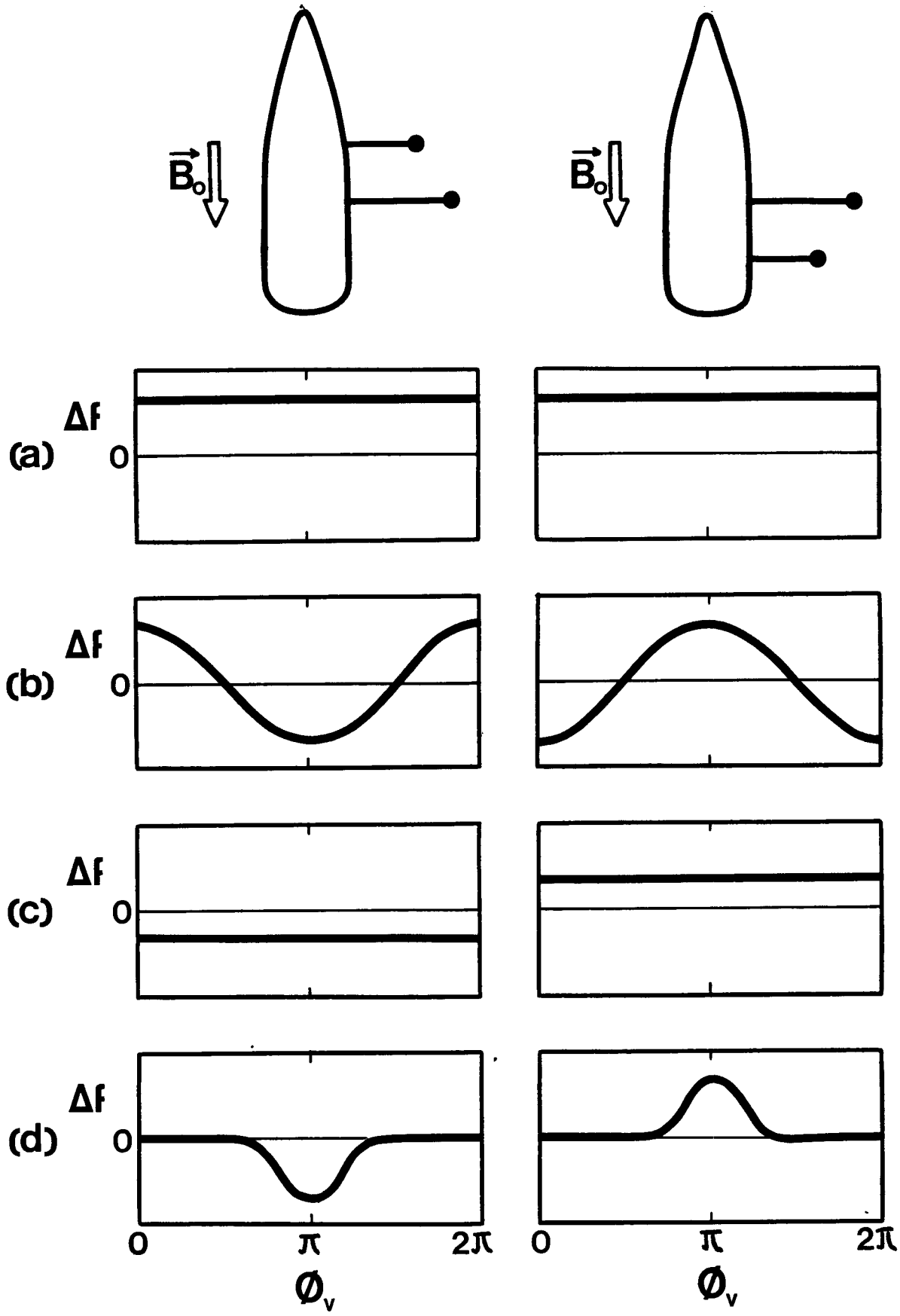

FIGURE 23

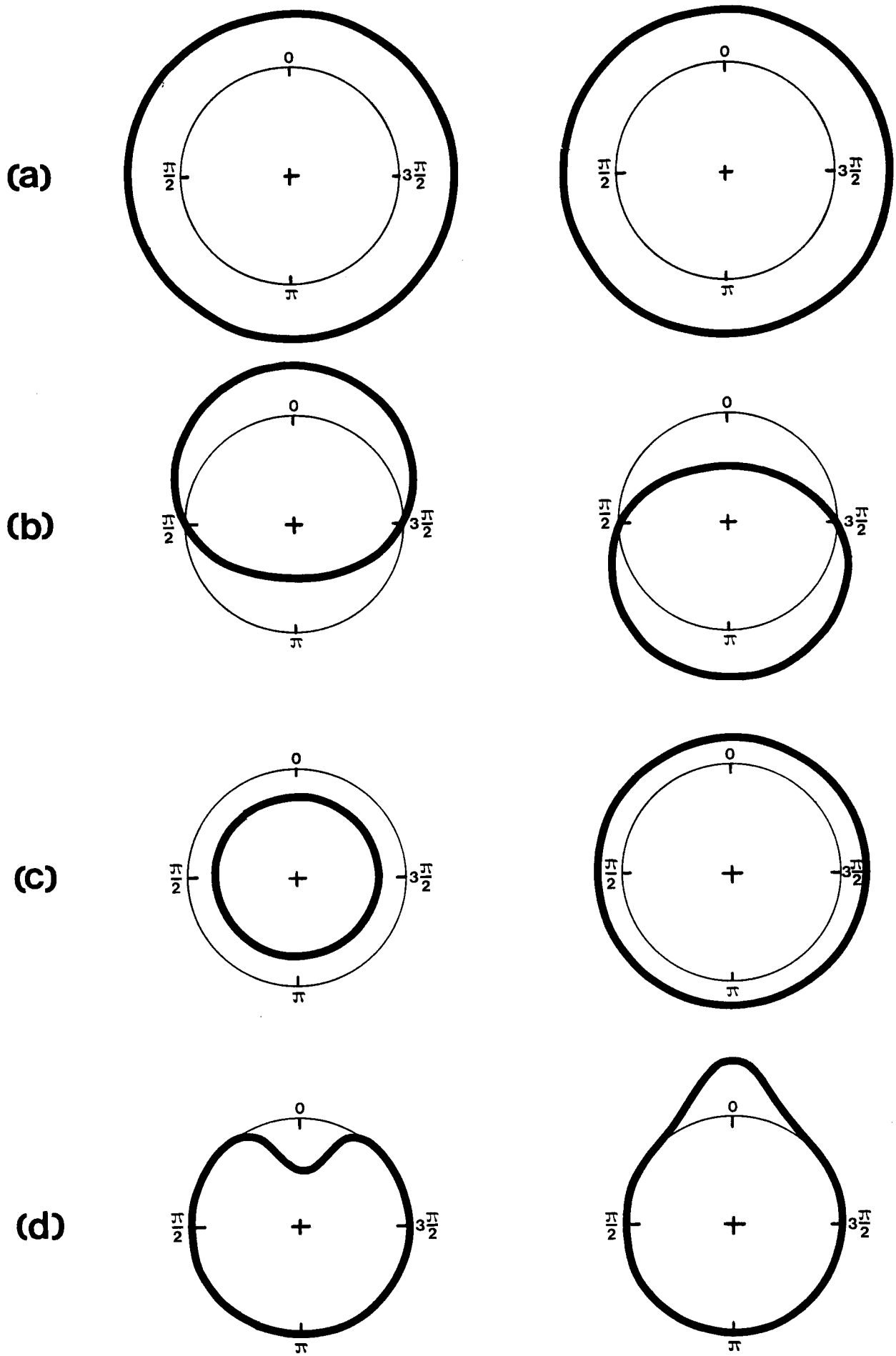

FIGURE 24

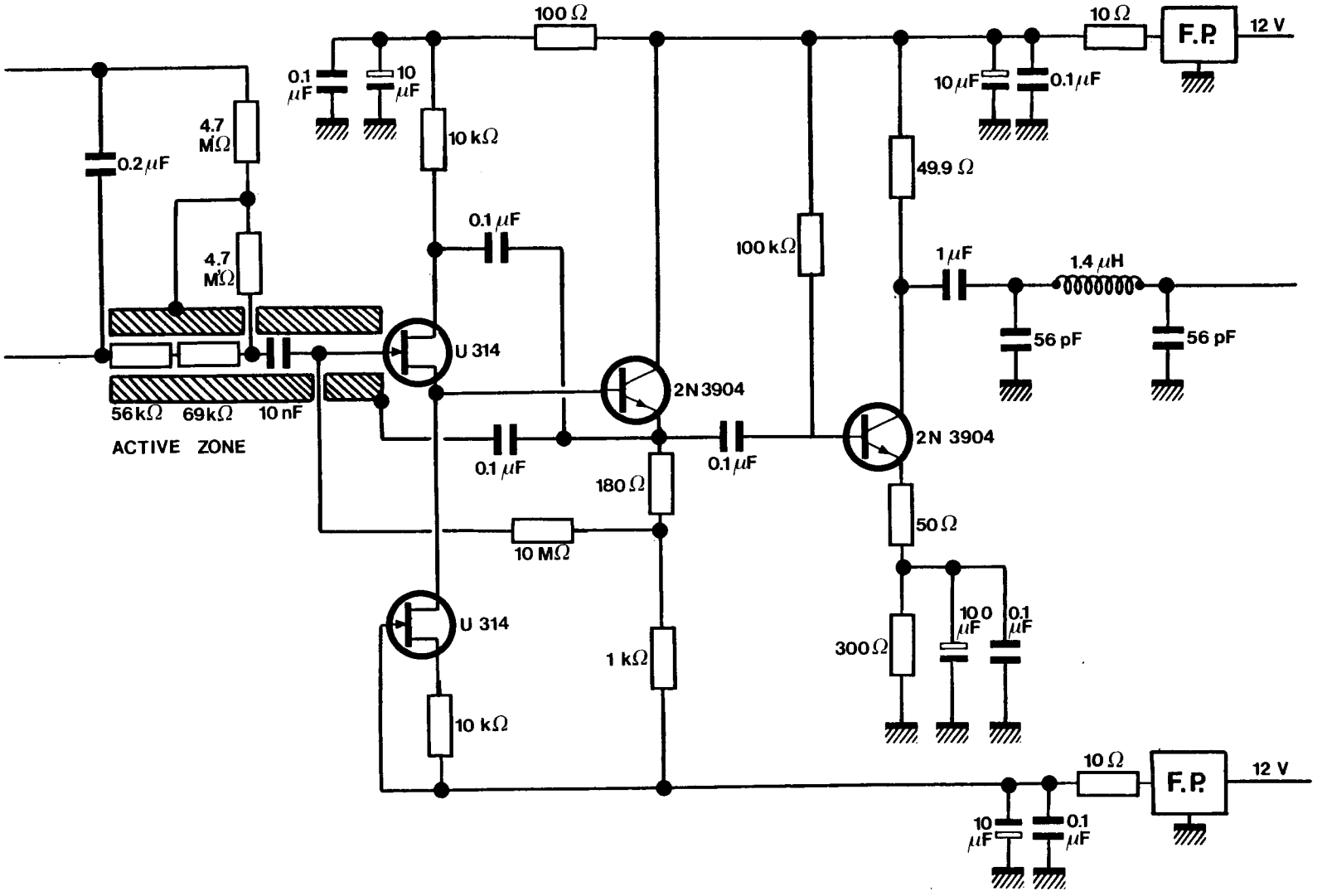
100 Ω
10 Ω
F.P.
12 V
0.1 μF
10 μF
10 kΩ
10 μF
0.1 μF
0.2 μF
4.7 MΩ
49.9 Ω
0.1 μF
100 kΩ
1 μF
1.4 μH
4.7 MΩ
U 314
2N3904
56 pF
56 pF
56 kΩ
69 kΩ
10 nF
ACTIVE ZONE
2N 3904
0.1 μF
180 Ω
0.1 μF
50 Ω
10 MΩ
U 314
100 μF
0.1 μF
300 Ω
1 kΩ
10 kΩ
10 Ω
F.P.
12 V
10 μF
0.1 μF

FIGURE 25

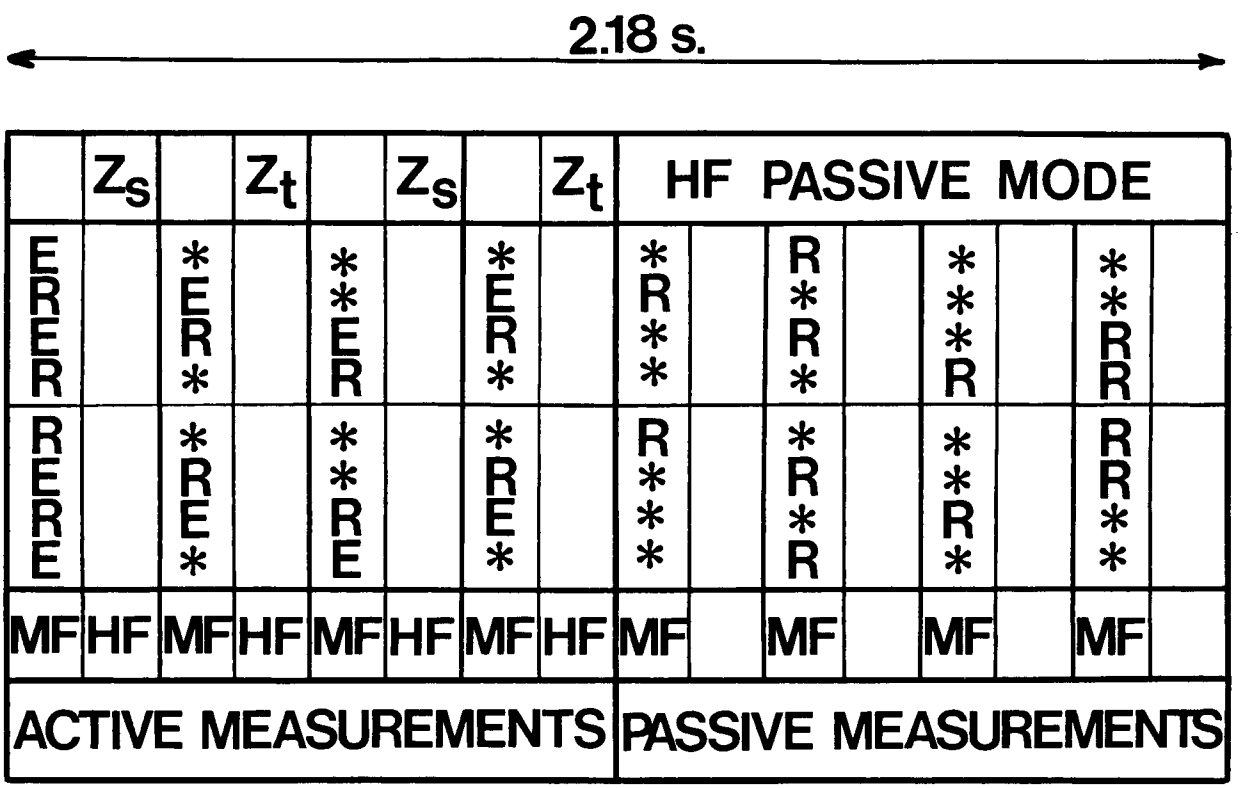
2.18 s.
Z_s
Z_t
Z_s
Z_t
HF PASSIVE MODE
ERER
ER
***ER
ER
*R**
R***
***R
**RR
RERE
RE
***RE
RE
R***
RR
***R*
RR**
MF HF MF HF MF HF MF HF MF MF MF MF
ACTIVE MEASUREMENTS
PASSIVE MEASUREMENTS

FIGURE 26

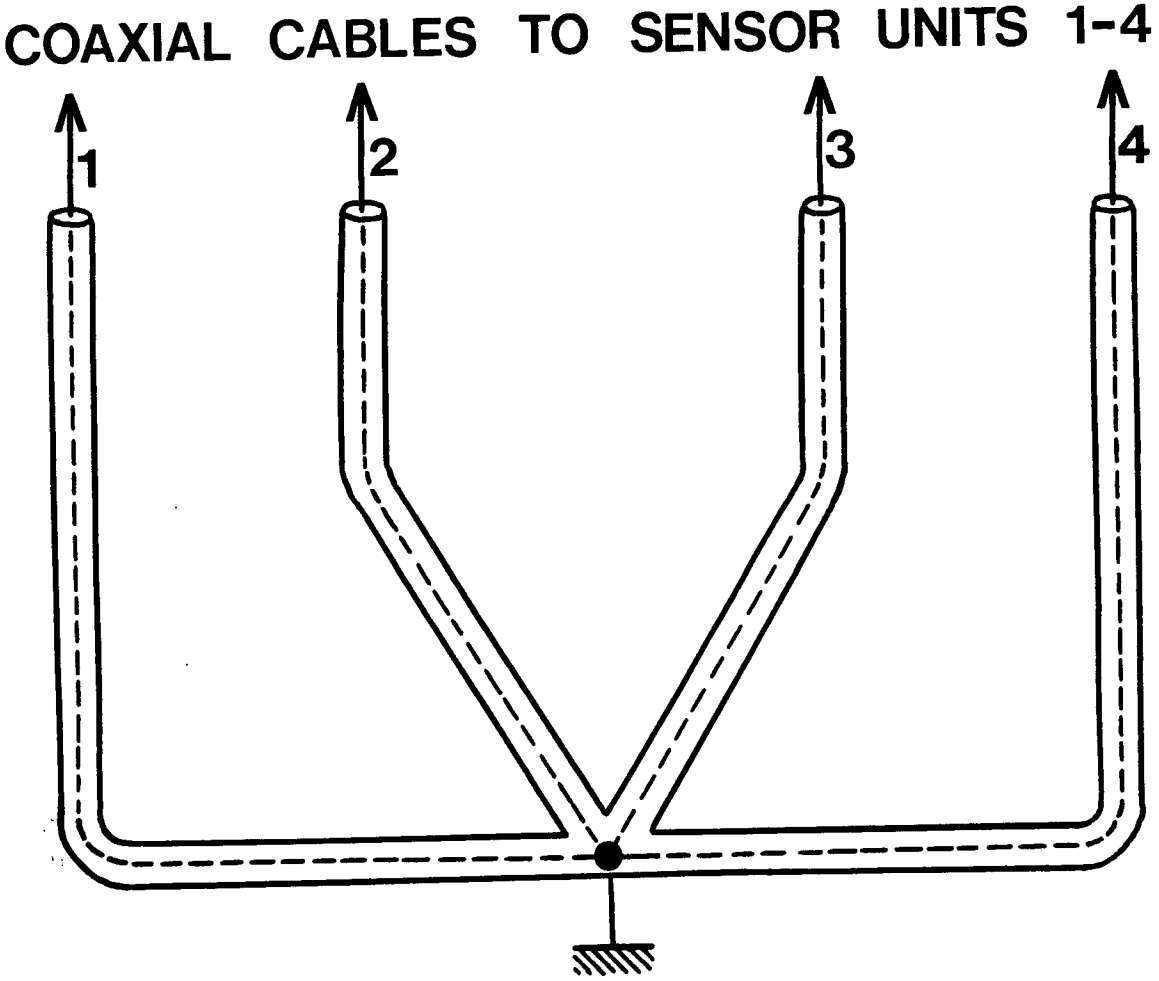

FIGURE 27

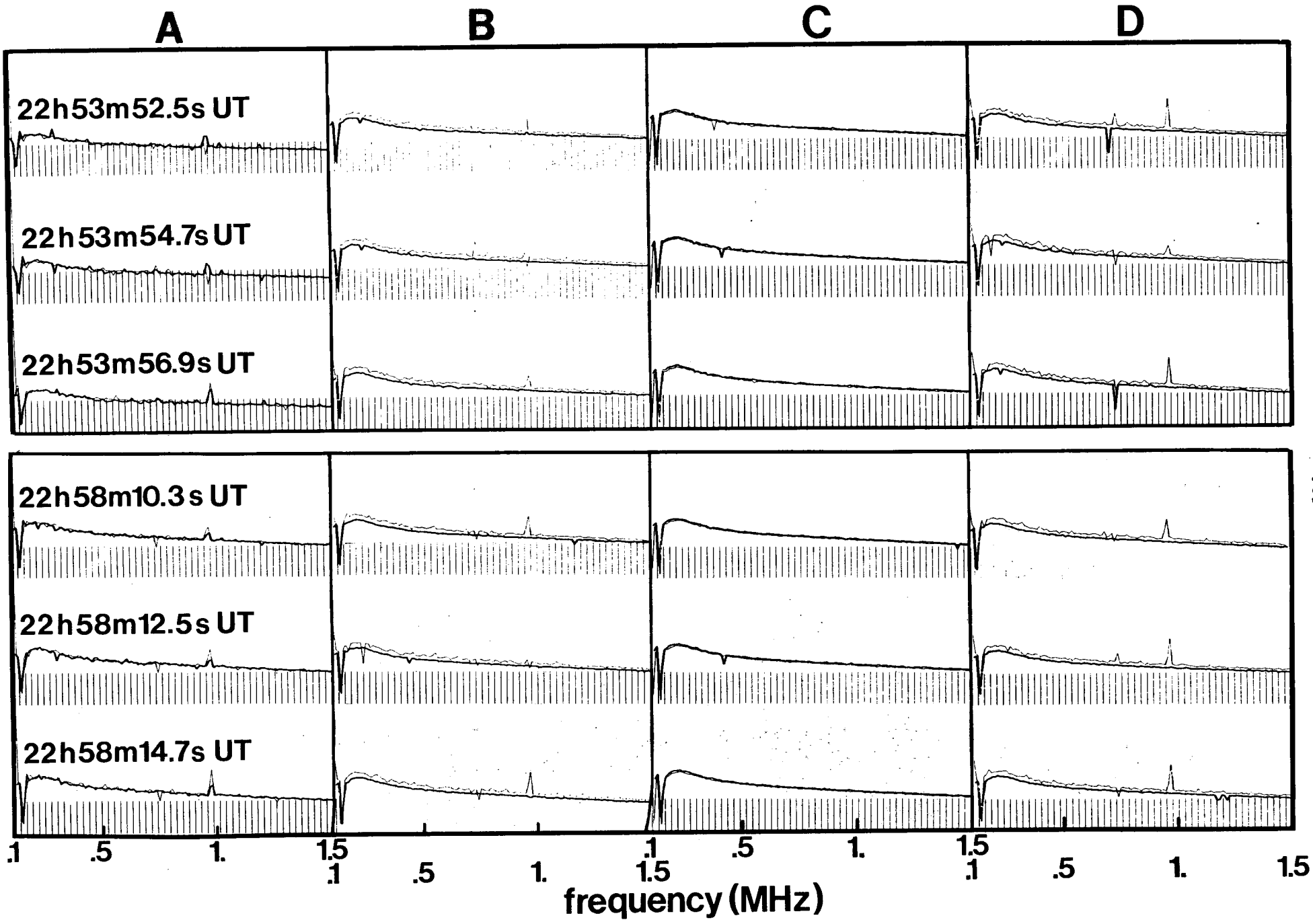
A
B
C
D
22h53m52.5s UT
22h53m54.7s UT
22h53m56.9s UT
22h58m10.3s UT
22h58m12.5s UT
22h58m14.7s UT
.1
.5
1.
1.5
frequency (MHz)

FIGURE 28

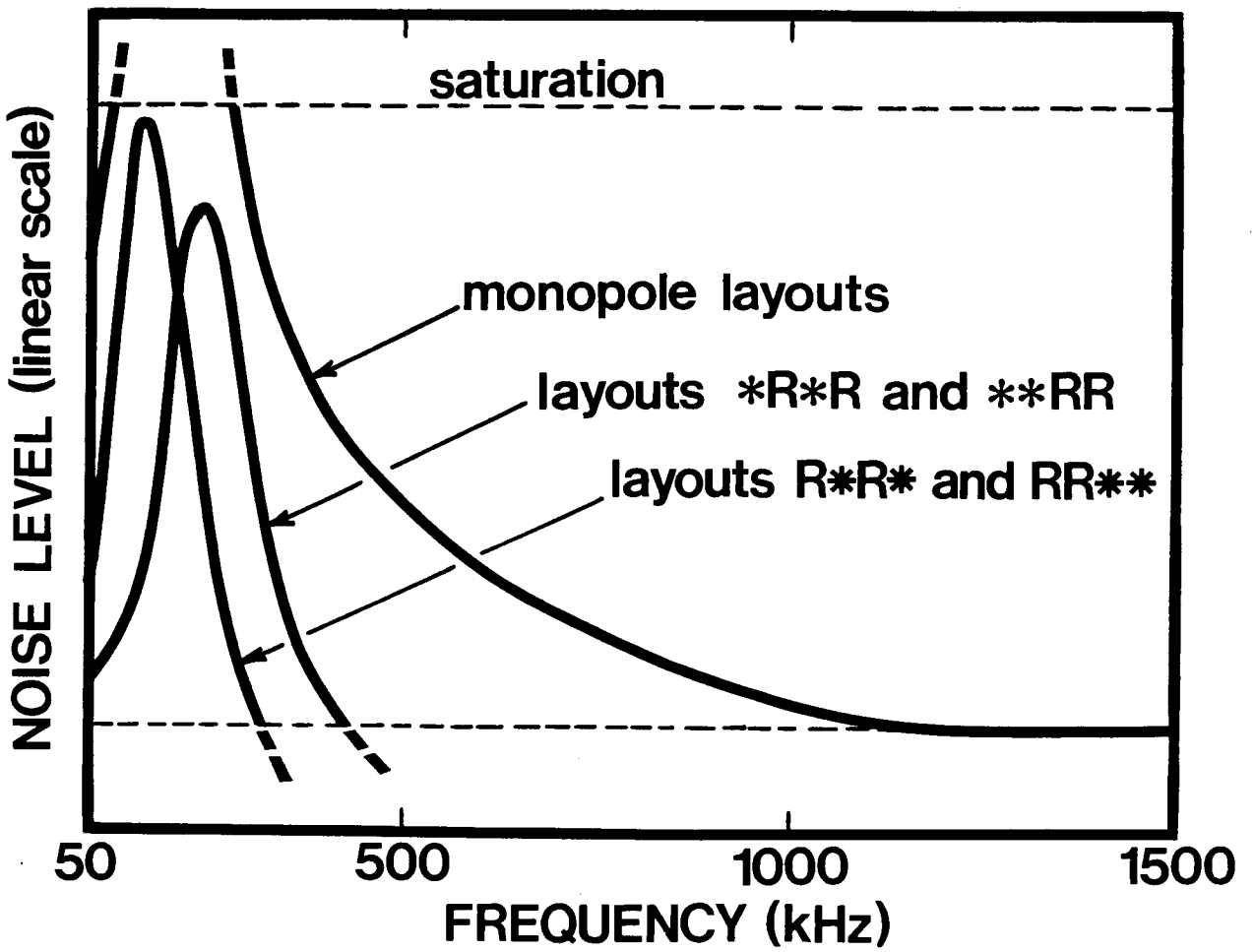
saturation
monopole layouts
layouts *R*R and **RR
layouts R*R* and RR**
NOISE LEVEL (linear scale)
50
500
1000
1500
FREQUENCY (kHz)

FIGURE 29

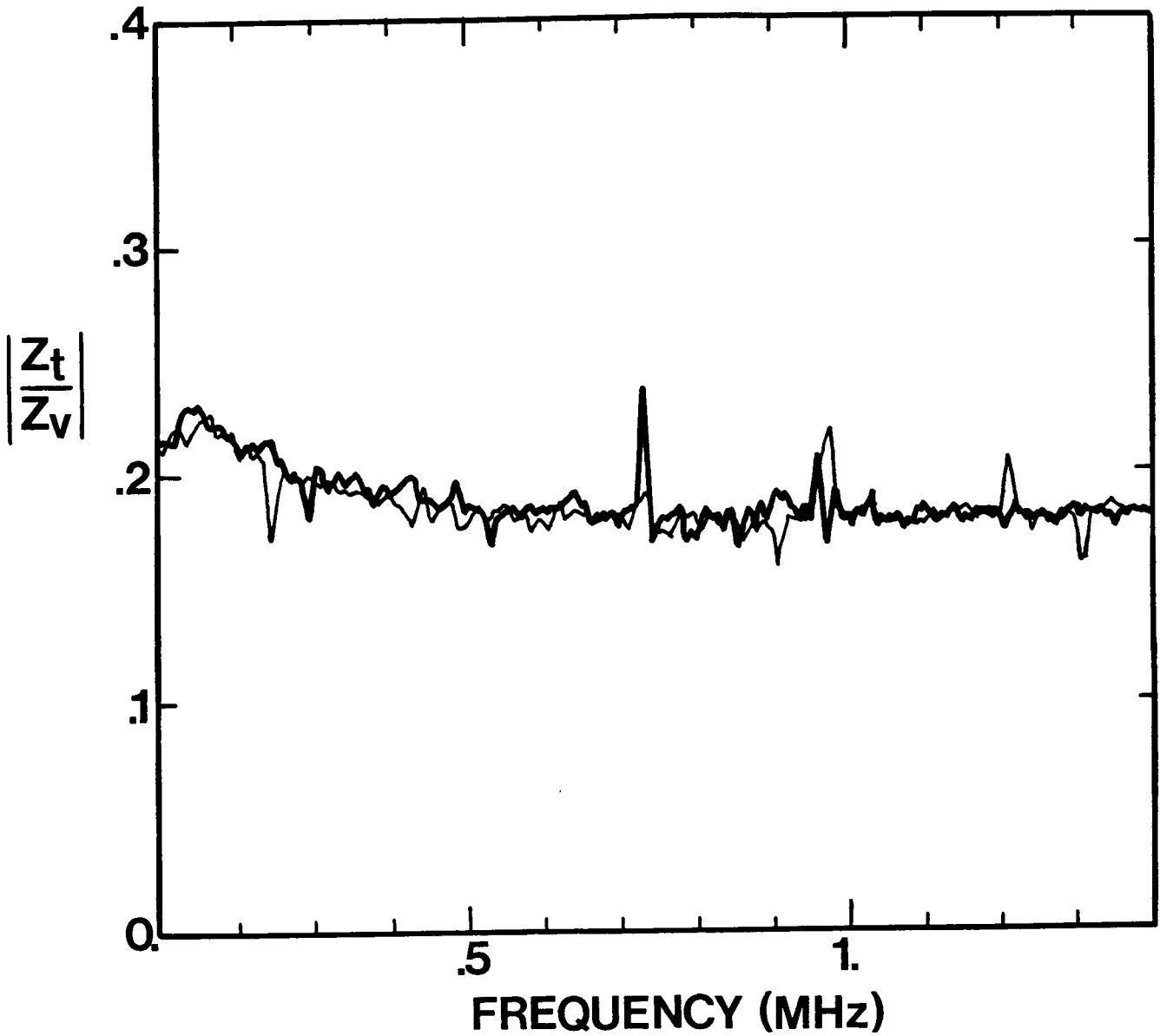

FIGURE 30

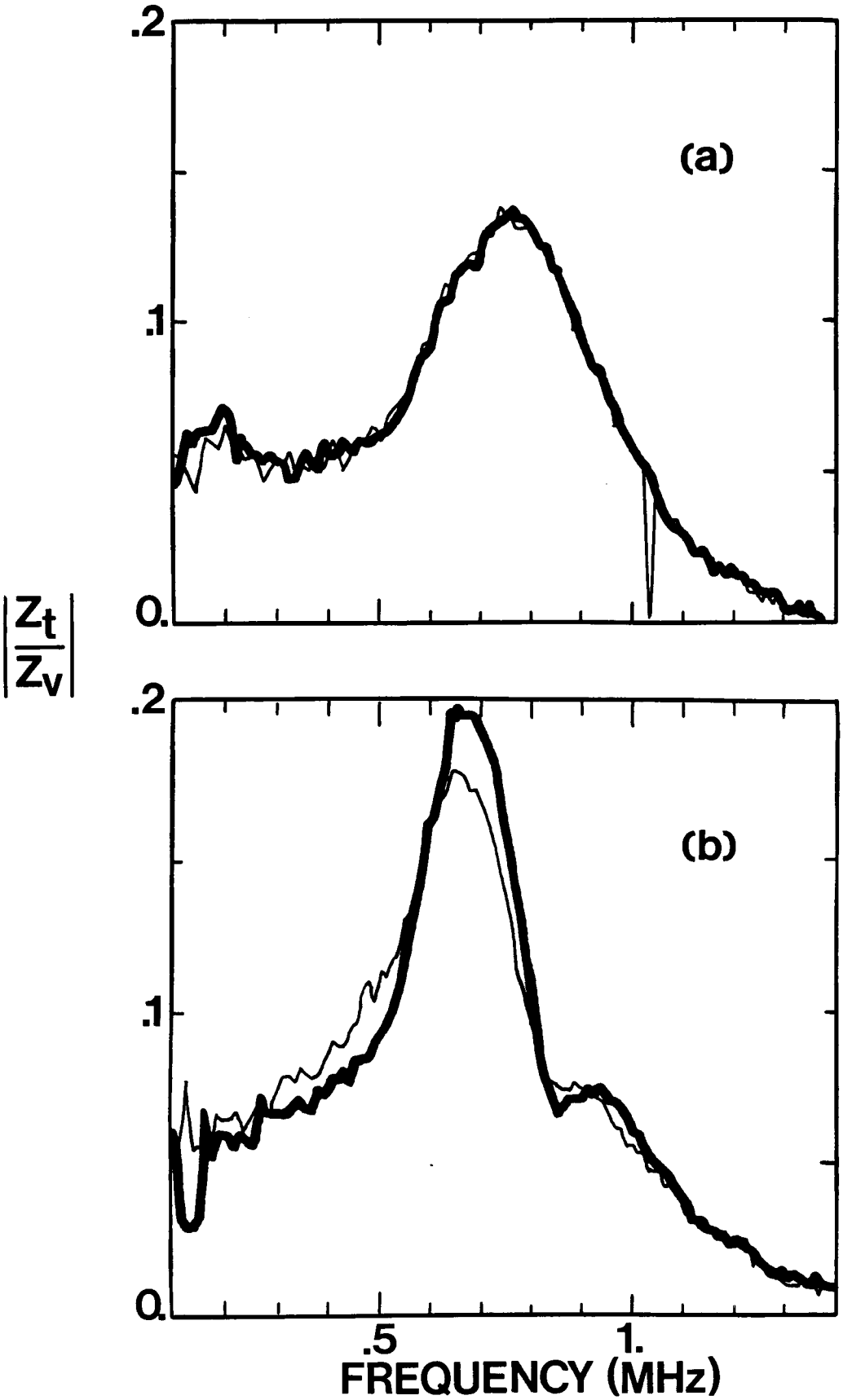

FIGURE 31

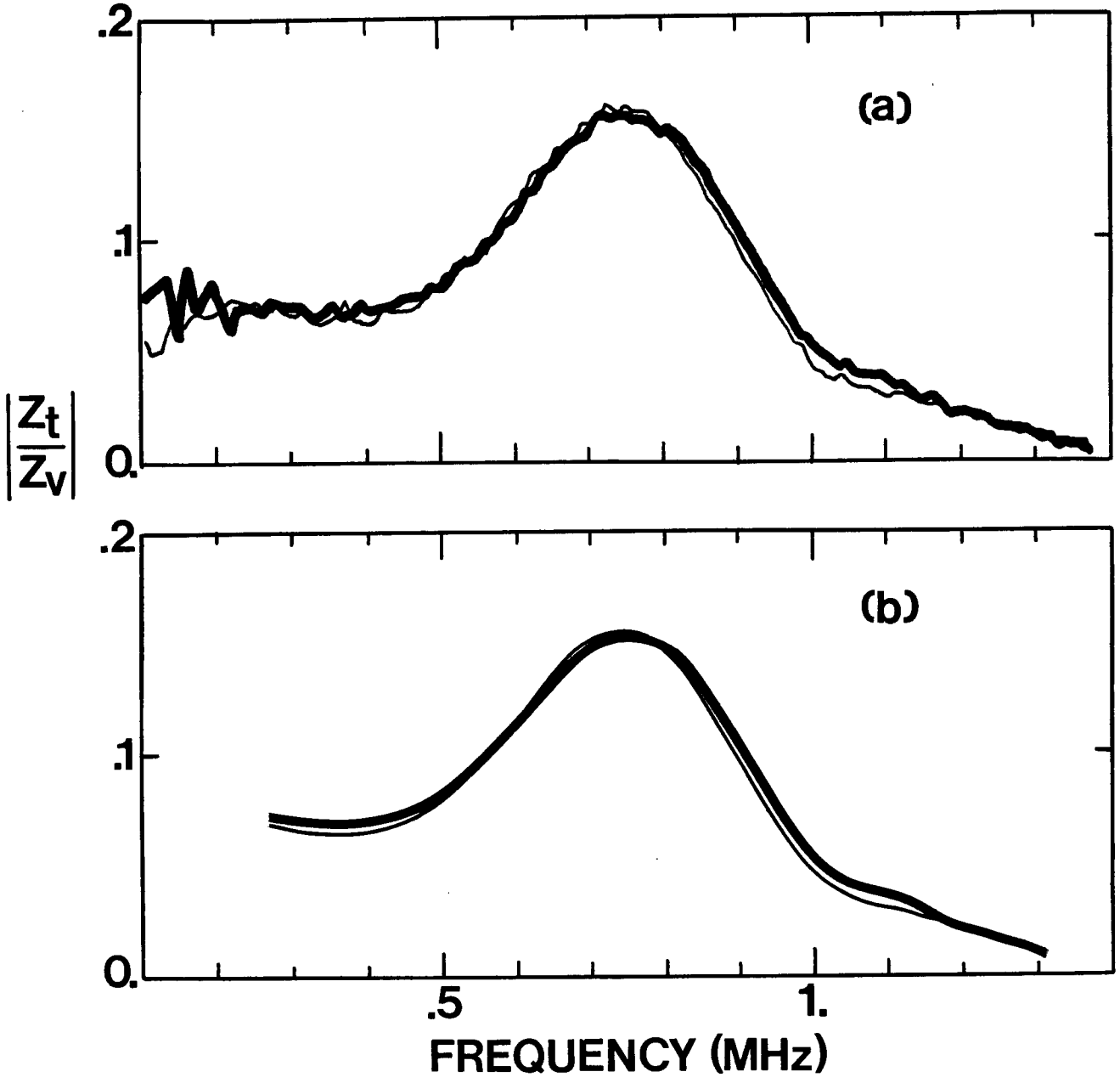

FIGURE 32

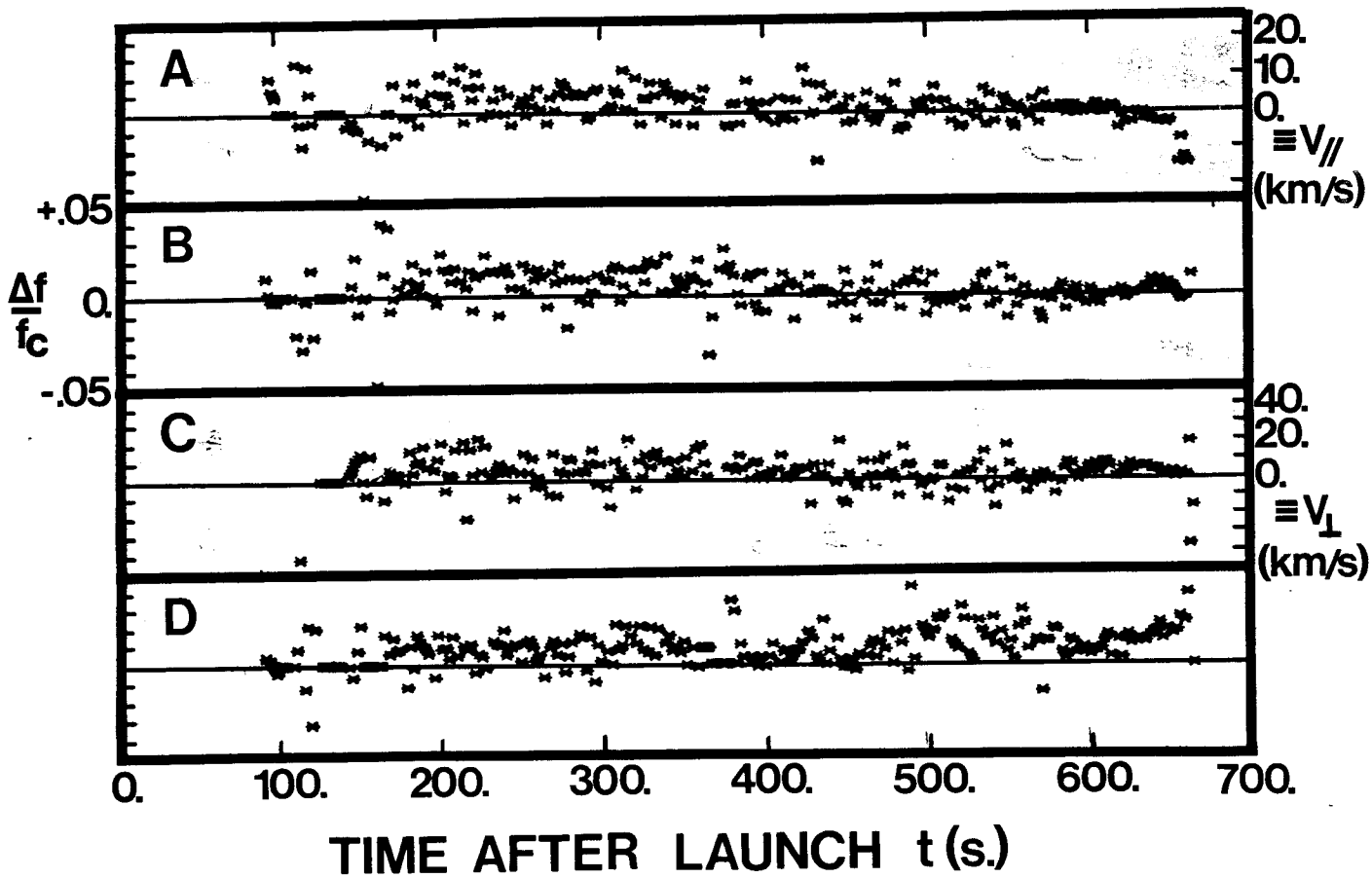
A
B
C
D
+.05
0.
-.05
Δf/fc
20.
10.
0.
≡V//
(km/s)
40.
20.
0.
≡V⊥
(km/s)
0.
100.
200.
300.
400.
500.
600.
700.
TIME AFTER LAUNCH t (s.)

FIGURE 33

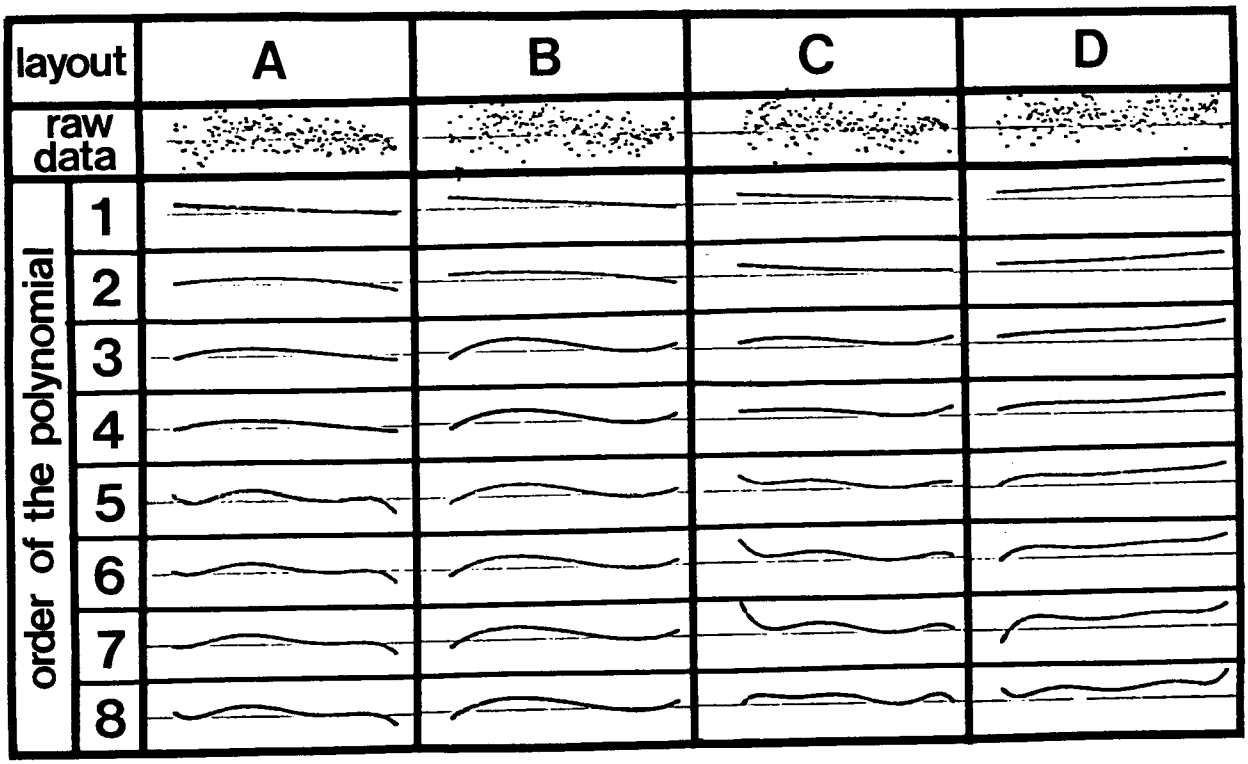
layout
A
B
C
D
raw data
order of the polynomial
1
2
3
4
5
6
7
8

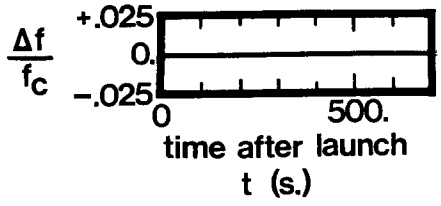
Δf/fc
+.025
0.
-.025
0
500.
time after launch
t (s.)

FIGURE 34

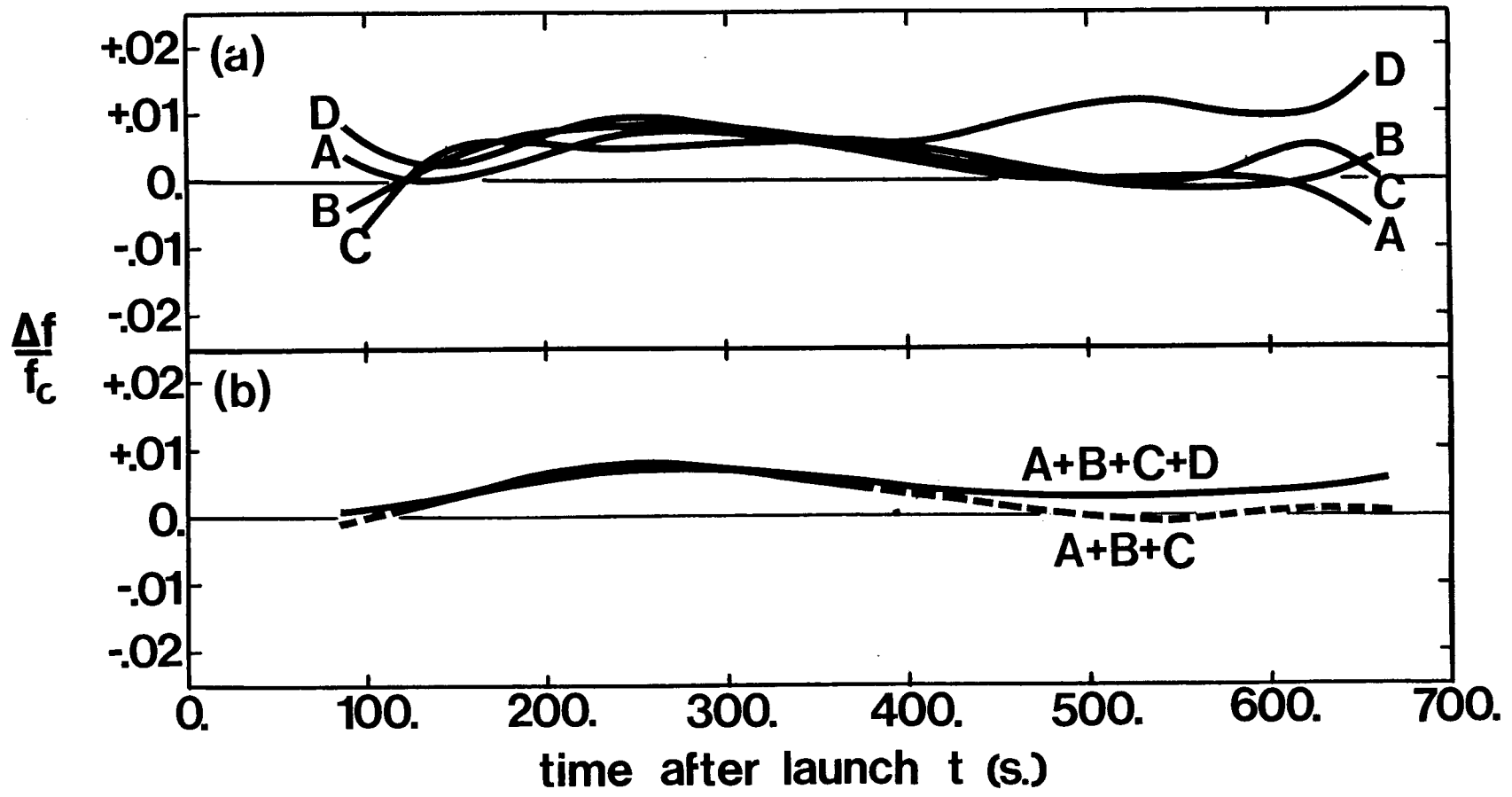
(a)
(b)
+.02
+.01
0.
-.01
-.02
Δf/f_c
D
A
B
C
A+B+C+D
A+B+C
0.
100.
200.
300.
400.
500.
600.
700.
time after launch t (s.)

FIGURE 35

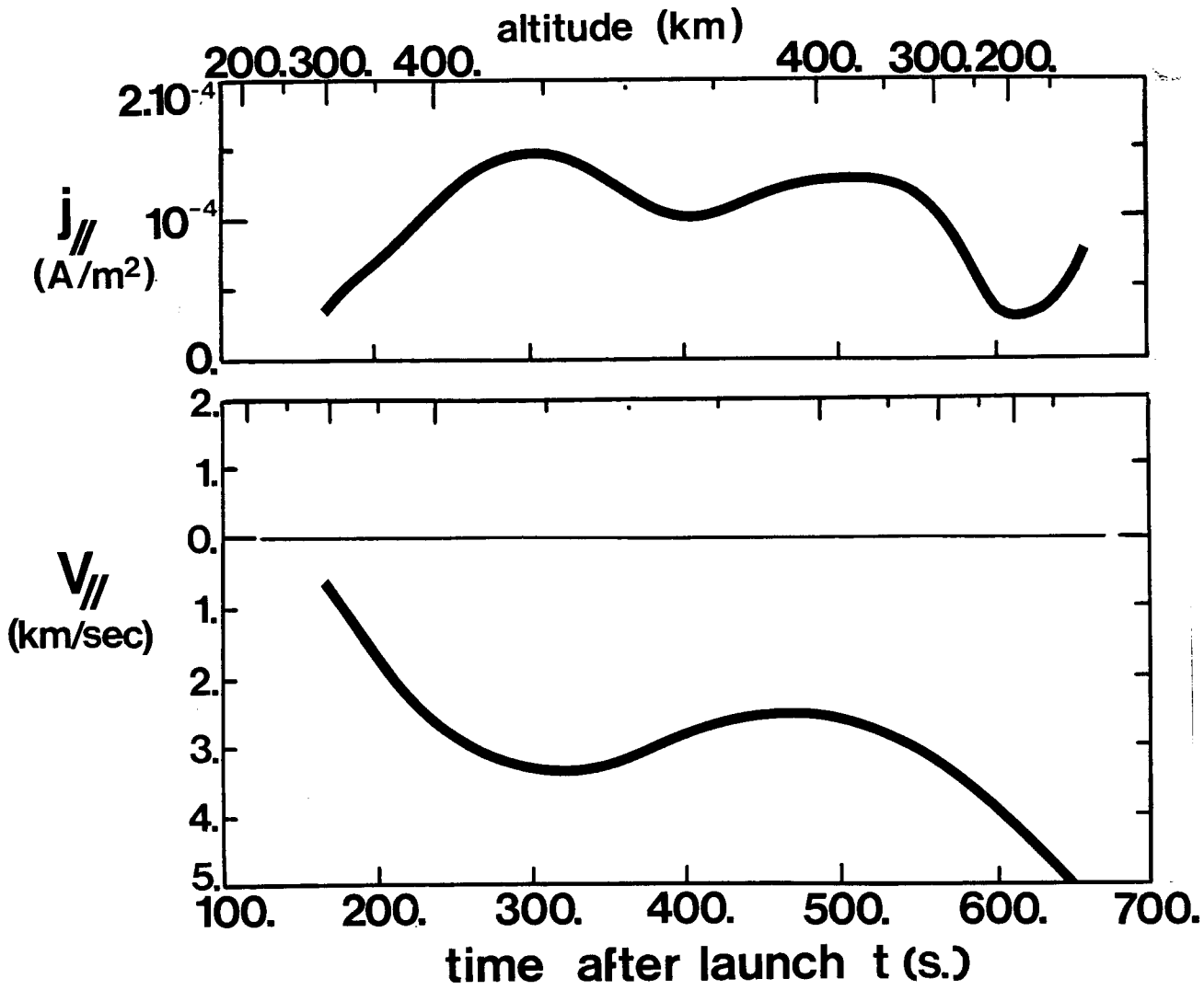
altitude (km)
200. 300. 400.
400. 300. 200.
2.10⁻⁴
10⁻⁴
0.
j// (A/m²)
2.
1.
0.
1.
2.
3.
4.
5.
V// (km/sec)
100. 200. 300. 400. 500. 600. 700.
time after launch t (s.)

FIGURE 36

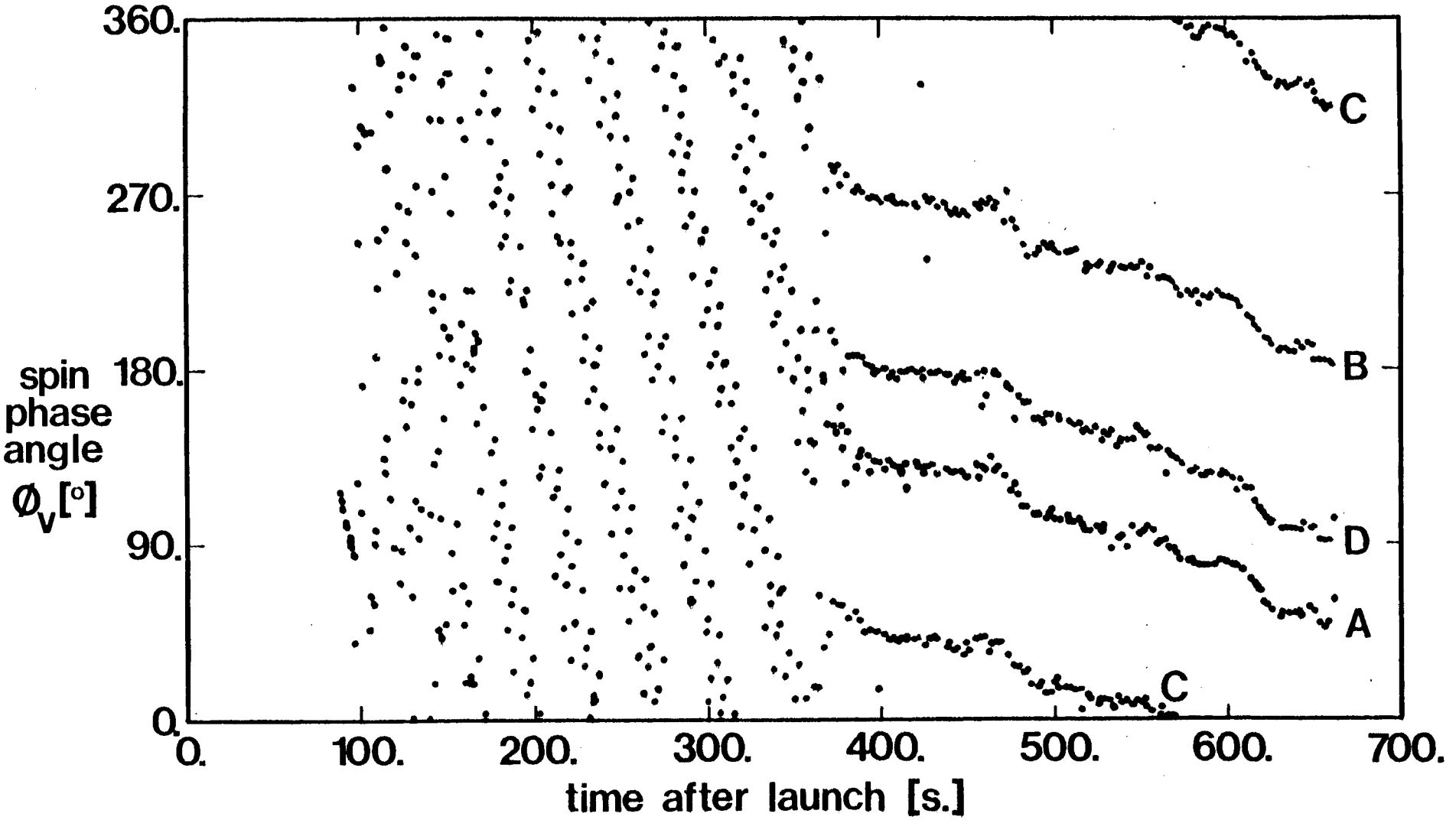
360.
270.
180.
90.
0.
spin phase angle ϕ_V[°]
0.
100.
200.
300.
400.
500.
600.
700.
time after launch [s.]
C
B
D
A
C

FIGURE 37

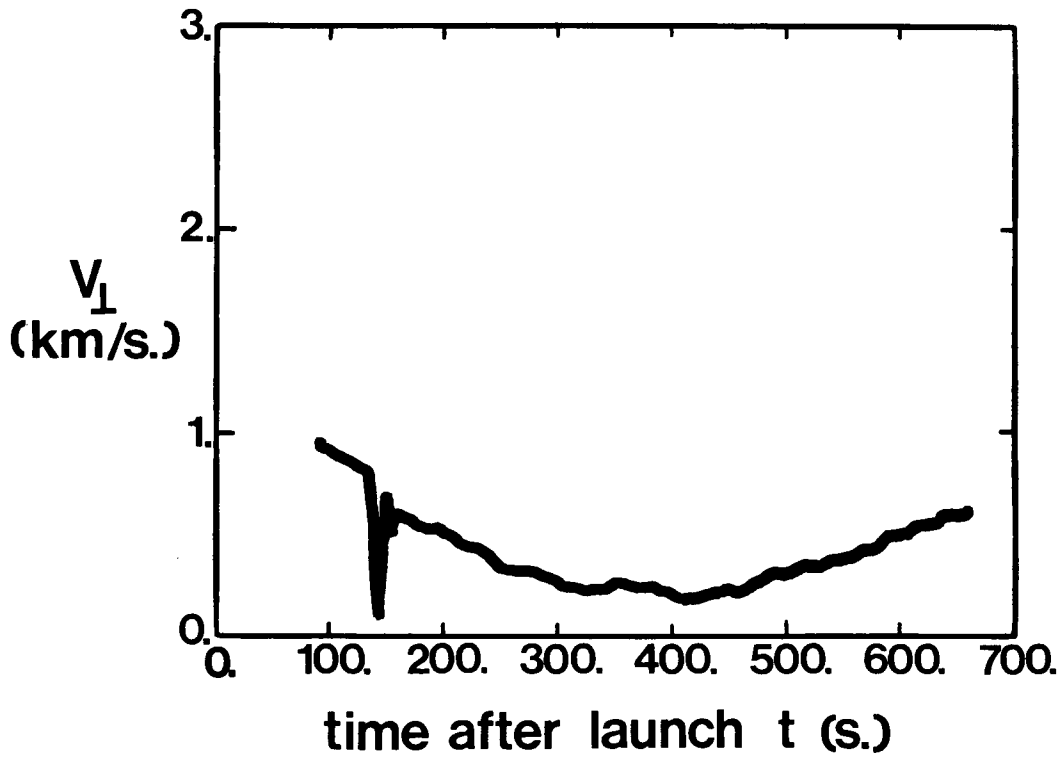
3.
2.
$V_\perp$
(km/s.)
1.
0.
0.
100.
200.
300.
400.
500.
600.
700.
time after launch t (s.)

FIGURE 38

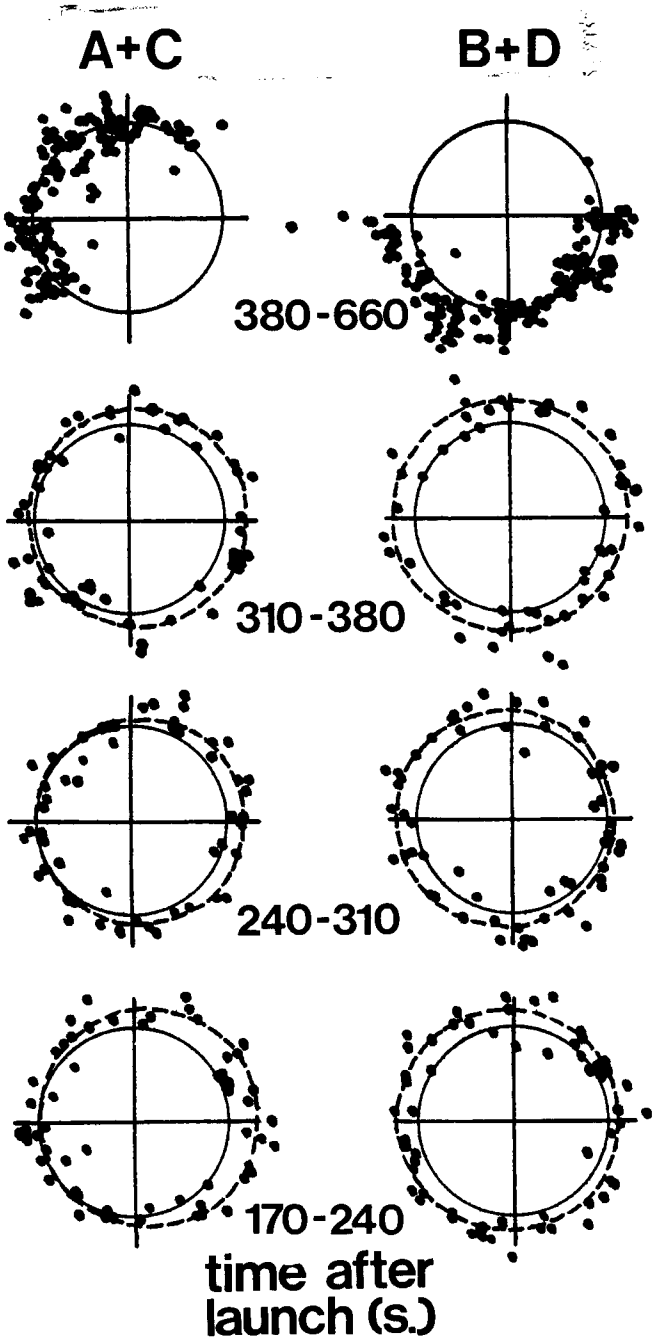

FIGURE 39

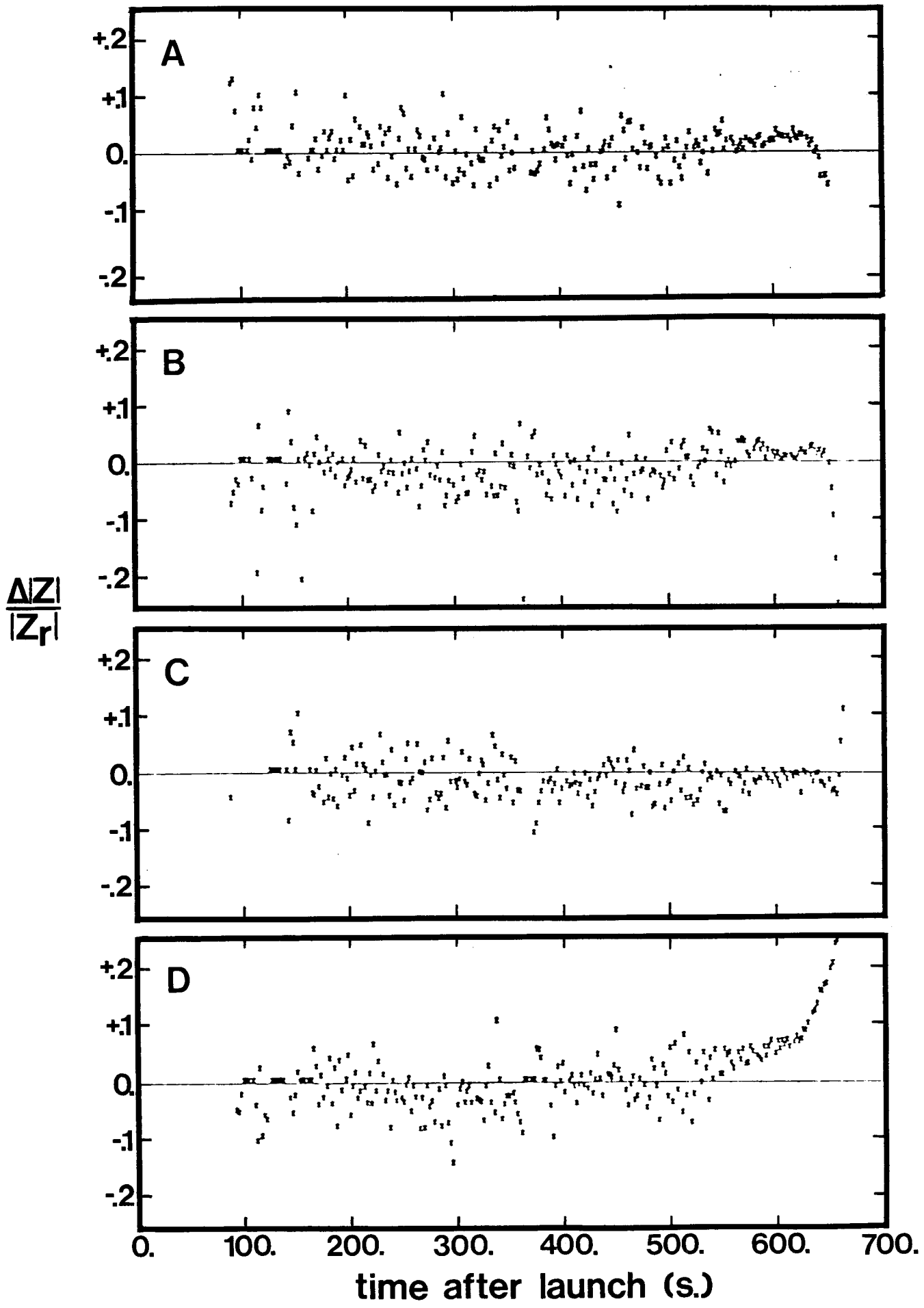
A
B
C
D
+.2
+.1
0.
-.1
-.2
$\frac{\Delta|Z|}{|Z_r|}$
0.
100.
200.
300.
400.
500.
600.
700.
time after launch (s.)

FIGURE 40

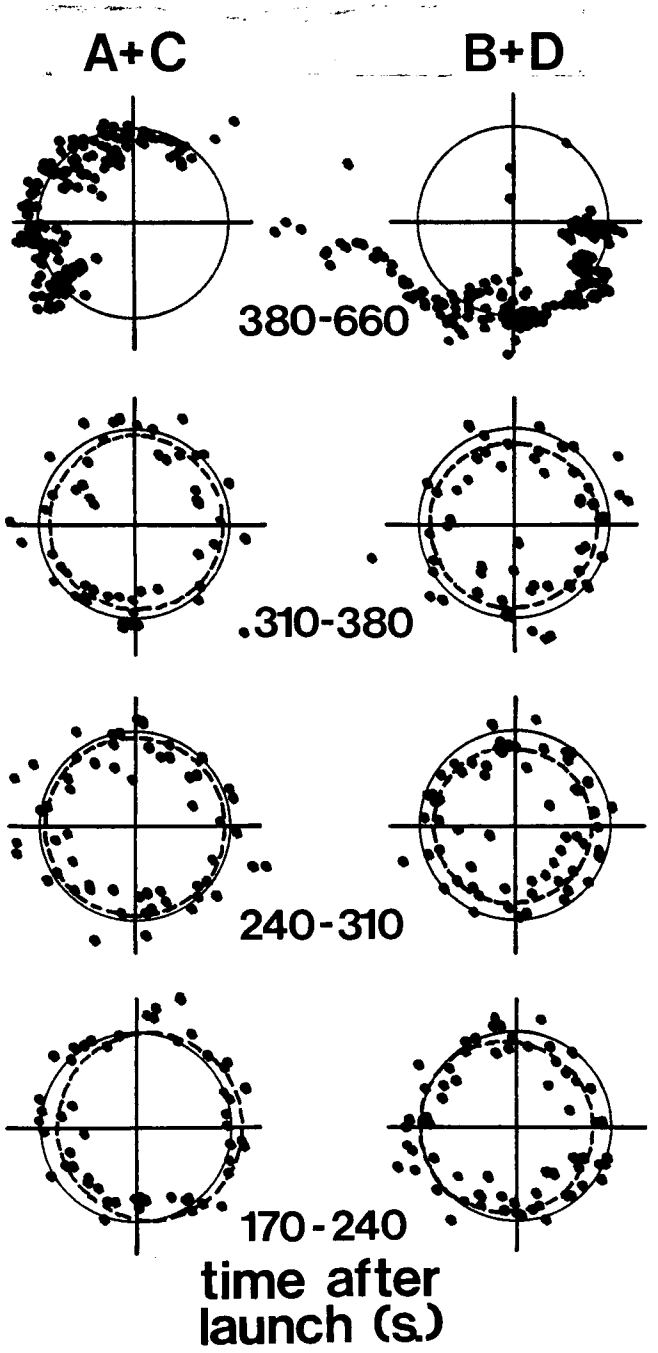

FIGURE 41

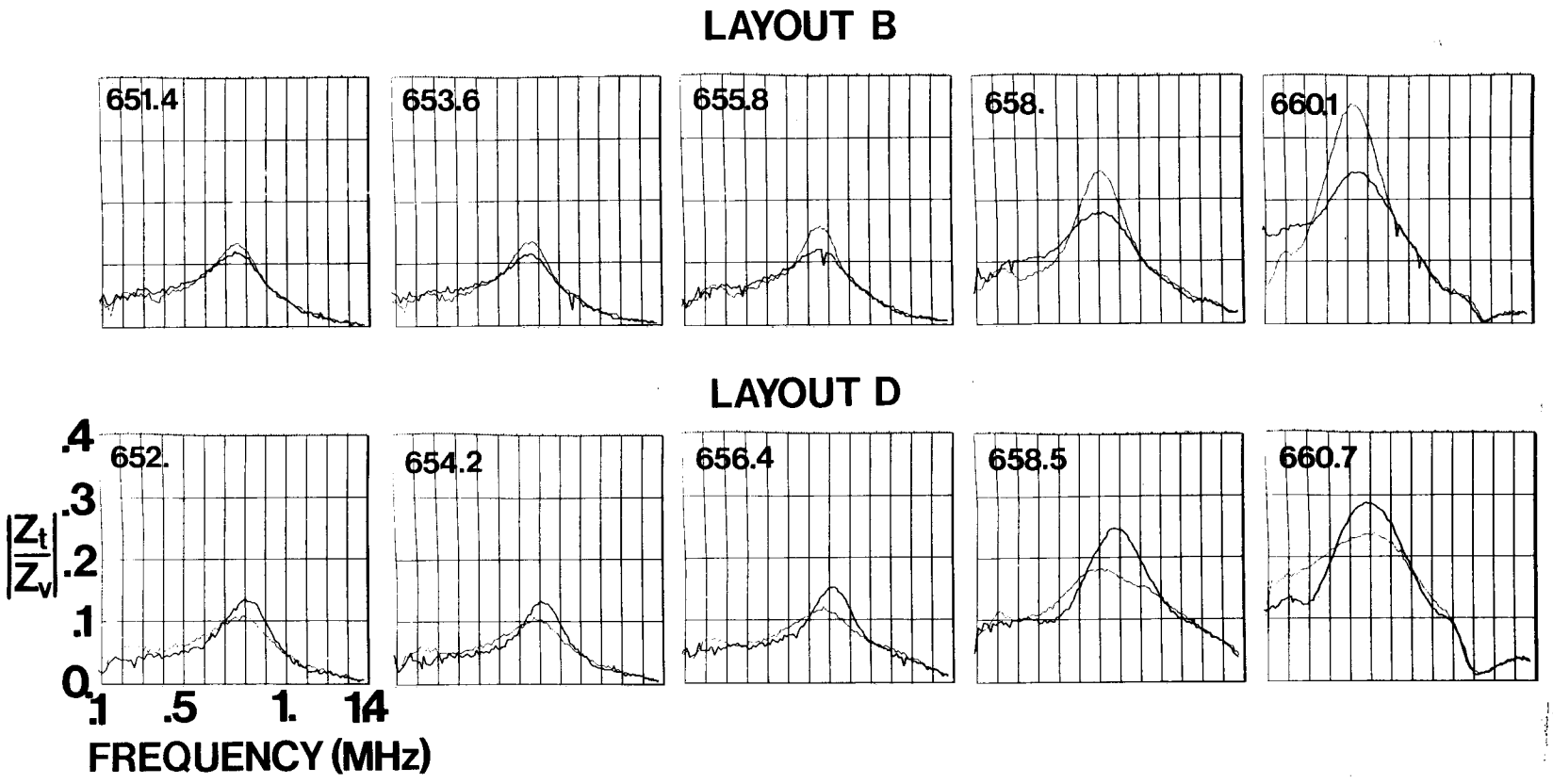
LAYOUT B
651.4
653.6
655.8
658.
660.1
LAYOUT D
652.
654.2
656.4
658.5
660.7
.4
.3
.2
.1
0
|Zt|/|Zv|
.1
.5
1.
14
FREQUENCY (MHz)

FIGURE 42

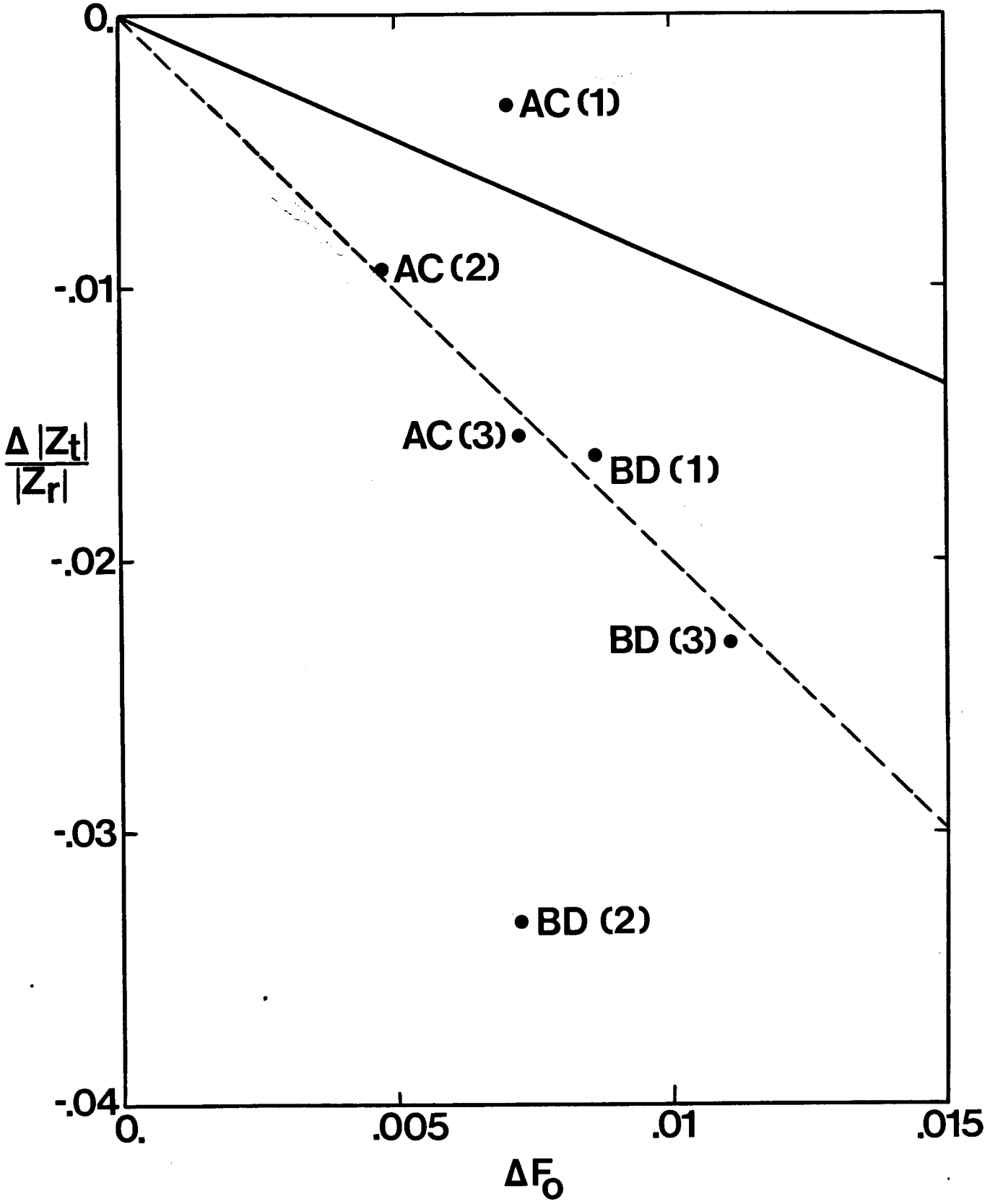
0.
-.01
-.02
-.03
-.04
0.
.005
.01
.015
$\frac{\Delta |Z_t|}{|Z_r|}$
ΔF_o
AC (1)
AC (2)
AC (3)
BD (1)
BD (2)
BD (3)

FIGURE 43

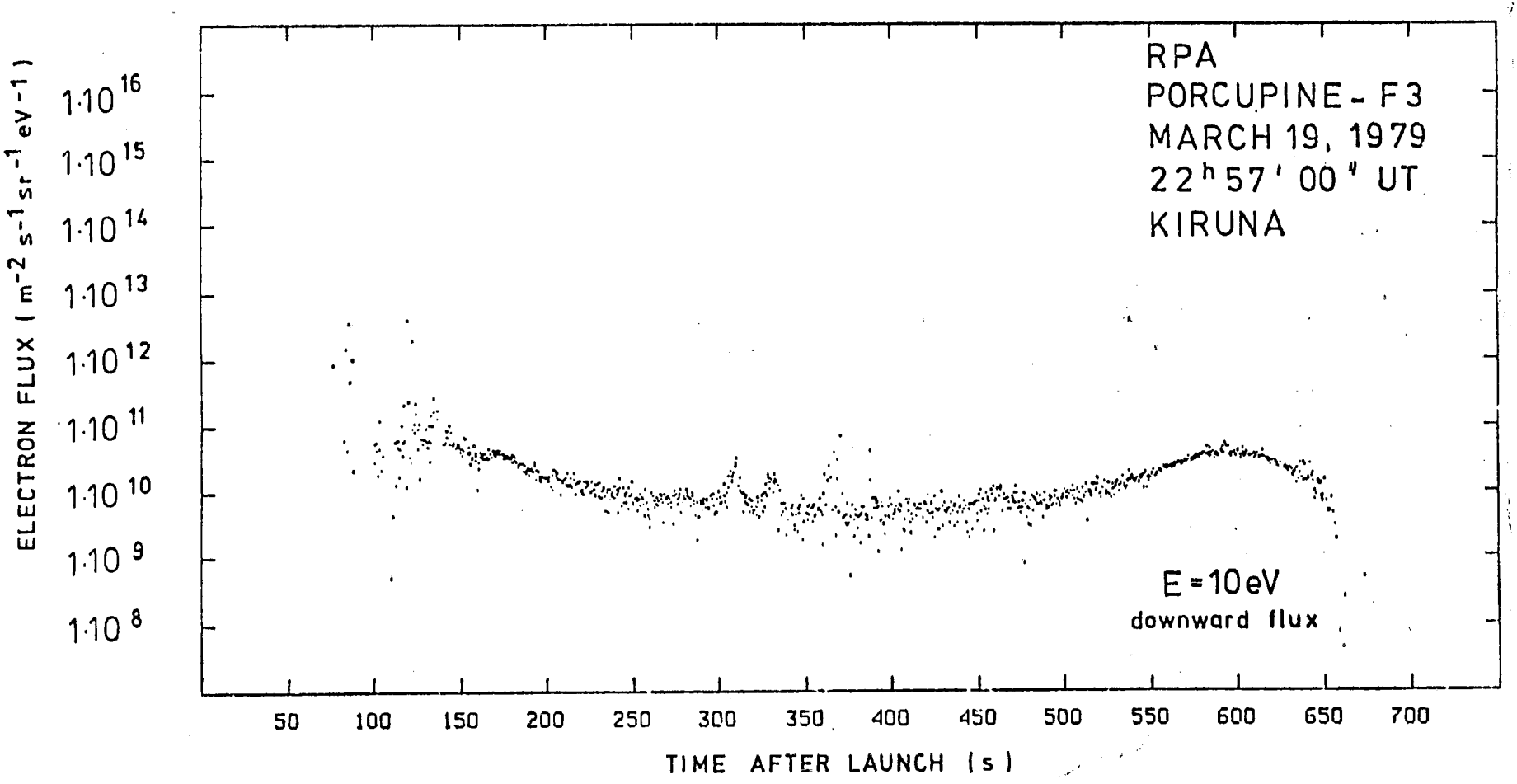
RPA
PORCUPINE - F3
MARCH 19, 1979
22h57'00" UT
KIRUNA
E = 10 eV
downward flux
ELECTRON FLUX (m-2 s-1 sr-1 eV-1)
1·10 16
1·10 15
1·10 14
1·10 13
1·10 12
1·10 11
1·10 10
1·10 9
1·10 8
50
100
150
200
250
300
350
400
450
500
550
600
650
700
TIME AFTER LAUNCH (s)

FIGURE 44

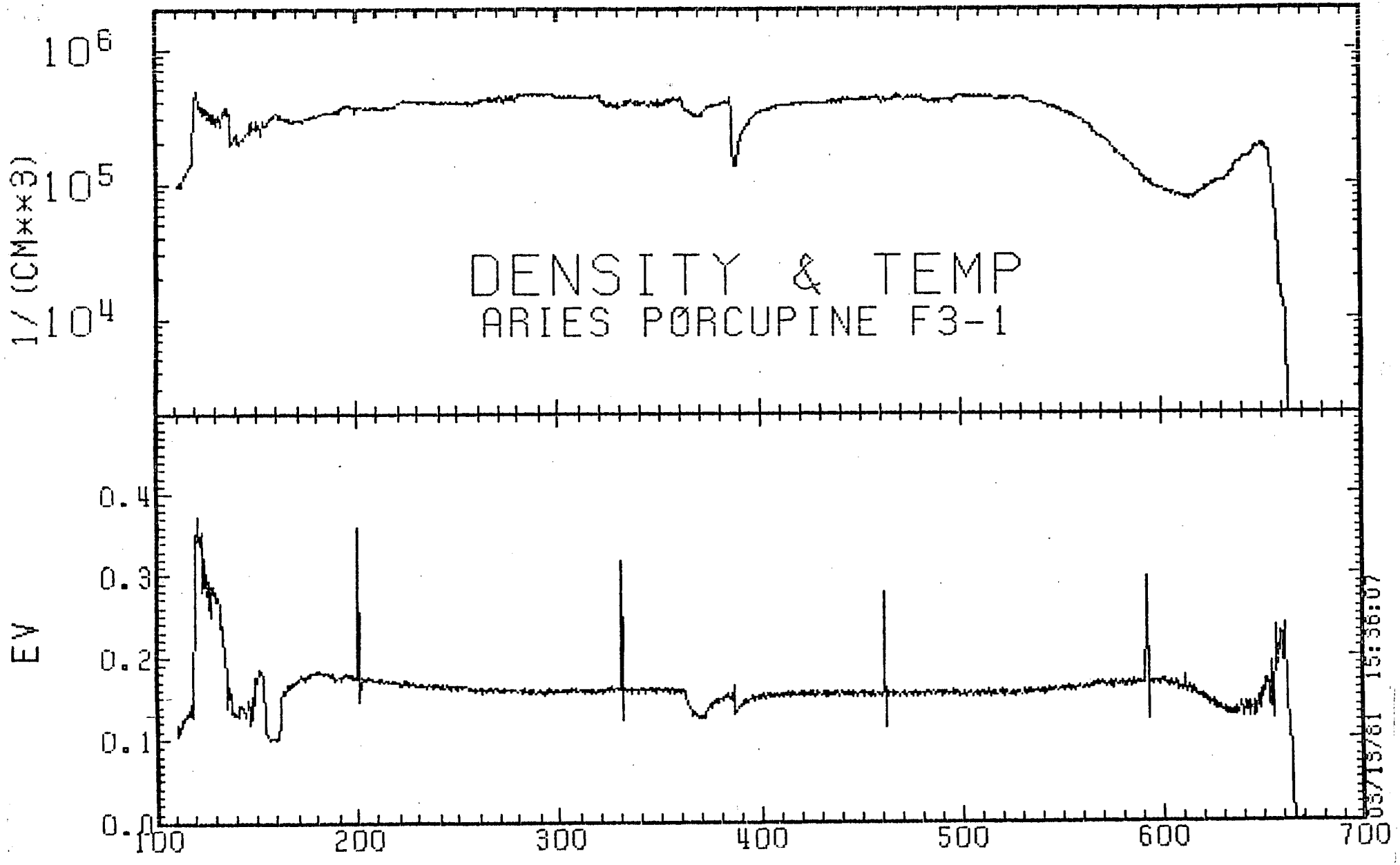
DENSITY & TEMP
ARIES PØRCUPINE F3-1
1/(CM**3)
10^6
10^5
10^4
EV
0.4
0.3
0.2
0.1
0.0
100
200
300
400
500
600
700
05/19/81 15:56:07

FIGURE 45

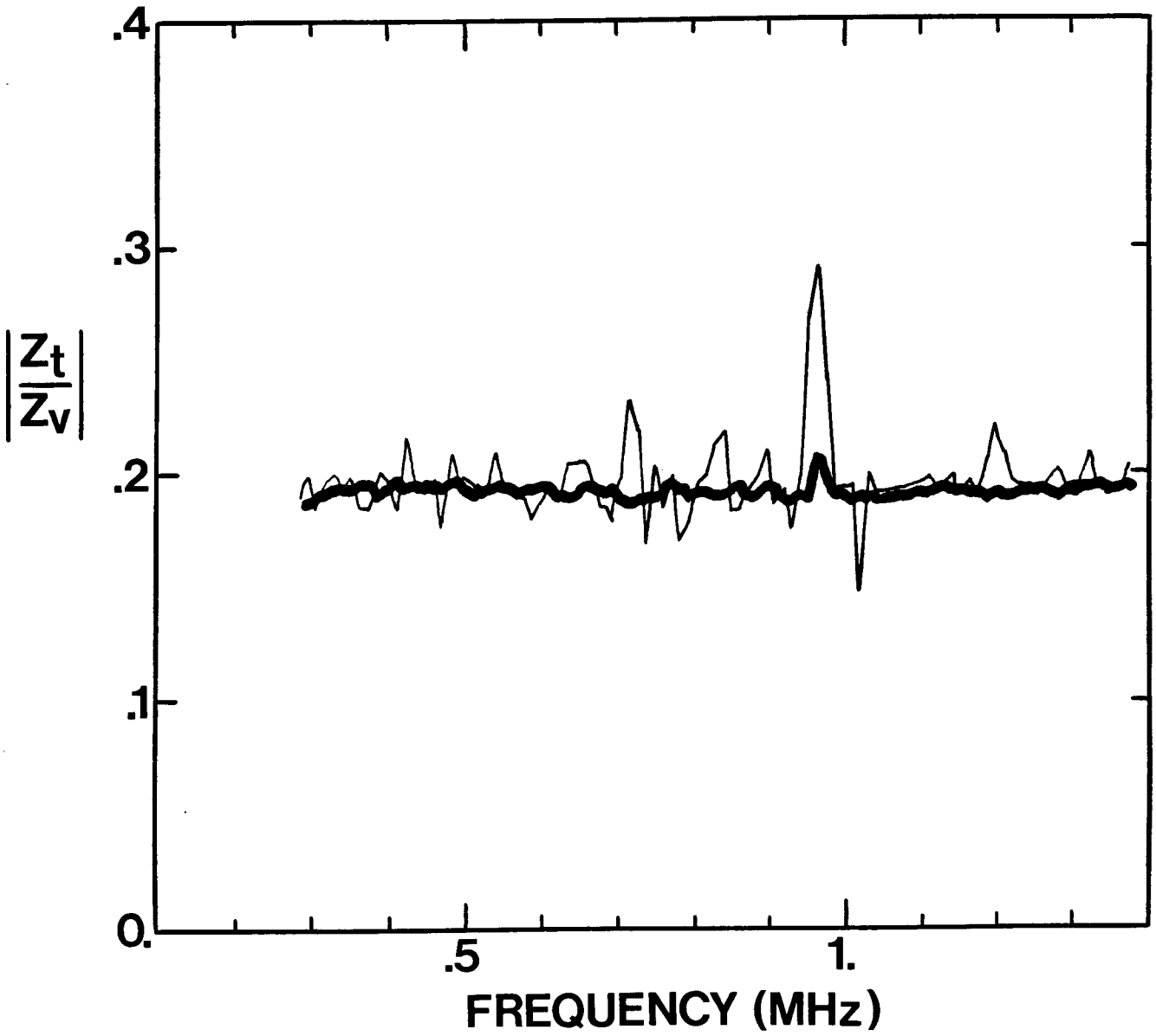

FIGURE 46

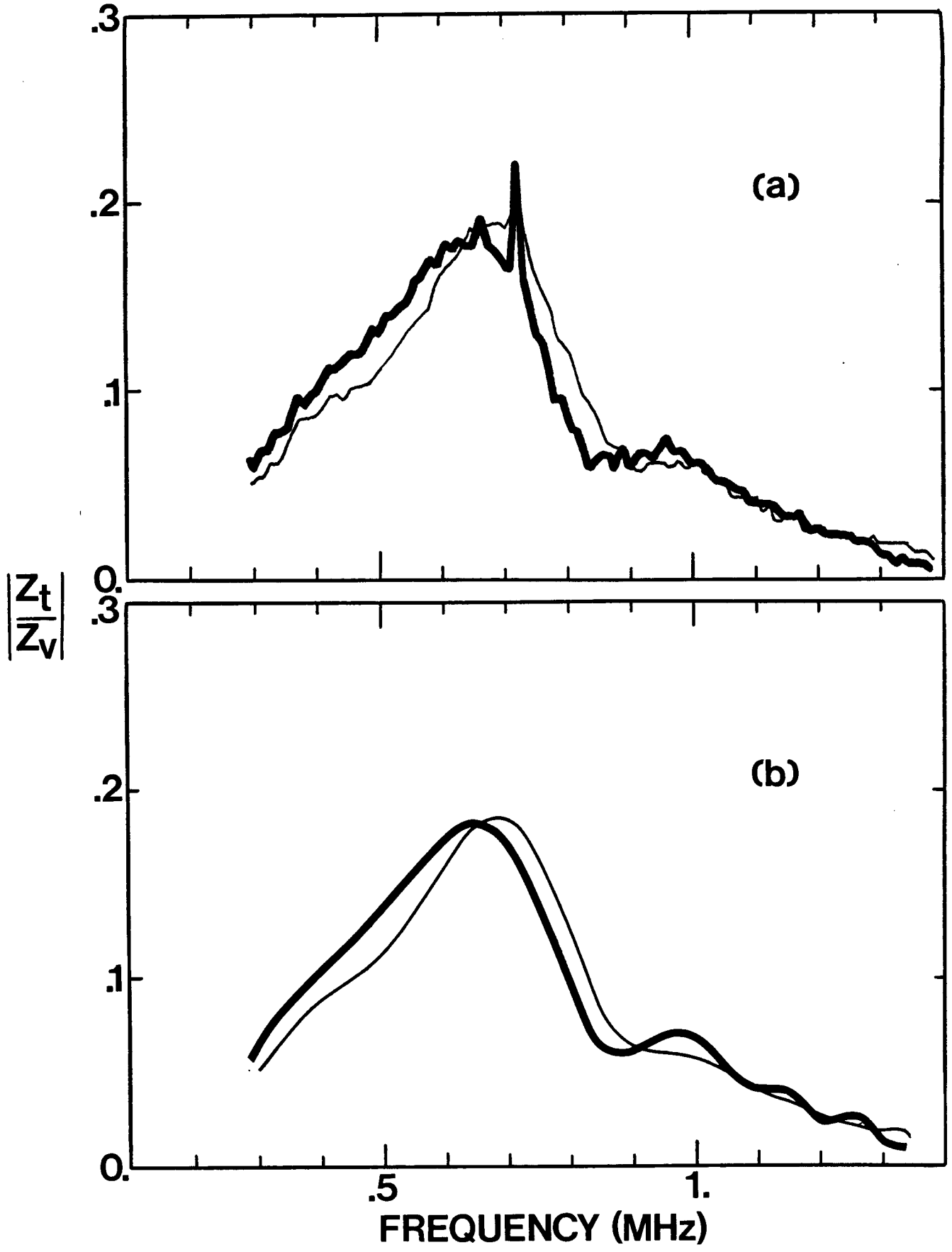

FIGURE 47

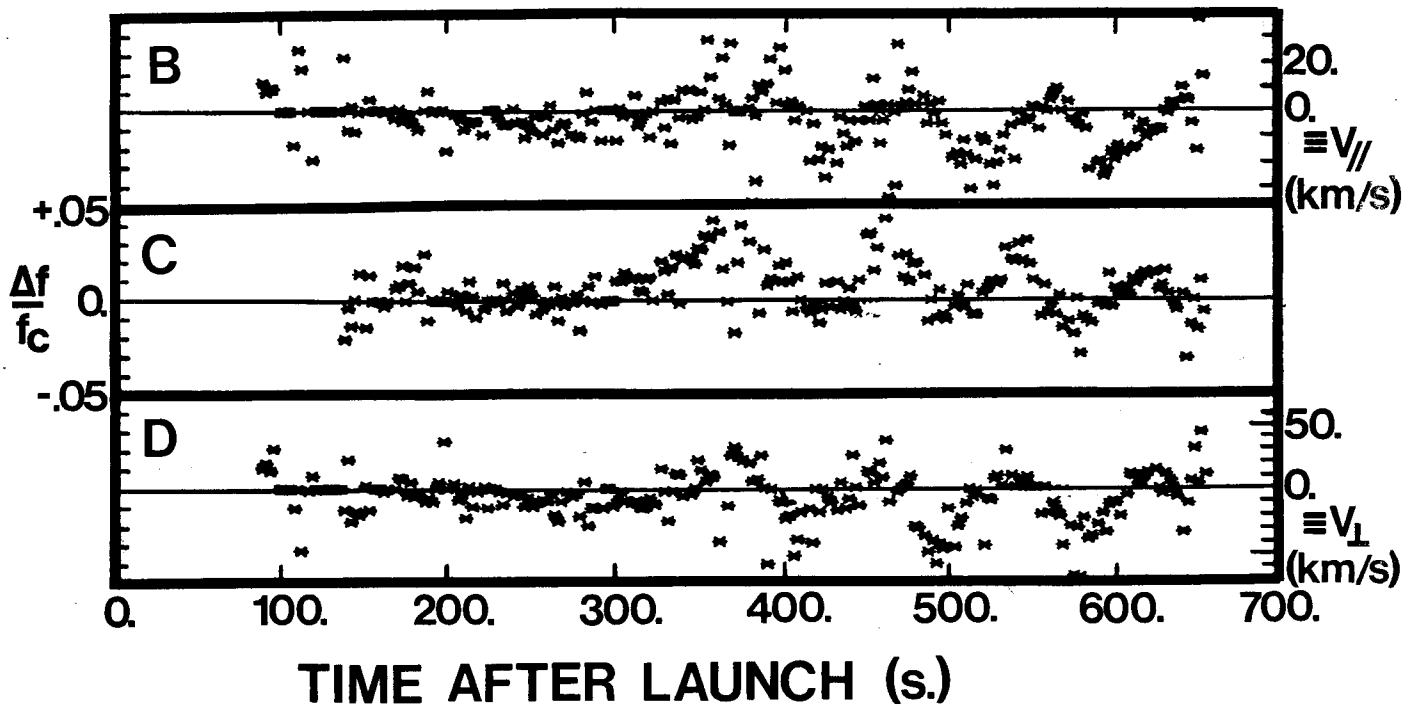
B
C
D
+.05
Δf/fc
0.
-.05
20.
0.
≡V//
(km/s)
50.
0.
≡V⊥
(km/s)
0.
100.
200.
300.
400.
500.
600.
700.
TIME AFTER LAUNCH (s.)

FIGURE 48

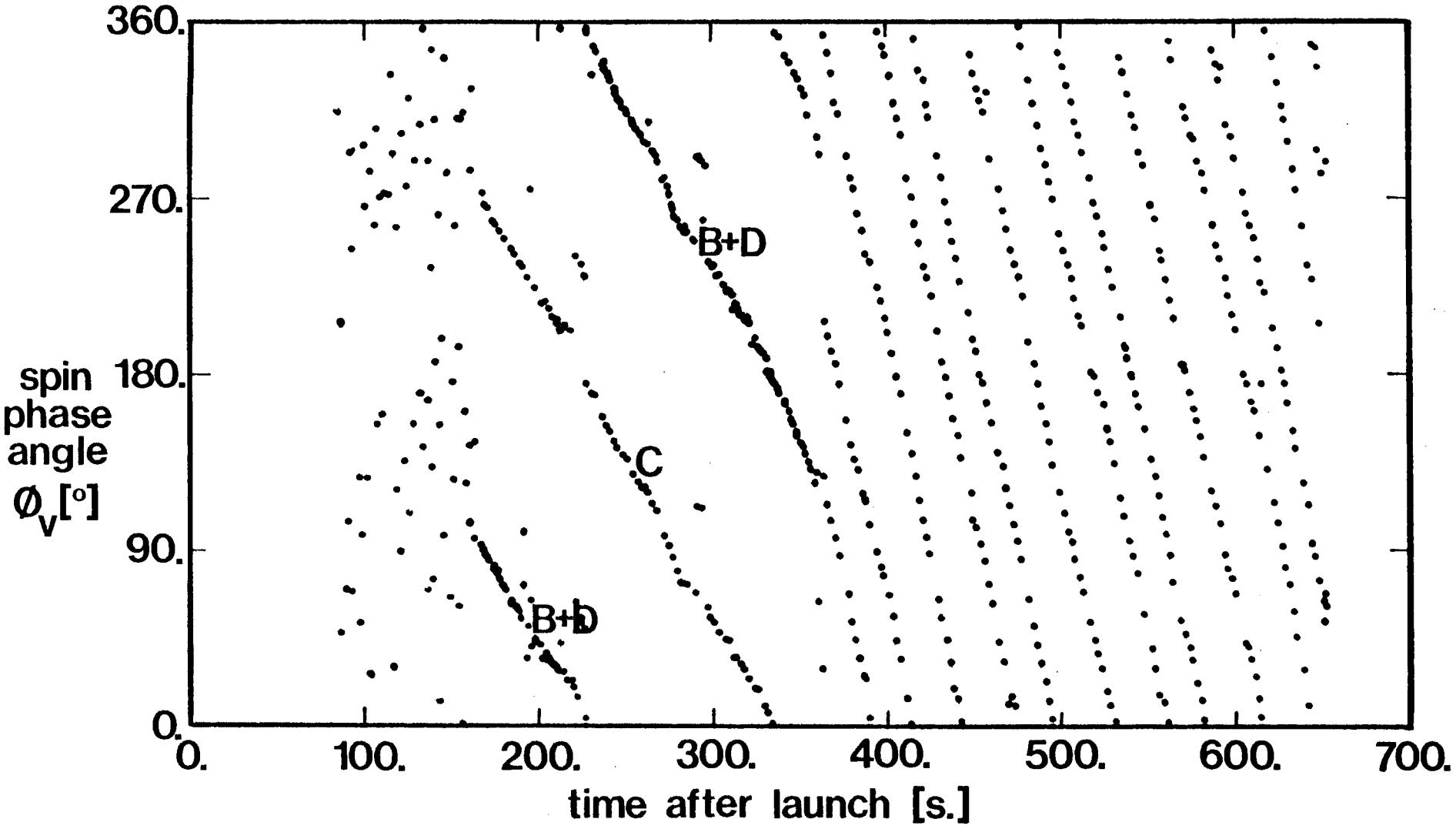
360.
270.
180.
90.
0.
spin phase angle ϕ_v[°]
B+D
C
B+D
0.
100.
200.
300.
400.
500.
600.
700.
time after launch [s.]

FIGURE 49

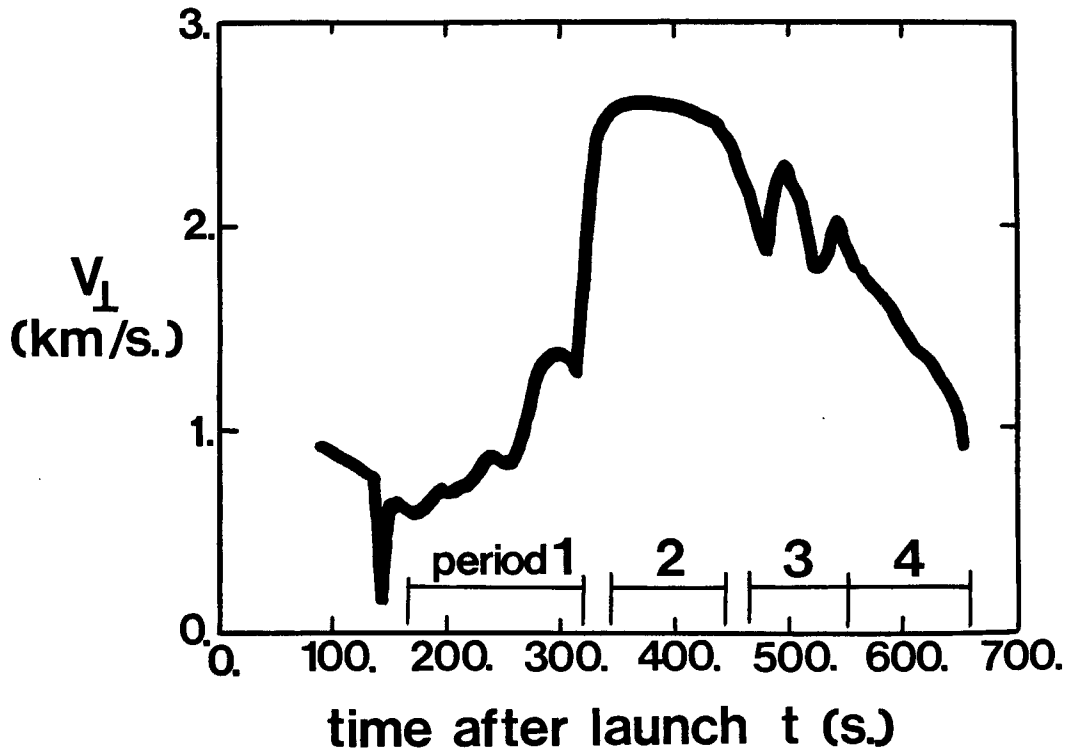
3.
2.
1.
0.
$V_\perp$
(km/s.)
period 1
2
3
4
0.
100.
200.
300.
400.
500.
600.
700.
time after launch t (s.)

FIGURE 50

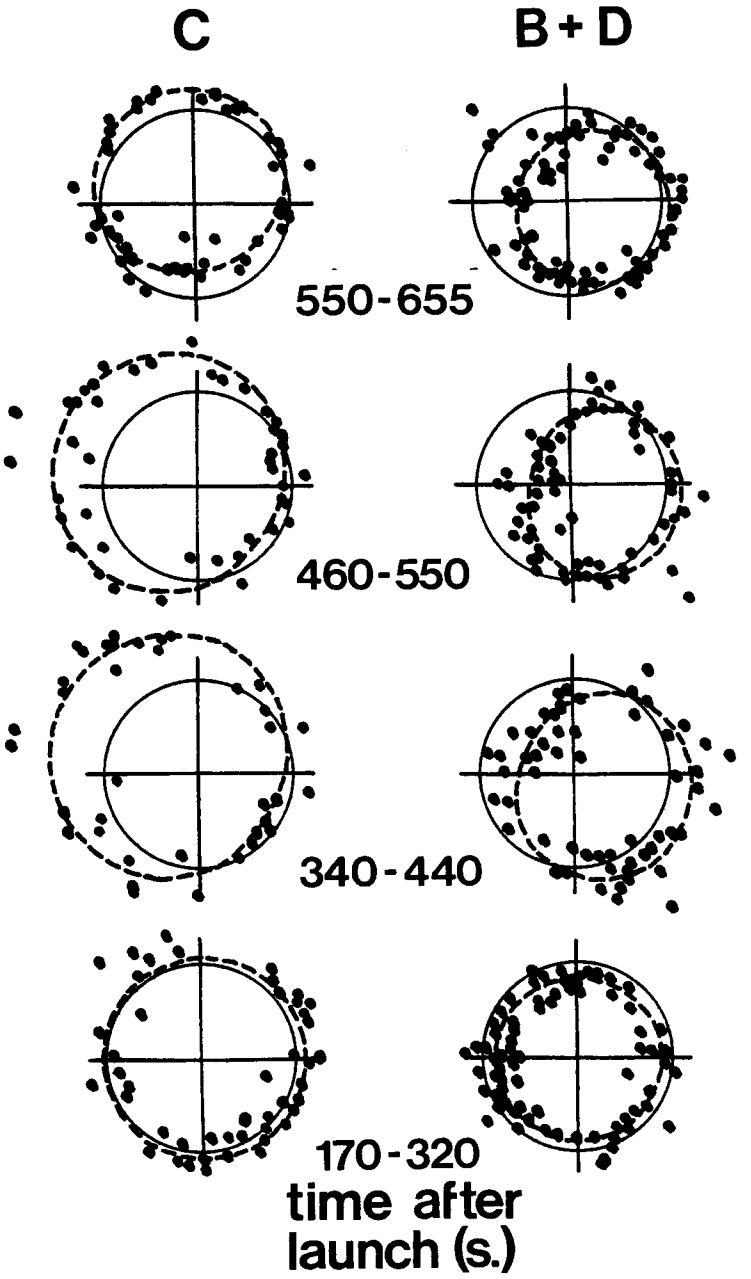

FIGURE 51

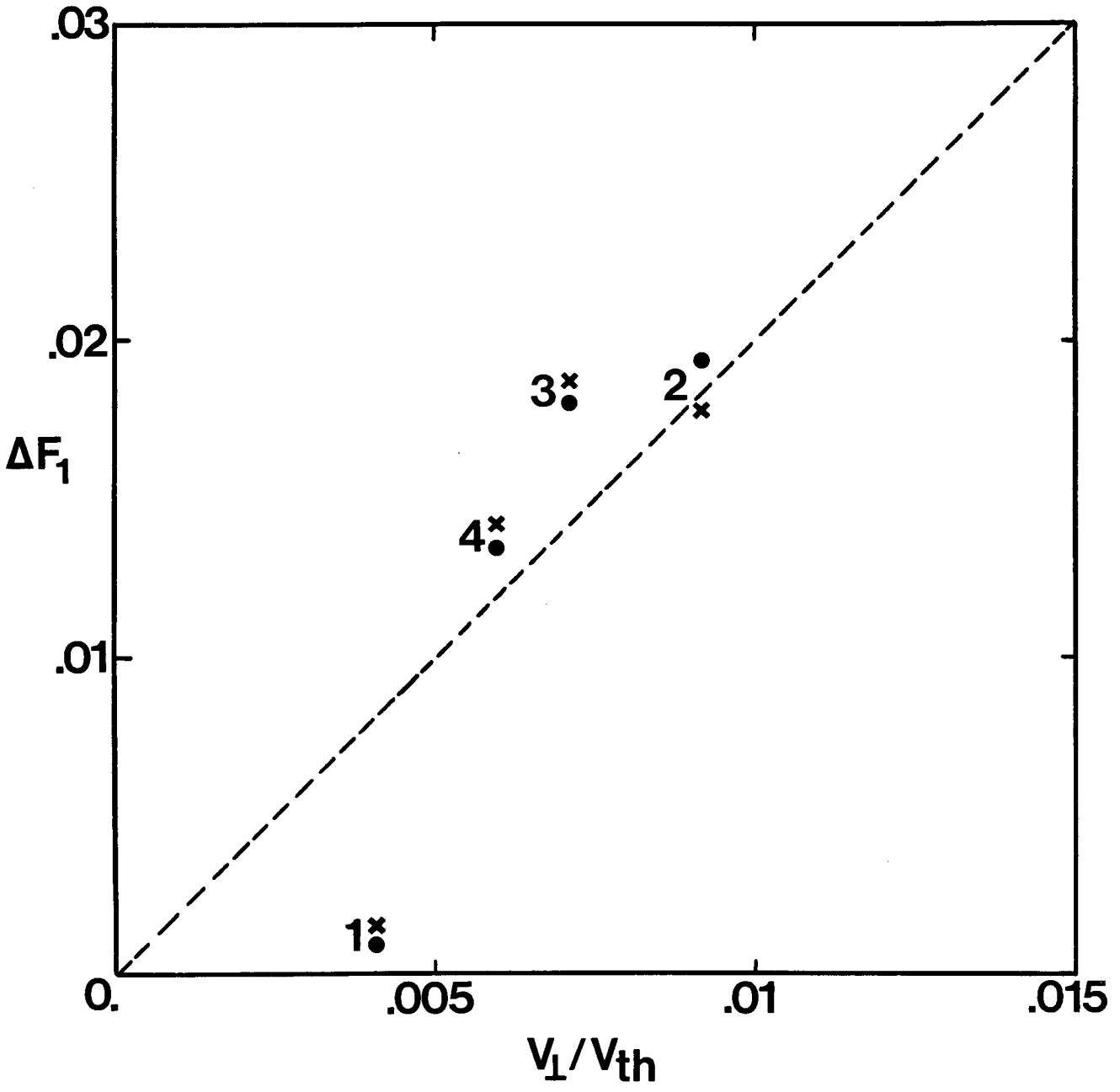

FIGURE 52

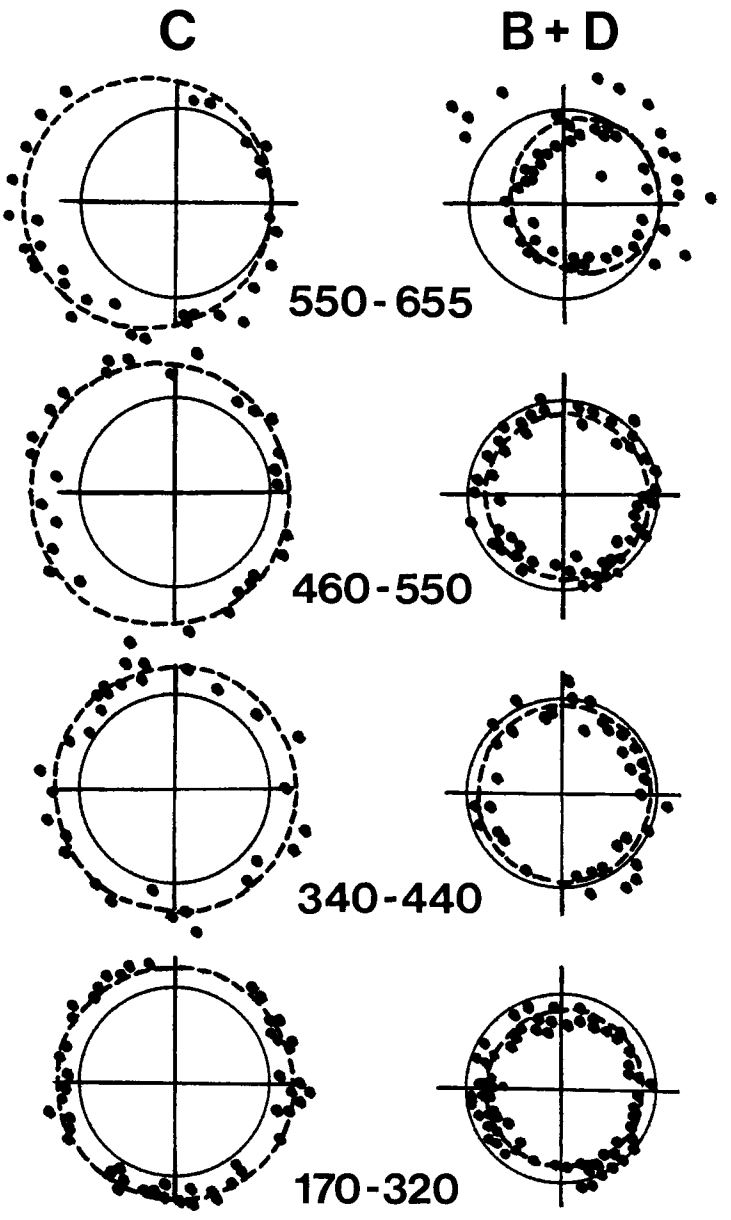

FIGURE 53

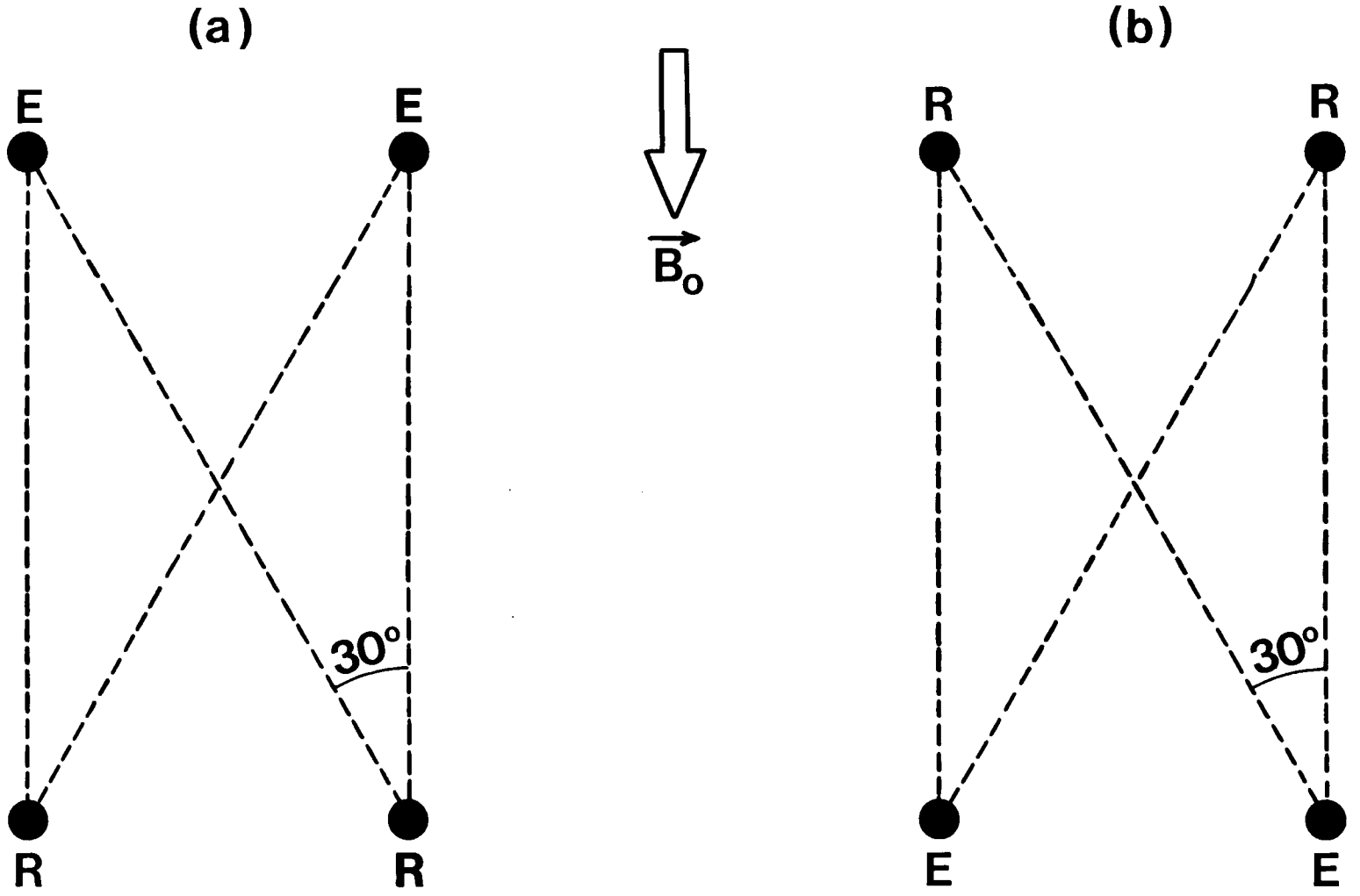

FIGURE 54

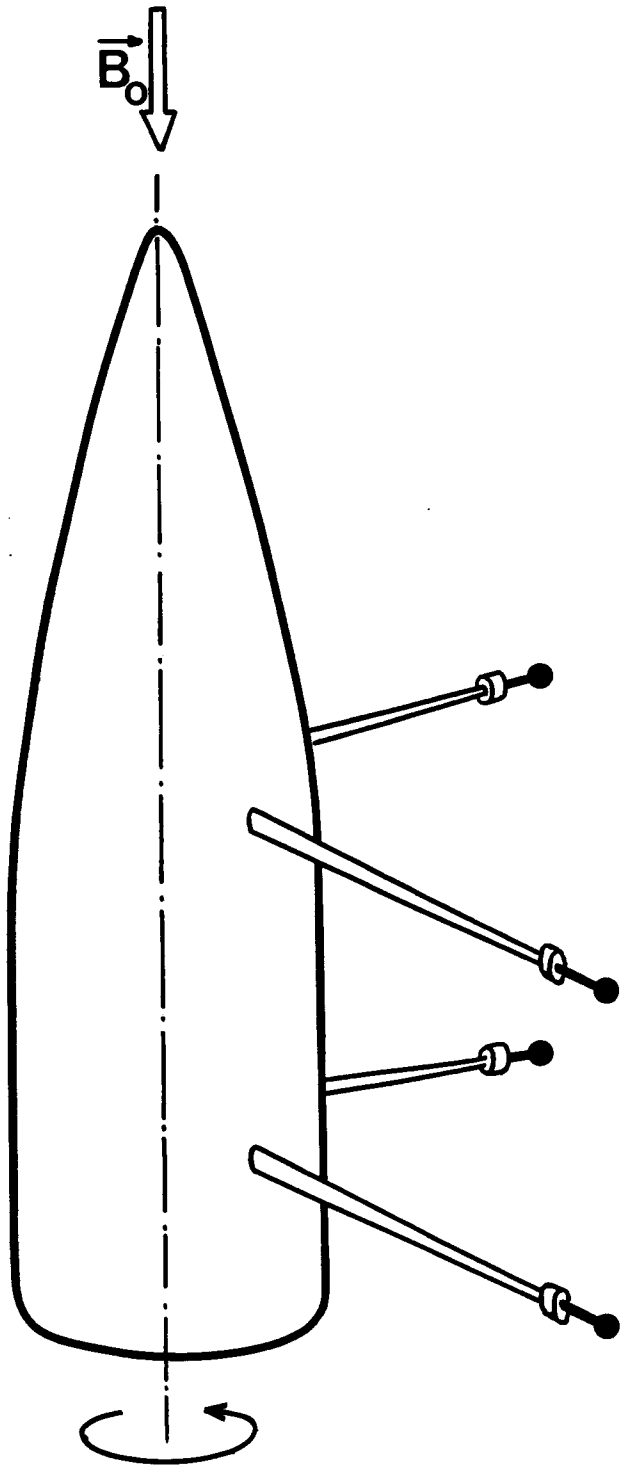

FIGURE 55